Analyse der Cadherin-Expression im Cortex cerebri und der Amygdala in der Reeler-Mausmutante

Dissertation

zur Erlangung des akademischen Grades
Doctor rerum naturalium
(Dr. rer. nat.)

vorgelegt dem Rat der Medizinischen Fakultät der
Friedrich-Schiller-Universität Jena

von
Diplom-Biologin Nicole Hertel
geboren am 27. September 1982 in Borna

Analysis of cadherin expression in the cerebral cortex and the amygdala of the Reeler mutant mouse

Dissertation

for obtaining the academic degree Doctor rerum naturalium (Dr. rer. nat.)

from the Faculty of Medicine,
Friedrich-Schiller-University Jena

submitted by
Diploma-Biologist Nicole Hertel
born on September, 27th, 1982 in Borna, Germany

Reviewer 1: Prof. Dr. Dr. Christoph Redies
Institute of Anatomy I
University Hospital Jena
Teichgraben 7
07743 Jena, Germany

Reviewer 2: OA PD Dr. Hubertus Axer
Department of Neurology
University Hospital Jena
ErlangerAllee 101
07747 Jena, Germany

Reviewer 3: Prof. Dr. Loreta Medina
Laboratory of Brain Development and Evolution
Institute of Biomedical Research of Lleida
University of Lleida
25008 Lleida, Spain

Day of the public defence: 04.10.2011

CONTENTS

ABBREVIATIONS

General abbreviations

°C	degree Celsius
Cdh	cadherin
CNS	central nervous system
d	dorsal
DIG	digoxigenin
D-ISH	double-label *in situ* hybridization
E	embryonic day
e.g.	for example (lat.: exempli gratia)
Fig	figure
Fluo	fluorescein
for	forward
g	gravity
ISH	*in situ* hybridization
kDa	kilodalton
l	lateral
µg	microgram
µm	micrometer
m	medial
M	molar
mA	milliampere
ml	milliliter
ng	nanogram
nm	nanometer
reln	Reelin
rpm	rotations per minute
rev	reverse
P	postnatal day
Pcdh	protocadherin
pg	picogram
thio	thionin
v	ventral

V	volt
wt	wild type
w/v	weight per volume
v/v	volume per volume

Neuroanatomical abbreviations

I-IV	cortical layers
1-3	amygdaloid layers 1-3
AA	anterior amygdaloid area
AAD	anterior amygdaloid area, dorsal part
AAV	anterior amygdaloid area, ventral part
ACo	anterior cortical amygdaloid nucleus
AD	dentate area
AHip	amygdalohippocampal area
alv	alveus of the hippocampus
APir	amygdalopiriform transition area
AStr	amygdalostriatal transition area
BAOT	bed nucleus of the accessory olfactory tract
BL	basolateral amygdaloid nucleus
BLA	basolateral amygdaloid nucleus, anterior part
BLP	basolateral amygdaloid nucleus, posterior part
BLV	basolateral amygdaloid nucleus, ventral part
BM	basomedial amygdaloid nucleus
BMA	basomedial amygdaloid nucleus, anterior part
BMP	basomedial amygdaloid nucleus, posterior part
BSTIA	bed nucleus of the stria terminalis, intraamygdaloid division
CA1	cornu ammonis, field 1
CA2	cornu ammonis, field 2
CA3	cornu ammonis, field 3
cc	corpus callosum
Ce	central amygdaloid nucleus
CeC	central amygdaloid nucleus, capsular part
CeC/L	central amygdaloid nucleus, capsular/lateral division
CeL	central amygdaloid nucleus, lateral division

CeM	central amygdaloid nucleus, medial division
cg	cingulum
Cg	cingulate cortex
cp	cortical plate
CPu	caudate putamen
CxA	cortex-amygdala transition zone
DEn	dorsal endopiriform nucleus
ec	external capsule
EAM	extended amygdala, medial part
Ent	entorhinal cortex
fi	fimbria of the hippocampus
GD	dentate gyrus
GP	globus pallidus
HF	hippocampal fissure
Hil	hilus
I	intercalated nuclei of the amygdala
IG	indusium griseum
IM	intercalated amygdaloid nucleus, main part
IPAC	interstitial nucleus of the posterior limb of the anterior commissure
iz	intermediate zone
La	lateral amygdaloid nucleus
LaD	lateral amygdaloid nucleus, dorsal part
LaDL	lateral amygdaloid nucleus, dorsolateral part
LaV	lateral amygdaloid nucleus, ventral part
LaVL	lateral amygdaloid nucleus, ventrolateral part
LaVM	lateral amygdaloid nucleus, ventromedial part
LOT	nucleus of the lateral olfactory tract
LV	lateral ventricle
M	motor cortex
MeA	medial amygdaloid nucleus, anterior part
MEnt	medial entorhinal cortex
MeP	medial amygdaloid nucleus, posterior part
MePD	medial amygdaloid nucleus, posterodorsal part
MePV	medial amygdaloid nucleus, posteroventral part

mz	marginal zone
PaS	parasubiculum
Pir	piriform cortex
PLCo	posterolateral cortical amygdaloid nucleus
PMCo	posteromedial cortical amygdaloid nucleus
PRh	perirhinal cortex
PrS	presubiculum
SI	primary somatosensory cortex
sp	subplate
spp	superplate
st	stria terminalis
sub	subiculum
VEn	ventral endopiriform nucleus
vz	ventricular zone
WM	white matter

1. SUMMARY

The brain is a complex organ that develops on the basis of various morphogenetic processes. The capability of cells to bind specifically and strongly to other cells is a key function in the evolution of multicellular organisms. This binding between cells is based on the mechanism of cell-cell adhesion, in which members of the cadherin superfamily are involved. Cadherins are multifunctional adhesion molecules and represent Ca^{2+}-dependent glycoproteins with more than 100 members. They play a critical role during the development of the vertebrate nervous system. By their predominantly homophilic binding, cadherins are involved in many morphogenetic processes during neuronal development, e.g., in cell proliferation, migration, axon guidance, neurite outgrowth, development of neural circuits and synaptogenesis. Previous studies of the Redies group have shown that cadherins are molecular markers for the layers of the cerebral cortex (Krishna-K et al., 2009).

Cell migration is an important mechanism en route to a mature nervous system. Reelin, an extracellular glycoprotein, plays a role in the radial migration of nerve cells. Mutations within the Reelin gene lead to disturbances of neuronal migration, e.g., in the cerebral cortex, the hippocampus and the cerebellum. Therefore, the Reeler mutant mouse is a suitable model to study corticogenesis. In the present thesis, I analyzed the effect of the Reeler mutation on the expression of cadherins in the cerebral cortex and the amygdala, a functional and morphogenetically highly complex area that mediates emotions and behaviour.

By *in situ* hybridization, the expression of 13 cadherins was examined in three neocortical regions (primary somatosensory cortex, motor cortex, cingulate cortex) at three different points of development (E18, P5, adult) and in one allocortical region, the adult hippocampus. The cerebral cortex of wild-type mice shows layer-specific cadherin expression profiles, with each layer expressing more than one cadherin. This result supports the notion that cadherins provide a combinatorial code of potentially adhesive cues for cortical layers and regions.

The expression patterns of cadherins in the Reeler mutant mouse reveal that layering is disturbed in the different regions of cerebral cortex and partly replaced by roundish aggregates (patches) of cells that express the same cadherin. However, the appearance of individual cadherins in the different cortical regions is not changed in the

mutant. These results are surprising because it is generally believed that layering is inverted in the cerebral cortex of the Reeler mutant mouse.

I performed similar investigations in the amygdala. The development and functional connections of this complex telencephalic brain region are not completely understood to date. By analyzing 13 cadherins in the amygdala of wild-type mice, it was possible to define several novel subdivisions within the amygdala that were unknown from previous morphological studies. Because Reelin is also expressed in cortical regions of the amygdala (Remedios et al., 2007), I asked whether the mutation of the Reelin gene has an effect on the morphology of this brain area. My results show strong alterations in morphology of the cortical amygdaloid areas whereas deep pallial areas and subpallial nuclei are not affected by the Reeler mutation.

The disorganization and the structural deficits of the cerebral cortex and the amygdala in the Reeler mutant brain may coincide with changes in the establishment of neural circuits. In this context, I discuss the possible involvement of Reelin in several neurodevelopmental psychotic disorders, e.g. schizophrenia, bipolar disorder and autism.

2. ZUSAMMENFASSUNG

Das Gehirn ist ein komplexes Organ, an dessen Entwicklung verschiedene morphogenetische Prozesse beteiligt sind. Die Fähigkeit einzelner Zellen, spezifisch und stark an andere Zellen zu binden, ist eine Schlüsselfunktion in der Evolution multizellulärer Organismen. Diesen Bindungen zwischen Zellen liegt der Mechanismus der Zell-Zell-Adhäsion zu Grunde, in dem die Molekülfamilie der Cadherine involviert ist. Cadherine sind multifunktionelle Adhäsionsmoleküle und stellen Ca^{2+}-abhängige, transmembrane Glycoproteine mit über 100 Subtypen dar. Sie spielen eine entscheidende Rolle in der Entwicklung des Nervensystems von Vertebraten. Durch ihre überwiegend homophilen Bindungen sind sie an vielen morphogenetischen Prozessen während der neuronalen Entwicklung beteiligt, wie z.B. an Zellproliferation, Migration, Axonlenkung, Neuritenwachstum, Bildung neuronaler Schaltkreise und Synaptogenese. Frühere Studien der Arbeitsgruppe Redies zeigten, dass Cadherine als Schichtenmarker im cerebralen Cortex dienen können (Krishna-K et al., 2009).

Die Zellmigration ist ein wichtiger Entwicklungsmechanismus auf dem Weg zu einem ausgereiften Nervensystem. Reelin, ein extrazelluläres Glykoprotein, ist maßgeblich an der radialen Migration von Nervenzellen beteiligt. Mutationen des Reelin-Gens führen zu Störungen der neuronalen Migration, beispielsweise im cerebralen Cortex, im Hippocampus und im Cerebellum. Die Reeler-Mausmutante dient daher als Modell für das Studium der Corticogenese. In der vorliegenden Arbeit untersuchte ich, in wie weit die Reeler-Mutation Einfluss auf die Expression von Cadherinen im cerebralen Cortex hat. Dieselbe Frage stellte ich für die Amygdala, einem funktionell und morphogenetisch hoch komplexen Kerngebiet, das an der Ausbildung von Emotionen und sozialem Verhalten beteiligt ist.

Die Expressionsanalyse von 13 Cadherinen mit Hilfe der *In-situ*-Hybridisierung wurde in drei neocorticalen Arealen (primärer somatosensorischer Cortex, motorischer Cortex und cingulärer Cortex) zu drei verschiedenen Entwicklungszeitpunkten (E18, P5, adult) sowie in einer allocorticalen Region, dem adulten Hippocampus, untersucht. Der cerebrale Cortex der Wildtypmaus weist ein schichtspezifisches Expressionsmuster der Cadherine auf. Jede corticale Schicht zeigt dabei eine Expression mehrerer Cadherine. Diese überlappende Expression ist mit der Hypothese vereinbar, dass

Cadherine einen kombinatorischen adhäsiven Code für die corticalen Schichten und Areale liefern.

Die Verteilungsmuster der Cadherine in der Reeler-Maus zeigen, dass in den verschiedenen Regionen des cerebralen Cortex die Schichtung aufgehoben ist und teilweise durch rundliche Aggregate von Zellen (Patches), die das gleiche Cadherin exprimieren, ersetzt ist. Das spezifische Vorkommen einzelner Cadherine in den verschiedenen corticalen Regionen ist jedoch nicht verändert. Die Ergebnisse dieser Arbeit sind insofern überraschend, als man bisher davon ausging, dass die Schichtung des cerebralen Cortexes in der Reeler-Mutante invertiert ist.

Ähnliche Untersuchungen führte ich in der Amygdala durch. Die Amygdala ist ein komplexes Kerngebiet des Telencephalons, deren Entwicklung und funktionelle Verbindungen bis heute noch nicht vollständig verstanden sind. Die Analyse von 13 Cadherinen in der Amygdala der Wildtyp-Maus erlaubte es mir, mehrere neue Unterbereiche innerhalb der Amygdala zu definieren, die bislang von morphologischen Studien her nicht bekannt waren. Da Reelin auch in den corticalen Gebieten der Amygdala exprimiert ist (Remedios et al., 2007), untersuchte ich, ob die Mutation des Reelin-Gens in diesem Hirnareal ebenfalls mit einer Störung der Morphologie einhergeht. Meine Ergebnisse zeigen, dass die morphologische Organisation der corticalen amygdaloiden Gebiete in der Reeler-Mutante stark verändert ist, während tiefe palliale Strukturen und subpalliale Kerne nicht betroffen sind.

Die Veränderungen der morphologischen Organisation sowohl des cerebralen Cortex als auch der Amygdala in der Reeler-Mutante führen möglicherweise auch zu Veränderungen in der Ausbildung neuraler Schaltkreise. In diesem Zusammenhang wird die Rolle von Reelin in einigen entwicklungsabhängigen, psychischen Erkrankungen, wie z. B. der Schizophrenie, den bipolaren Störungen und dem Autismus diskutiert.

3. INTRODUCTION

3.1 Basics and principles of brain development

The mammalian brain is perhaps one of the most complex objects in our universe. It is composed of billions of cells and trillions of connections that process information and mediate behavior. These connections develop in several steps, beginning with the decision of few early embryonic cells to become neural progenitors.

The vertebrate nervous system is a derivative of the ectoderm, one of the three germ layers of the gastrula-stage embryo that forms during early cleavage stages. Following gastrulation, the ectoderm gives rise to different tissues, depending on the position along the mediolateral and anteroposterior axes of the embryo. Along the dorsal midline, the ectoderm thickens to form the neural plate. During a complex morphogenetic process called neurulation, the neural plate folds onto itself to form a tube-like structure, the neural tube. The neural tube gives rise to nearly all the neurons and glia of the central nervous system (CNS). Cells at the junction between the tube and the ectoderm form the neural crest. The neural crest is the source of most of the neurons and glia of the peripheral nervous system (Kandel et al., 2000; Squire et al., 2003; Sanes et al., 2006).

In the vertebrate embryo, the caudal part of the neural tube gives rise to the spinal cord, while the rostral end enlarges to form the three primary brain vesicles: the prosencephalon (or forebrain), the mesencephalon (or midbrain) and the rhombencephalon (or hindbrain). The three primary brain vesicles become further subdivided into five vesicles. The prosencephalon gives rise to both the telencephalon (major mature derivatives are: neocortex, basal ganglia, hippocampal formation, amygdala and olfactory bulb) and the diencephalon (gives rise to the thalamus, the hypothalamus, the retina, the optic nerve and the optic tract). The mesencephalon remains a single vesicle and does not expand. The rhombencephalon divides into the metencephalon and the myelencephalon. These two vesicles form the pons/cerebellum and the medulla oblongata, respectively (Kandel et al., 2000; Squire et al., 2003; Sanes et al., 2006).

3.1.1 Corticogenesis

The most elaborate part of the human CNS is the cerebral cortex, part of the telencephalon. Here, afferent (sensory) information is processed and integrated, and

passed on to efferent (motor) systems. Based on differences in its laminar structure, the murine cortex, like that of all mammals, can be subdivided into neocortex and allocortex. The allocortex is the phylogenetically older cortex; it encompasses those regions that show a highly variable laminar structure and comprises both the paleo- and the archicortex (Vogt and Vogt, 1919). The term neocortex (Vogt and Vogt, 1919) comprises the phylogenetically younger cortical regions, which in general show a lamination into six layers (isocortex). These layers are generated in an inside-out fashion, with early-born neurons located in the deep layers and late-born neurons located in the superficial layers (Angevine and Sidman, 1961; Rakic and Caviness, 1995; Takahashi et al., 1999). To generate this inside-out pattern, cortical cells migrate radially by somal translocation followed by tangential locomotion (Rakic, 1972; Nadarajah et al., 2001). The first step of neocortical development is the formation of the preplate above the ventricular zone (the principal germinal center of the brain) around embryonic day 10 in the mouse (E10; Fig. 3.1). The preplate is composed of the earliest generated neurons, including the Cajal-Retzius cells and the subplate neurons (Marin-Padilla, 1998). In the second step (E13-E18), cortical plate neurons are generated in the ventricular zone and these neurons invade the preplate. Migrating neurons move past the subplate, splitting this layer away from the preplate. Therefore, the preplate is split into a superficial marginal zone, in which the Cajal-Retzius cells remain adjacent to the pial surface, and a deep subplate. Later-born neurons are generated in the ventricular zone and migrate radially; they pass through the developing intermediate zone, which consists of pioneer axons, and then move past the subplate and earlier generated neurons of the cortical plate. The systematic migration of later-generated neurons past their predecessors results in the inside-out pattern of cortical layering. In adulthood, a six-layered neocortex is thus formed superficial to the deep white matter comprising the axonal tracts (Fig. 3.1; Angevine and Sidman, 1961; Rakic, 1974; Kubo and Nakajima, 2003).

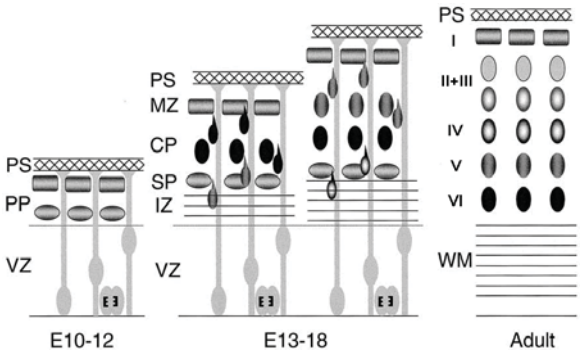

Figure 3.1. Development of the neocortex. I-VI, cortical layers; CP, cortical plate; IZ, intermediate zone; MZ, marginal zone; PP, preplate; PS, pial surface; SP, subplate; VZ, ventricular zone; WM, white matter. Adapted from Kubo and Nakajima, 2003.

3.1.2 The hippocampal region

The hippocampal region is a prominent component of the allocortex. It comprises two structures, the hippocampal formation (Fig. 3.2A) and the parahippocampal region (Fig. 3.2B). The hippocampal formation consists of three cytoarchitectonically distinct regions: the dentate gyrus, the hippocampus proper (also called Ammon´s horn), which is subdivided into three fields (CA1, CA2 and CA3), and the subiculum. All three areas of the hippocampal formation share the characteristic three-layered appearance of allocortex. The parahippocampal region includes the entorhinal cortex, the parasubiculum and the presubiculum. The entorhinal cortex contains six layers that, with the exception of layer I, are substantially different from those found in the neocortex. There are four cellular layers (layers II, III, V and VI) and two acellular or plexiform layers (layers I and IV).

There are three characteristic gradients of formation within the hippocampal region. First, deep cells are generated before superficial cells. Second, cells closer to the rhinal fissure are formed before those lying farther away ("rhinal-to-dentate" gradient). The entorhinal cortex starts to develop first, next is the subiculum, then field CA3 of Ammon's horn, and finally, the dentate gyrus. Two structures are exceptions to this gradient. The para- and presubiculum form significantly later than the subiculum, and CA1 forms significantly later than adjacent CA3 cells; this late neurogenesis may be related to prominent thalamic input to both structures (Angevine, 1965; Bayer, 1980). Third, later forming cells are flanked by superficial and deep cells ("sandwich gradient") that form earlier in the entorhinal cortex (where layer III cells originate after layers II and IV), in the Ammon's horn (where pyramidal cells originate after large cells in the stratum oriens, stratum radiatum, and stratum lacunosum-moleculare), and in the dentate gyrus, where granule cells originate after large cells in the hilus and molecular layer (Bayer, 1980).

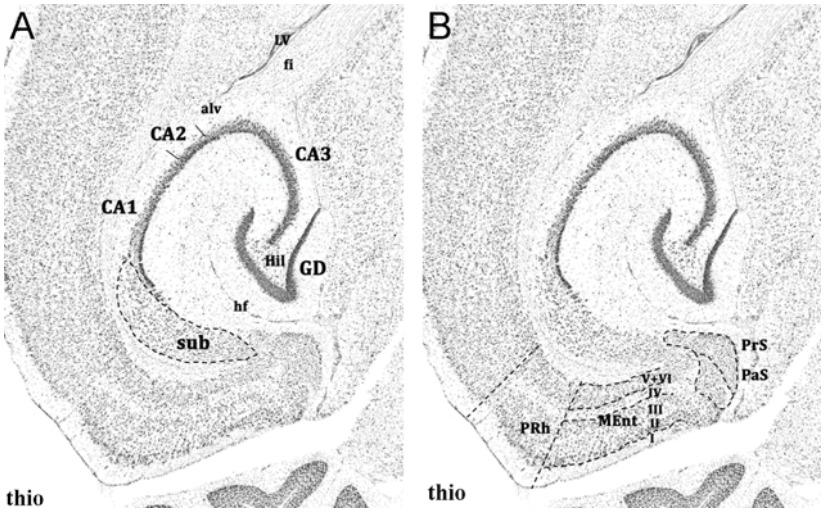

Figure 3.2. A neuroanatomical overview of the adult mouse hippocampal region (Nissl [thionin] stain of a horizontal section). The Ammon´s horn of the hippocampus proper, the dentate gyrus and the subiculum form the hippocampal formation (**A**). The parahippocampal region consists of the entorhinal cortex, the parasubiculum and the presubiculum (**B**). I-VI, cortical layers; alv, alveus of the hippocampus; CA, cornu ammonis (Ammon´s horn); fi, fimbria of the hippocampus; GD, dentate gyrus; hf, hippocampal fissure; Hil, hilus; LV, lateral ventricle; MEnt, medial entorhinal cortex; PaS, parasubiculum; PRh, perirhinal cortex; PrS, presubiculum; sub, subiculum; thio, thionin.

3.1.3 The amygdaloid complex

The amygdala, part of the telencephalon, is a key mediator of emotional and social behavior (Alheid et al., 2000; Davis, 2000; LeDoux, 2000). Furthermore, the amygdala controls instinctive reflexes, like defense, ingestion and reproduction (Davis, 2000; LeDoux, 2000; de Olmos et al., 2004). The amygdala lies in the depth of the anteromedial temporal lobe ventral to the lentiform nucleus. To grasp the complex function of the amygdala, it is important to understand both its morphological divisions and their neural connectivity. The amygdala has a highly intricate organization and development. It consists of several amygdaloid nuclei and cortical areas (see Chapter 5, Results, pages 32 - 79), which are formed as the results of a complex migration of neural precursor cells. Current models of amygdaloid complex development postulate that amygdalar structures originate around the pallial-subpallial boundary (Puelles et al., 2000; Nery et al., 2002). Several components of the amygdala are pallial and subpallial derivatives and belong to distinct functional systems (Puelles et al., 2000; Tole et al., 2005; Remedios et al., 2007; Garcia-Lopez et al., 2008). This complexity is the basis for the elaborate function of the amygdala.

3.1.4 From embryonic divisions to functional modularity

Embryonic modularity and functional modularity are two principles of brain organization. Embryonic modules are histogenetic fields, in which pattern formation takes place during development. Embryonic modules finally give rise to brain nuclei and cortical layers. Defined subsets of these gray matter structures become connected by fiber tracts to form the neural circuits, which represent the information-processing modules of the brain. Many of the genes that are involved in the formation of the embryonic divisions of the brain have been identified. They belong to several families of transcription factors or gene regulatory proteins, that are expressed in restricted neuroepithelial regions (e.g. Hox, Dlx, Pax, Otx, Gbx, Emx, Wnt, Sox, and Nkx genes; Puelles and Rubenstein, 1993; Shimamura et al., 1995; Lumsden et al., 1996; Rubenstein et al., 1998). This initial patterning of the embryonic brain must be translated into expression patterns of genes that are involved in the various processes of brain morphogenesis, circuit formation and synaptogenesis (Redies and Puelles, 2001). Factors, which regulate these processes, include molecules that mediate cell-cell and cell-substrate adhesion (e.g., integrins and members of the Ig superfamily; Stoeckli and Landmesser, 1998; Kaprielian et al., 2000), diffusible molecules that set up molecular gradients for cell and axon migration (e.g., netrins, slit; Brose and Tessir-Lavigne, 2000), and molecules that mediate attraction and repulsion between the neural cells and their processes (e.g., ephrins, Eph receptors, neuropilin; O´Leary and Wilkinson, 1999; Marin et al., 2001). I will focus on a family of cell-cell adhesion molecules, the cadherins, which provide a combinatorial adhesive code for both embryonic divisions and functional neural circuits in the vertebrate brain (Redies, 2000).

3.2 Cadherins – From molecules to neural networks

The ability of cells to form specific and strong connections among each other is one of the key functions during the evolution of multicellular organisms. This ability is based on the mechanism of cell adhesion. Cells aggregate with the help of integral membrane proteins, the cell adhesion molecules (CAMs), and specific cell populations accumulate to form specific types of tissue. Cell adhesion is mediated by two different systems (Takeichi, 1977; Takeichi, 1988): a calcium-dependent cell adhesion system (CADS) with cadherins, selectins and integrins, and a calcium-independent adhesion system (CIDS) that is regulated by members of the immunoglobulin superfamily (Petruzzelli et al., 1999).

Cadherins play a crucial role in cell-cell adhesion during the differentiation and morphogenesis of the developing nervous system and other tissues. Initially, cadherins were named after the tissue, in which they were first identified. It is now clear that most cadherins are expressed widely and not limited to a single tissue or organ. For example, N-cadherin (N-Cdh), which was first discovered in neural tissue, is also found in diverse epithelia and mesenchymal cells; E-cadherin (E-Cdh), which was initially discovered in various epithelia, has also been localized to non-epithelial tissues (Takeichi, 1988; Redies, 2000); and R-cadherin (R-Cdh), which was isolated in the retina, is also expressed strongly in the brain and other organs (Obst-Pernberg et al., 2001). So far, more than 100 members of the cadherin superfamily were confirmed from vertebrates and invertebrate species (e.g., *Drosophila melanogaster* and *Caenorhabditis elegans*). These members were classified into several subfamilies (Fig. 3.3): classic cadherins, desmosomal cadherins, Flamingo cadherins, fat-like cadherins and protocadherins (Hirano et al., 2003; Redies et al., 2005; Halbleib and Nelson, 2006; Takeichi, 2007; Hulpiau and van Roy, 2011).

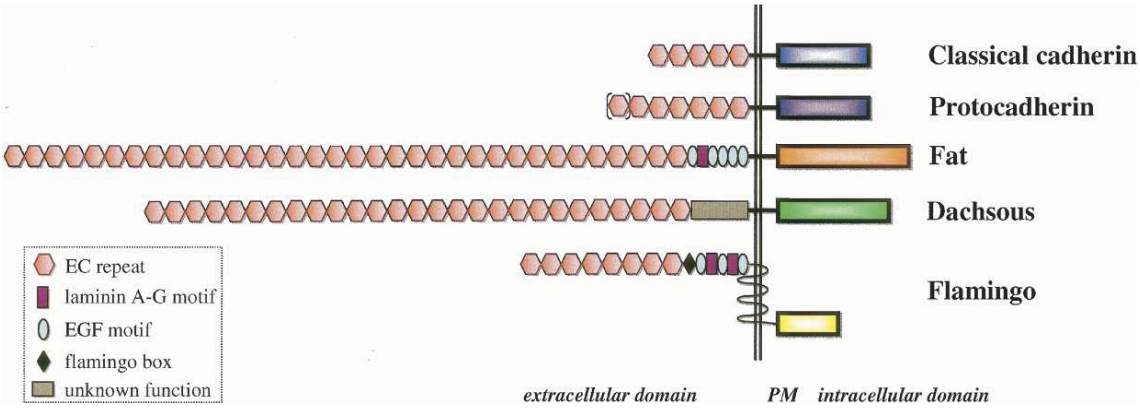

Figure 3.3. Overview of the cadherin superfamily. The domain structure of representative members of the cadherin family of vertebrates is shown. In most cases, the cytoplasmic domains are completely different from each other. This suggests that members of different cadherin subfamilies participate in distinct signalling pathways and protein interactions. Adapted from Halbleib and Nelson, 2006.

Cadherins are cell surface gycoproteins with a transmembrane domain, an extracellular domain and a highly conserved cytoplasmic region. The main characteristics of this protein family are about 110 amino acids-long cadherin repeats in the extracellular domain (Overduin et al., 1995; Shapiro et al., 1995) that comprise Ca^{2+}-binding motifs. The cytoplasmic domain interacts with the actin cytoskeleton. This linkage is regulated by cadherin-binding proteins, e.g. the catenins (Hirano et al. 1992). Cadherins mediate

cell-cell adhesion via homophilic binding, which means that cadherins preferentially bind to the same cadherin subtype (Nose et al., 1988). For example, E-Cdh interacts with E-Cdh, whereas N-Cdh interacts with N-Cdh (Hirano et al., 2003). This binding specificity is thought to provide a molecular basis for the sorting of cells and/or their processes during morphogenesis (Takeichi, 1995; Redies and Takeichi, 1996; Redies, 2000; Hirano et al., 2003).

The present thesis project mainly focuses on classic cadherins (Cdhs) and protocadherins (Pcdhs). Classic cadherins are composed of five conserved extracellular domains, of which the fifth domain shows lower sequence identity between different cadherins than the other domains. On the basis of characteristic amino acid sequences in the cytoplasmic domain, classic cadherins can be further divided into type I and type II classic cadherins. Type I classic cadherins have been named according to the organ or tissue, in which they were first identified (see above). Type II classic cadherins, which differ from type I cadherins in specific amino acids sequences, were numbered according to the order of their discovery (Hirano et al., 2003). So far, type II cadherins include Cdh5 (VE-Cdh), Cdh6, Cdh7, Cdh8, Cdh9, Cdh10, Cdh11, Cdh12, Cdh14/18, Cdh19 and Cdh20; these genes were identified in human, mouse, rat, chicken, or *Xenopus*.

The first members of the protocadherin (Pcdh) family were identified in the early 1990s via PCR with degenerative primers, when scientists were searching for new cadherin-like molecules (Suzuki et al., 1991; Sano et al., 1993). Since then, diverse subgroups of Pcdhs were identified, e.g. the α-, β-, and γ-protocadherin subgroups that are located on three gene clusters on the human chromosome 5q31 ("clustered" Pcdhs). Other subgroups are the Flamingo (CELSR) cadherins and the fat protocadherins (Fig. 3.4; Hulpiau and van Roy, 2009). In a phylogenetic study of all murine and human protocadherin subgroups (Redies et al., 2005; Vanhalst et al., 2005), Frans van Roy, Christoph Redies and their collaborators identified a new subfamily, the δ-protocadherins (Fig. 3.4). This subgroup includes nine members and can be further subdivided into two subgroups (δ1-Pcdhs and δ2-Pcdhs), based on structural differences. The δ1-protocadherins (Pcdh1, Pcdh7, Pcdh9, and Pcdh11) are the only protocadherins with seven extracellular cadherin-domains (Nollet et al., 2000; Hirano et al., 2003; Vanhalst et al., 2005). In addition to the conserved cytoplasmic motifs (CM) 1 and CM2 (Wolverton and Lalande, 2001), the cytoplasmic domain of δ1-protocadherins contains the small and highly conserved CM3 motif (Redies et al., 2005; Vanhalst et al.,

2005) that is necessary for the interaction with protein phosphatase 1α (PP1α; Wolverton and Lalande, 2001).

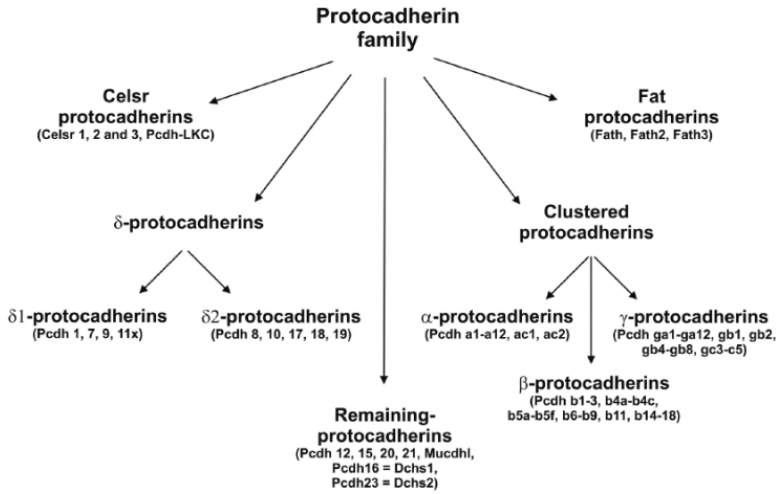

Figure 3.4. Schematic overview of the protocadherin classification. Four subgroups are distinguishable: Flamingo protocadherins, Fat protocadherins, clustered protocadherins, and δ-protocadherins. Representative cadherin members are listed in parentheses (from Redies et al., 2005).

Members of the second subgroup, the δ2-Pcdhs, are Pcdh8, Pcdh10, Pcdh17, Pcdh18 and Pcdh19. The cytoplasmic domain of δ2-Pcdhs consists of CM1 and CM2 motifs that are more highly conserved than in δ1-Pcdhs (Wolverton and Lalande, 2001; Vanhalst et al., 2005; Fig. 3.5). Furthermore, δ2-Pcdhs have six extracellular domains instead of seven.

As adhesion molecules, the principal function of cadherins is to mediate cell-cell adhesion. Moreover, cadherins have been implicated in a number of signalling pathways (Hirano et al., 2003), in cell proliferation, differentiation, and migration (Winklbauer et al., 1992; Goichberg and Geiger, 1998; Nakagawa and Takeichi, 1998), in axonal outgrowth, fasciculation, and pathfinding (Treubert-Zimmermann et al., 2002), as well as in synaptogenesis and synaptic plasticity (Fannon and Colman, 1996; Tanaka et al., 2000; Suzuki et al., 2007; Takeichi, 2007). In the CNS, cadherin-mediated adhesive specificity has been proposed to provide a molecular code for early embryonic regionalization as well as for the development and maintenance of functional structures (Redies, 2000; Redies et al., 2003; Hertel et al., 2008; Krishna et al., 2009). Abnormal alteration of cadherin function results in malformation and tumor genesis (Takeichi,

1995; Peinado et al., 2004). For example, N-Cdh is of critical importance as an adhesive molecule in early development. N-Cdh-deficient mouse embryos die around embryonic day 10.5 with multiple defects, including malformed somites, an undulated neural tube and severe heart defects (Luo et al., 2001).

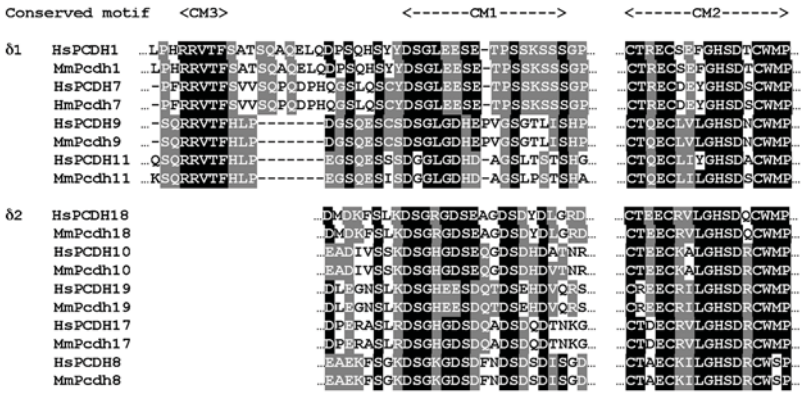

Figure 3.5. Multiple amino acid alignment of selected parts of the cytoplasmic domains of all nine δ-protocadherins. Overall, the CM1 motif is less conserved than the CM2 motif. The highly conserved CM3 domain is absent in δ2-protocadherins. Hs, *Homo sapiens*; Mm, *Mus musculus*. From Vanhalst et al., 2005.

3.3 The Reeler mutant mouse

The molecular signals that regulate the interaction between migrating cells and their environment have been studied during the last decades (for a review, see Marin and Rubenstein, 2003). One pathway regulating radial migration involves the extracellular matrix protein Reelin (Dulabon et al., 2000; Tissir and Goffinet, 2003; Fig. 3.6), a glycoprotein with a relative molecular mass of 400 kD. The Reelin protein comprises 3461 amino acids and possesses a serine protease activity. It contains a signal peptide followed by a F-spondin-like region at the N-terminus, a hinge region upstream of eight Reelin repeats (R), and ends with a highly basic C-terminus of 33 amino acids that is required for secretion. The protein is cleaved at two cleavage sites extracellularly. The first cleavage by a metalloprotease is located at the N-terminal site between R2 and R3, and the second cleavage is located at C-terminus between R6 and R7 (Lambert de Rouvroit et al., 1999; Jossin et al., 2007). This generates three major fragments *in vivo*: an N-terminal fragment (~180 kDa, corresponding to the N-terminal region up to R2), a central fragment (~120 kDa, corresponding to R3 to R6) and a C-terminal fragment (~100kDa, corresponding to R7 and the C-terminus; Lambert de Rouvroit et al., 1999; Jossin et al., 2004, 2007). An epitope known as the CR-50 is localized near the N-

terminus and is composed of 230-346 amino acids. This epitope is essential for Reelin-Reelin electrostatic interactions that result in a soluble string-like homopolymer, composed of up to 40 or more regularly repeated monomers. Mutated Reelin that lacks the CR-50 epitope fails to form homopolymers, and is, thereby, unable to transduce the Reelin signal (Ogawa et al., 1995; Utsunomiya-Tate et al., 2000). Each Reelin repeat is composed of 350-390 amino acids and contains two sub-repeats separated by an epidermal growth factor (EGF)-like motif of 30 amino acids. The presence of amino-acid sequences similar to those conserved in several ECM proteins, such as tenascin, laminin and in cell adhesion molecules, suggests a function of Reelin in neuronal process extension and in determining the destination of migrating neurons (Hirotsune et al., 1995; Frotscher, 1997).

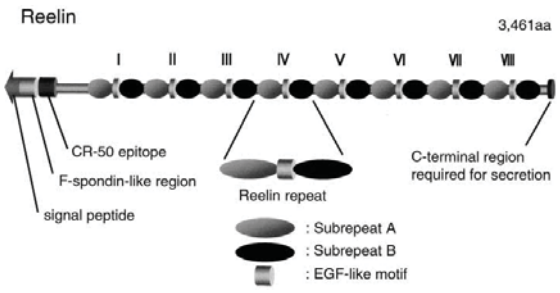

Figure 3.6. A scheme of the Reelin structure. The N-terminus of Reelin has 25% identity with that of F-spondin. Eight Reelin repeats are following. Each Reelin repeat contains two related subrepeats A and B, separated by an EGF-like motif. Adapted from Kubo and Nakajima, 2003.

Receptors for Reelin are apolipoprotein E receptor 2 (ApoER2), very-low-densitiy lipoprotein receptor (VLDLR) and α3β1 integrin protein (D´Arcangelo et al., 1999; Hiesberger et al., 1999; Dulabon et al., 2000). Reelin binding to its receptors causes dimerization/oligomerization of the adapter protein disabled-1 (Dab1; Strasser et al., 2004) and activates members of the Src-tyrosine kinase family/Fyn-kinase leading to phosphorylation of Dab1 (Cooper and Howell, 1999). This initiates a signaling system in the effector cells. Interaction between Dab1 with various kinases (e.g. PI3K, PKB/Akt, GSK3β, Cdk5) leads to important processes including cell migration (Suetsugu et al., 2004), synaptic and dendritic spine plasticity (Rodriguez et al., 2000), neurotransmission (Keshvara et al., 2001; Beffert et al., 2002; Arnaud et al., 2003a,b), cell survival and growth (Beffert et al., 2002, Ohkubo et al., 2007), as well as cognition and memory processing (Fatemi, 2005; Jossin and Goffinet, 2007; Ohkubo et al., 2007).

Mutations in the Reelin gene cause a disruption in neuronal migration, for example in the cerebral cortex, hippocampus and cerebellum (for reviews, see Lambert de Rouvroit and Goffinet, 1998; Rice and Curran, 2001; D´Arcangelo, 2006; Fatemi, 2008). In the neocortex of the Reeler mutant, the initial formation of the preplate proceeds normally. Cortical neurons that are generated in the ventricular zone, however, fail to invade the preplate. Consequently, the subplate remains adjacent to the marginal zone and a "superplate" is formed (Caviness, 1982). As a result, cortical layers are inverted (Caviness and Sidman, 1973; Kubo and Nakajima, 2003; Tissir and Goffinet, 2003; Fig. 3.7). However, Caviness (1982) noted an increased scatter of cells in an overall reversed lamination. Pinto Lord et al. (1979) described a mixed population of projection neurons with aberrant neurite orientations. Some researchers even claimed that cortical layering is disturbed in the Reeler mutant (Hamburgh, 1963; for a review see, Katsuyama and Terashima, 2009) or replaced, at least in part, by a patchy type of gray matter architecture (Ichinohe et al., 2008).

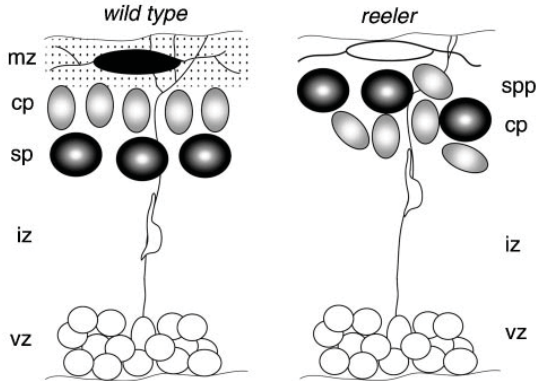

Figure 3.7. A simplified current view of the malformation of the Reeler cortex. In wild-type cortex, the first cohort of cortical plate neurons (gray) positions itself between the Cajal-Retzius cells (black) that produce Reelin (stipples) and the subplate layer. In Reeler mutants, the first cohort of cortical plate neurons fails to migrate past the subplate and instead accumulates in a disorganized fashion in the superplate. cp, cortical plate; iz, intermediate zone; mz, marginal zone; sp, subplate; spp, superplate; vz, ventricular zone. Adapted from Rice and Curran, 2001.

The homozygous Reeler mutant mouse, the model in which the gene for Reelin is mutated (Goffinet, 1979, 1984), exhibits a special phenotype characterized by ataxia. Beside the described defects in the cerebral cortex of the forebrain (see above), the Reeler cerebellum is hypoplastic (Magdaleno et al., 2002) and the Purkinje cell number is reduced (Hadj-Sahraoui et al., 1996). Additionally, neuronal microtubule function is dysregulated (Hiesberger et al., 1999).

Different models of Reelin action have been proposed to explain the Reeler phenotype by direct effects on migrating neuroblasts and their final positioning. For example, Reelin may act as a stop signal (Curran and D´Arcangelo, 1998; Dulabon et al., 2000, Chai et al., 2009), a chemoattractant (Gilmore and Herrup, 2000), or a detachment signal for migrating neurons (Hack et al., 2002; Sanada et al., 2004), or it may influence neuronal migration by altering adhesive properties (Hoffarth et al., 1995). One current model suggests that Reelin could either increase or arrest motility, depending on the concentration of Reelin (D´Arcangelo, 2006; Jossin et al., 2007). At low levels, in the developing cortical plate, it promotes the extension of a leading edge and the radial migration of neurons. At high levels, on the pial surface, Reelin prompts cells to stop migration, detach from radial fibers and associate into layers. How a deficit in any of these mechanisms can cause a loss of layer formation in the Reeler mutant remains obscure at present.

3.4 Aims of the study

Cadherin expression by functional brain divisions persists in the adult brain and, therefore, cadherins can be used as markers for the functional organization of the mature brain (Hertel et al., 2008; Krishna-K. et al., 2009; Kim et al., 2010). In cerebral cortex, some cadherins have already been used as markers for cortical regions in genetically altered mice (Cdh6, Cdh8, Cdh11, Miyashita-Lin et al., 1999; Nakagawa et al., 1999; Rubenstein et al., 1999; Bishop et al., 2000). Here, I use cadherin markers to investigate the functional differentiation in the Reeler mutant mouse in two telencephalic regions, the cerebral cortex and the amygdaloid complex.

To determine in detail how the layer-specific expression of cadherins is perturbed in different regions of the Reeler cortex, I studied the effect of the Reeler mutation in three neocortical regions (cingulate cortex, motor cortex and primary somatosensory cortex) and the allocortical hippocampal region by comparing the expression of thirteen different classic cadherins and δ-protocadherins in the Reeler mutant mouse and wild-type littermates, both in the mature cerebral cortex and during corticogenesis (at embryonic day 18 [E18] and at postnatal day 5 [P5]). My results show that the cortical layer-specific expression of cadherins is almost completely abolished and replaced by a patchy type of gray matter organization in the Reeler mutant mouse.

In addition, in the postnatal (P5) and adult amygdaloid complex in the Reeler mutant mouse, the combinatorial study of multiple (proto-)cadherins allows the

distinction of molecular subdivisions within the amygdala that go beyond the previously known morphological divisions. Reelin is expressed in cortical areas of the amygdala, but not in deep nuclei (Remedios et al., 2007). My results provide evidence that the cortical pallial parts of the amygdaloid complex are disorganized in the Reeler mutant but the deep pallial and subpallial nuclei seem to be largely unaffected.

4. MATERIALS AND METHODS

A complete list of the materials used is attached to Appendix (pages xi to xxii).

4.1 Animals

The mice used in this study were homozygous Reeler mice (reln) and their wild-type (wt) littermates from the B6C3Fe a/a-Reln strain (Jackson Laboratories, Bar Harbor, ME, USA; stock number: 000235). The animals were obtained from a colony maintained at the animal facilities of the University Hospital Jena. Heterozygous mice were intercrossed to obtain wild-type mice. Efforts were made to minimize animal suffering and to use only the number of animals necessary to produce reliable scientific data.

4.2 Dissection of embryonic, postnatal and adult mouse brains

All experimental procedures were in accordance with current versions of institutional regulations and national laws on the use of animals in research.

Embryonic stages: Pregnant adult mice were deeply anesthetized with chloroform and quickly decapitated with a large scissor. With the aid of forceps and scissors, the abdominal cavity was opened and the uterus was dissected. Immediately, the uterus was stored on ice. In a Petri dish under a stereo microscope, each embryo was removed from its amniotic cavity and separated from its placenta. Embryos were quickly decapitated and the brains were removed. Brains were fixed in 4% formaldehyde in HBSS solution overnight on ice on a rocking platform. Fixed brains were incubated for three hours in 12% w/v sucrose solution followed by three hours in 15% w/v sucrose solution and overnight in 18% w/v sucrose solution. Afterwards, specimens were embedded in Tissue Tec O.C.T. compound, frozen in liquid nitrogen, and stored at -80°C.

Postnatal stages: Postnatal mice (P5 to P7; P0 was defined as day of birth) were deep anesthetized on ice and quickly decapitated. The following dissection was carried out on ice. In a Petri dish under a stereo microscope, the skin and remaining muscles of the neck were removed with forceps and scissors. The skull was opened by a midsagittal cut and removed via forceps. Thereby, the dorsal aspect of the brain was visible. A spatula was positioned ventral to the bulbs and the brain was carefully turned caudally. Thus the brain was removed from the head. Dissected brains were fixed in 4%

formaldehyde in HBSS solution overnight on ice on a rocking platform. Fixed brains were incubated for several hours (see above) each in a graded series of sucrose solutions (12%, 15%, and 18% w/v). Afterwards, specimens were embedded in Tissue Tec O.C.T. compound, frozen in liquid nitrogen, and stored at -80°C.

Adult stage: Adult mice were deeply anesthetized with chloroform and quickly decapitated. The same dissection procedure was used as at *postnatal stages* (see above). Dissected brains from adult mice were immediatly frozen by immersion in 2-methyl butane chilled with dry ice to about -40°C and stored at -80°C until sectioning.

4.3. Preparation of cryostat sections

Specimens of freshly frozen brains were removed from the -80°C freezer and equilibrated in the cooling chamber of the cryostat for at least 30 minutes. For sectioning, frozen brains were mounted onto the cutting stage of a refrigerated microtome by Tissue Tec O.C.T. compound. Series of coronal and horizontal sections (20 µm slice thickness) of the whole forebrain were cut at a specimen temperature of -12°C and a knife temperature of -13°C. For each brain, alternating series of sections were necessary. Sections were thawed directly onto SuperFrost plus glass slides. After cutting, slices were allowed to dry for at least 1 hour at 37°C on a prewarmed slide stretching table. Slides were stored at -80°C.

4.4 Molecular biological techniques

4.4.1 Genotype identification of the Reeler mutant mice

4.4.1.1 Isolation of total DNA

A piece of tail (0.5cm to 1.0cm in length) was cut from each individual mouse. Each piece was placed individually into a 1.5ml microcentrifuge tube followed by the addition of 180µl lysis buffer ATL (DNeasy Blood and Tissue Kit, Qiagen GmbH, Germany). 10µl proteinase K (DNeasy Blood and Tissue Kit) was added to the lysis buffer. Each mixture was vortexed and incubated in a rocking thermomixer at 56°C overnight. On the next day, the mixture was vortexed for 15 seconds to disperse the sample until the tissue was completely lysed. After vortexing, 200µl of buffer AL (DNeasy Blood and Tissue Kit) was added to the sample, vortexed thoroughly and then 200µl of 100% ethanol were added to the mixture. The complex was mixed vigorously by vortexing. A white DNA precipitate may form on addition of ethanol. It was essential to apply all of the precipitate to the DNeasy Mini Spin Columns (DNeasy

Blood and Tissue Kit). The complete mixture was pipetted into a DNeasy Mini Spin Column placed in a 2ml collection tube (DNeasy Blood and Tissue Kit) and centrifuged at 6000 x g for 1 minute. The flow-through and the collection tubes were discarded. The spin column was placed in a new 2ml collection tube. 500µl wash buffer AW1 (DNeasy Blood and Tissue Kit) were added to each sample, followed by a centrifugation step for 1 minute at 6000 x g to remove remaining contaminants. The flow-through and the collection tubes were discarded. Each spin column was placed in a new 2ml collection tube and mixed with 500µl AW2 wash buffer (DNeasy Blood and Tissue Kit). The samples were centrifuged for 3 minutes at 13,800rpm. The flow-through and the collection tubes were discarded. After the spin, the DNeasy columns were transferred into a new 1.5ml collection tube. 200µl of elution buffer AE (DNeasy Blood and Tissue Kit) was directly pipetted onto the membrane. To allow the DNA to be adsorbed to the membrane, spin columns were incubated for 1 minute at room temperature. Then the DNA was eluted by centrifuging the spin columns for 1 minute at 8,000rpm. The spin column was discarded and the tube was put on ice for the following quantification.

4.4.1.2 Quantification of total DNA

DNA yield was determined by measuring the concentration of DNA in the eluate by its absobance at 260nm (A_{260}) and 280nm (A_{280}) in a spectrophotometer. An absorbance of 1 unit at 260nm corresponds to 50µg of DNA per ml. The ratio between the values taken at 260nm and 280nm (A260/A280) provides an estimate of the purity of DNA with respect to contaminats that absorb UV. Pure DNA has an A_{260}/A_{280} ratio of 1.8 - 2.0.

The DNA quantification was carried out as followed: At first, 75µl of AE buffer (DNeasy Blood and Tissue Kit) were used to calibrate the photometer before measuring each sample. Second, 5µl of each DNA sample solution were diluted in 70µl buffer AE (1/15 dilution). Third, each diluted sample was transferred into a 100µl cuvette. Finally, each DNA sample was measured.

4.4.1.3 Touch-down real-time PCR analysis

Three primers were used for PCR and amplification of probes. Primer 1 (rev-wt), a wild type-specific upstream primer, binds to a sequence of 79 base pairs downstream of the breakpoint. This sequence is absent in the Reeler genome. Primer 2 (rev-Reeler), a

second upstream primer, binds to a sequence which is located 176 base pairs downstream of the breakpoint. This sequence is presumbly located much farther away in the wildtype genome. Primer 3 (for-wt), the downstream primer, binds to a sequence 187 base pairs upstream of the breakpoint. Thus, PCR amplification of the wildtype Reelin gene results in a 266 base pair PCR fragment, whereas amplification of the mutant Reelin gene results in a 363 base pair fragment. In heterozygous mice, both PCR fragments are amplified.

Sequence of primers:

for-wt: 5´- AGA GCC TAG AGG TTA GGG ACA CAA CTC TTC -3´

rev-wt: 5´- CTG CTA CAC AGT TGA CAT ACC TTA ATC TAC -3´

rev-Reeler: 5`- TAA GGG AGT CCT GGT CTC TTT CTG TCT TTA -3´

Per tube:

Reagent	Final concentration
REDTaq® ReadyMix™ PCR Reaction Mix	0.5x v/v
Primer 1 (rev-wt)	0.4pg/µl
Primer 2 (rev-Reeler)	0.4pg/µl
Primer 3 (for-wt)	0.6pg/µl
Template DNA	10ng/µl

The amplifications were performed in a Biometra Cycler with the following cycling scheme:

2 minutes at 95°C (initial denaturation)

45 seconds at 94°C (denaturation)
45 seconds at 64°C → 53°C (touch-down, annealing)
45 seconds at 72°C (extension)
10 minutes at 72°C (final extension)
} 33 cycles

store at 4°C until further use

4.4.1.4 Electrophoresis analysis of PCR-amplified DNA fragments

20µl of each PCR sample together with 3µl Mid Range DNA Ladder as DNA size marker were loaded on a 2% agarose gel containing 0.005% ethidium bromide. Electrophoresis was performed in an electrophoresis chamber containing 1 x TAE running buffer at 100V for 45 minutes. Then the gel was transferred to an ultraviolet

light station and photographed with a digital camera. An example of a genotype result is shown in Figure 4.1.

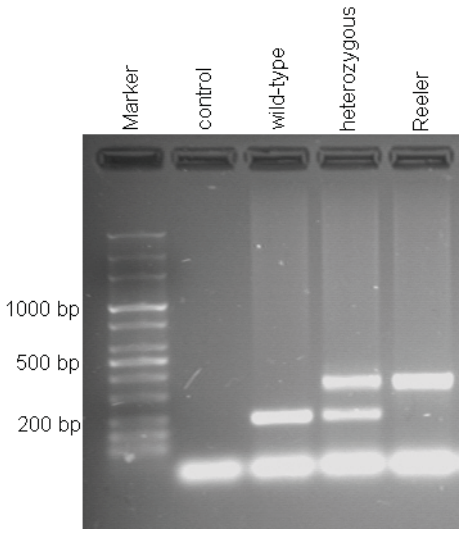

Figure 4.1. Example of genotype identification of the B6C3Fea/a-Reln strain using PCR. The wild-type sample shows a 266 base pair band. The heterozygous sample consists of a 266 base pair fragment and a 366 base pair fragment. The Reeler sample results in a 366 base pair band. The control sample is a negative control that contains all PCR reagents except of DNA.

4.4.2 cRNA Probe Synthesis

4.4.2.1 Transformation of competent *E. coli* cells

Transformation is the process, by which plasmid DNA is introduced into a bacterial host cell. A 25µl aliquot of frozen competent *E.coli* Top 10F´ cells (Topo TA Cloning Kit, Invitrogen GmbH, Germany) was thawed on ice. 1µl plasmid DNA was transferred to the cell suspension, carefully mixed and kept on ice for 30 minutes. The microcentrifuge tube containing the sample was transferred to a 42°C heating block for 30 seconds (heat shock), followed by immediate storing on ice. 250µl SOC medium was added to the cells and incubated for 60 minutes at 37°C on a rocking heating block. The cells were plated out in 50µl, 80µl and 140µl aliquots on LB-agar plates containing 50µg/µl ampicillin antibiotic. The selective plates were incubated overnight at 37°C until bacterial colonies developed.

4.4.2.2 Preparation of starter cultures and glycerol stocks

A starter culture was prepared by inoculating a single colony from the freshly grown selective plates into 5ml LB medium containing 50µg/µl ampicillin. The starter cultures were grown overnight at 37°C with vigorous shaking (~300 rpm). 130µl sterilized glycerol (100% solution) was added to a 2ml screw-cap vial and 870µl of the starter

culture were added. The vials were mixed, carefully frozen in liquid nitrogen and stored at -80°C. The rest of the starter culture was harvested by centrifugation at 6,000 x g for 15 minutes at 4°C. The supernatant was removed. The bacterial cells were now ready for the lysis procedure to purify plasmid DNA.

4.4.2.3 Plasmid DNA purification

The bacterial cell pellets were resuspended in 250µl buffer P1 (QIAprep Spin Miniprep Kit, Qiagen GmbH, Germany). 250µl buffer P2 (lysis buffer; QIAprep Spin Miniprep Kit) was added and the sample was mixed thoroughly by inverting the tube for several times. For precipitation, 350µl buffer N3 (neutralization buffer; QIAprep Spin Miniprep Kit) was added and immediately mixed to avoid localized precipitation. The sample was centrifuged for 10 minutes at 13,000 rpm resulting in a white pellet. The supernatant was pipetted onto a spin column (QIAprep Spin Miniprep Kit) and centrifuged for 1 minute at full speed. The flow-through was discarded and the column was washed by adding 750µl buffer PE (QIAprep Spin Miniprep Kit). After an additional centrifugation for 1 minute, the flow-through was discarded. A second centrifugation for 1 minute was necessary to remove residual wash buffer. For eluation, the spin column was placed in a new 1.5ml microcentrifuge tube, 50µl buffer EB (QIAprep Spin Miniprep Kit) were added, incubated for 1 minute and the tube was centrifuged for 1 minute. The eluate contained the purified plasmid DNA.

4.4.2.4 DNA quantification by spectrophotometry

Plasmid DNA concentration was determined by measuring the absorbance at 260nm and 280nm in a spectrophotometer using a cuvette (see 4.4.1.2). The purified plasmid DNA samples were diluted 1:75 in EB buffer (QIAprep Spin Miniprep Kit).

4.4.2.5 Linearization of purified plasmid DNA

For RNA probe synthesis, the circled plasmid DNA has to be linearized using restriction endonucleases. Supercoiled plasmid DNA generally requires more than 1unit/µg to be digested completely. The digestions were carried out in a volume of 50µl. The reaction components (5µg purified DNA, 1x buffer, 1x BSA, appropriate restriction enzyme, pure water) were pipetted into a tube and mixed thoroughly. For digestion, the samples were incubated for 2 hours at 37°C in a heating block.

4.4.2.6 Alcohol precipitation and purification of linearized DNA

Precipitation is commonly used for concentrating, desalting and recovering nucleic acids. Precipitation is mediated by high concentrations of salt and the addition of ethanol. To each 50µl linearization sample, 100µl TE-buffer, 15µl 3M sodium acetate and 375µl ice-cold ethanol (100%) were added. Precipitation took place overnight at -80°C. The sample was centrifuged at 16,000 x g at 4°C for 20 minutes. The supernatant was discarded. The pellet was washed with 500µl ice-cold 70% ethanol and centrifuged at 4°C for 20 minutes at 16,000 x g. The supernatant was discarded and the pellet was allowed to dry. Dry pellet was eluted in 25µl TE buffer.

4.4.2.7 Quantification and electrophoresis analysis of DNA

Measuring of DNA concentration by spectrophotometry was carried out after the protocol given in 4.4.1.2. DNA was diluted 1:75 in TE buffer. 2µl of 6x DNA loading dye were added to 1µl DNA and 7µl pure water and mixed by pipetting. The DNA samples and 2µl of DNA size marker (MassRuler^{TM} DNA ladder; Fermentas) were loaded on a 1% agarose gel containing 0.005% ethidium bromide, and electrophoresed with 1x TAE running buffer at 80V for 45 minutes. Then, the gel was illuminated by ultraviolet light and DNA bands were photographed with a digital camera.

4.4.2.8 Synthesis of sense and antisense cRNA probes

Labeled antisense and sense cRNA probes were synthesized *in vitro* by using the plasmids listed in Table 1. Nonradioactive cRNA probes were produced for every cadherin and protocadherin with the digoxigenin (DIG) RNA Labeling Kit or the Fluorescein (Fluo) RNA Labeling Kit (Roche Diagnostics, Mannheim, Germany) according to the manufacturer's instructions. The linearized plasmids were transcribed with T7 or SP6 RNA polymerase (New England Biolabs, Ipswich, MA) or T3 RNA polymerase (Roche Diagnostics), followed by labeling with digoxigenin or fluorescein, to generate sense and antisense probes.

For the standard labeling assay the following reagents were added to a microcentrifuge tube on ice, mixed gently and centrifuged briefly:

Reagent	Volume
Linearized plasmid DNA	1µg/µl
10x Transcription buffer	2µl

10x BSA	2µl
RNA Inhibitor	0.5µl
10x Labeling mix (DIG or Fluo)	2µl
RNA Polymerase (SP6, T7 or T3)	2µl
Pure water	ad 20µl total volume

The samples were incubated for 2 hours at 37°C (T7, T3) or 40°C (SP6). After incubation, 1µl DNase was added to digest the template DNA. The samples were incubated for 15 minutes at 37°C. The reaction was stopped by adding 0.5µl of 0.5M EDTA. The probes were stored on ice.

Table 4.1. Plasmids used to obtain cRNA probes

Gene	Name of Plasmid	Position of Sequence	Gene Bank Accession Number	Reference
Cdh4	pBSMR4	55-2794	D14888	Matsunami et al., 1993
Cdh6	pBSII1.0B-mCdh6	202-1229	D82029	Inoue et al., 1997
Cdh7	TOPOII-mCdh7	182-1998	AK137369	Katayama et al., 2005
Cdh8	mcad8-12	504-1583	X95600	Korematsu and Redies, 1997a
Cdh11	BSSK11	452-2840	D31963	Kimura et al., 1995
Cux-2	pBC SK Cux2 5´	737-1895	U45665	Zimmer et al., 2004 Quaggin et al., 1996
ER81	BSK-mouse er81	668-3168	NM018781	Arber et al., 2000
Pcdh1	pGEMte-mPcdh1	1195-2781	NM029357	Vanhalst et al., 2005
Pcdh7	pGEMte-mPcdh7	1947-3575	NM018764	Vanhalst et al., 2005
Pcdh8	TOPOII-mPcdh8	201-1901	NM001042726	Vanhalst et al., 2005
Pcdh9	pGEMte-mPcdh9	961-2258	NM001081377	Vanhalst et al., 2005
Pcdh10	mOLe11	full lenght	U88549	Hirano et al., 1999
Pcdh11	pGEMte-mPcdh11	1581-2867	NM001081385	Vanhalst et al., 2005
Pcdh17	TOPOII-mPcdh17	985-3015	NM001013753	Visel et al., 2007
Pcdh19	TOPOII-mPcdh19	1827-4722	NM001105245	Gaitan and Bouchard, 2006

Tbr-1	Tbr-1 (IS6A)	689-949	NM009322	Bulfone et al., 1995

4.4.2.9 Purification of sense and antisense cRNA probes

Probes were purified by using Quick Spin Columns (Roche Diagnostics). A column was removed from the storage container and gently inverted for several times to resuspend the medium. The top cap of the column was removed followed by removal of the bottom tip. The buffer was allowed to drain by gravity and discarded. The column was placed in a microcentrifuge tube and centrifuged at 1,100 x g for 2 minutes. The eluted buffer and the tube were discarded. The column was kept in an upright position in a second tube and the RNA sample was applied to the center of the column bed. After centrifugation for 4 minutes at 1,100 x g at 4°C, the tube contained the purified RNA probe. The column was discarded.

4.4.2.10 Quantification and electrophoretic analysis of RNA probes

The concentration of RNA probes was quantified by spectrophotometry. RNA was eluted 1:75 in DEPC-treated water. Correct probe size and the overall quality of the RNA preparation were verified by formaldehyde agarose gel electrophoresis. At first, the gel was prepared by dissolving 0.6g agarose in 45ml DEPC-treated water. 5ml 10x MOPS running buffer, 0.9ml 37% formaldehyd and 0.005% ethidium bromide were added. The gel was poured and assembled in a tank. 1x MOPS running buffer was added to cover the gel. The gel was equilibrated for 30 minutes. In the meantime, the RNA probe samples were prepared. 2µl RNA probe, 2µl formaldehyd loading dye and 6µl DEPC-treated water were denatured by heating for 5 minutes at 65°C. Subsequently, the gel was loaded with the samples and 3µl RNA size marker (High Range RNA Ladder; Fermentas). Electrophoresis was carried out at 100V for 45 minutes. Then, the gel was transferred to an ultraviolet light station and RNA bands were photographed with a digital camera.

4.4.2.11 Northern blot analysis

Northern blot analysis was used as the standard method for detection and quantification of cRNA probes. After separation of the RNA samples by size via denaturing agarose gel electrophoresis (see 4.4.2.10), the labeled RNA probes were transferred to a nylon membrane, cross-linked and visualized.

The gel was washed three times for 10 minutes in DEPC-treated water to remove the formaldehyde. Then, the gel was equilibrated in 2x SSC buffer for 20 minutes. Filter paper and a nylon membrane were cut to roughly fit the dimensions of the gel and wet with 20x SSC buffer. On the top of 10 stacks of filter paper, the membrane was positioned within a blotting machine. A glass pipet was used to remove any air bubbles between the membrane and the filter paper. The gel was placed on the membrane and again any bubbles between gel and membrane were removed. Another wet filter paper stack was placed on top of the gel and bubbles were removed. The stack was covered with the gel casting tray and the transfer was carried out by applying 200mA for 60 minutes. For cross-linking, the membrane was exposed to UV light for 1 minute. Subsequently, the membrane was washed for 2 minutes in washing buffer, equilibrated in 1x blocking buffer for 30 minutes and then incubated with anti-digoxigenin or anti-fluorescein antibody solution (1:5,000) for 30 minutes. The membrane was washed twice in washing buffer for 15 minutes and then RNA probes were visualized by incubation with a solution containing 0.03% nitroblue tetrazolium salt (Fermentas, St. Leon-Rot, Germany) and 0.02% 5-bromo-4-chloro-3-indolyl phosphate, p-toluidine salt (Fermentas) as substrates. The developing process was stopped by washing the membrane with pure water. The membrane was dried and shrink-wrapped.

4.5 *In situ* hybridization procedures

4.5.1 In situ hybridization

The *in situ* hybridization technique is a method to detect specific nucleic acids at their origin (*in situ*), i.e. in morphologically preserved chromosomes, cells or tissues.

To prevent binding of probe to the coverslips, the coverslips were siliconized. Coverslips were incubated in a 0.2M HCl solution for 20 minutes followed by rinsing in 100% ethanol. The coverslips were air-dried and then baked for 6 hours at 180°C to destroy RNase. The chilled coverslips were dipped in a silicon solution (SERVA) and again baked for 2 hours at 120°C.

For wild-type and mutant mice, series of consecutive sections were hybridized in situ with antisense or sense RNA probes for Cdh4, Cdh6, Cdh7, Cdh8, Cdh11, Pcdh1, Pcdh7, Pcdh8, Pcdh9, Pcdh10, Pcdh11, Pcdh17, Pcdh19, ER81, Tbr-1, or Cux-2 (see Table 1).

Sections were removed from the -80°C freezer and dried on a 37°C heating plate for 1 hour. Then, sections were fixed in 4% formaldehyde/PBS for 30 minutes at 4°C,

washed twice for 5 minutes in 1x PBS and pretreated with 1µg/ml proteinase K (Sigma-Aldrich, Steinheim, Germany) for 5 minutes at room temperature to permeabilize the tissue. After an additional washing step in 1x PBS for 5 minutes, the sections were fixed again in 4% formaldehyde in 1x PBS for 30 minutes at 4°C. Then slices were rinsed in DEPC-treated water and pretreated in 0.25% acetic anhydride/PBS at room temperature for 20 minutes. This acetylation step neutralizes the positive ions and thus avoids unspecific binding of the probes. Sections were washed twice in 1x PBS for 5 minutes and hybridized overnight at 70°C (Tbr-1 probes at 63°C) with 0.5-1µg/ml cRNA probe in hybridization solution. For hybridization, sections were covered with siliconized coverslips and stored in a humid chamber in a prewarmed water bath. After posthybridization washings (5x SSC for 10 minutes to remove the coverslips, 5x SSC for 30 minutes at 60°C, and 50% formamide/2x SSC at 60°C for 60 minutes), unbound cRNA was removed by incubation of the sections with 20µg/ml RNase A in 1x NTE buffer for 30 minutes at 37°C. Sections were then washed again in 50% formamide/2x SSC solution at 60°C for 40 minutes, followed by washing in 2x SSC for 30 minutes at 60°C and 0.1x SSC buffer for 30 minutes at room temperature. After washing the sections twice in 1x PBS and pretreating with blocking solution for 30 minutes, slices were incubated with alkaline phosphatase-coupled anti-digoxigenin Fab fragments (Roche Applied Science) diluted in blocking solution at 4°C overnight. For visualization of the labeled mRNA, sections were washed three times in 1x TBS buffer for 20 minutes, pretreated in Buffer 3 for 10 minutes and incubated with a solution containing 0.03% nitroblue tetrazolium salt (Fermentas, St. Leon-Rot, Germany) and 0.02% 5-bromo-4-chloro-3-indolyl phosphate, p-toluidine salt (Fermentas) as substrates. After enough colored precipitate had formed, the reaction was stopped with water and slices were washed in Buffer 4 for 5 minutes. For dehydration and differentiation, sections were passed in an ascending ethanol series (70% ethanol for 10 minutes, 96% ethanol for 2 minutes, and 100% ethanol for 1 minute), cleared in xylenes, and mounted in Entellan (Merck, Darmstadt, Germany).

4.5.2 Double-labeling in situ hybridization

For double-labeling *in situ* hybridization, the above protocol (4.5.1) was modified in the pre- and posthybridization steps.

After fixation in 4% formaldehyde/PBS for 10 minutes at 4°C, sections were washed twice in 1x PBT for 5 minutes and pretreated with 1µg/ml proteinase K for 5

minutes at room temperature. Then sections were washed twice in 1x PBT for 5 minutes and post-fixed in 4% formaldehyde/PBS for 5 minutes at 4°C. After an additional washing step for 5 minutes in 1x PBT, sections were incubated in 0.25% acetic anhydride in 0.1M triethanolamine at room temperature for 10 minutes. Sections were washed twice in 1x PBT for 5 minutes, rinsed in DEPC-treated water and air-dried for 30 minutes. Slices were hybridized with a mixture of both digoxigenin- and fluorescein-labeled cRNA probes at a concentration of about 1µg/ml each overnight at 70°C in hybridization solution and covered by siliconized coverslips in a humid chamber. Sections were then washed with 5x SSC to remove the coverslips and incubated in 50% formamide/1x SSC at 60°C for 30 minutes. To remove unbound cRNA, 20µg/ml RNase A in 1x NTE buffer was used for 30 minutes at 37°C. Slices were then washed in 2x SSC and twice in 0.2x SSC each for 20 minutes at 60°C. After washing in 1x maleic acid buffer supplemented by 0.1% Tween-20 (MABT) for 5 minutes at room temperature, sections were blocked with 5% heat-inactivated sheep serum (Sigma-Aldrich) and 2% blocking reagent (Roche Applied Science) in 1x MABT buffer for 1 hour at room temperature. Sections were incubated for 4 hours with alkaline phosphatase-coupled anti-digoxigenin Fab fragments (Roche Applied Science) at room temperature, to detect digoxigenin-labeled mRNA, followed by three washing steps in 1x MABT for 5 minutes each. Sections were washed in Buffer 3 for 10 minutes and incubated with a solution containing 0.03% nitroblue tetrazolium salt (Fermentas) and 0.03% 5-bromo-4-chloro-3-indolyl phosphate, p-toluidine salt (Fermentas) as substrates. Subsequently, sections were washed twice in 1x PBS for 5 minutes and fixed in 4% formaldehyde/PBS. After washing in 1x MABT for 5 minutes, slices were blocked again in 5% heat-inactivated sheep serum and 2% blocking reagent in 1x MABT and incubated overnight with alkaline phosphatase-coupled anti-fluorescein Fab fragments (Roche Applied Science) at 4°C. To visualize the fluorescein-labeled mRNA, sections were incubated with a solution containing 0.1mg/ml Fast Red chromogen (Roche Applied Science), 0.025mg/ml naphthol substrate (Roche Applied Science) and 0.02mg/ml levamisole (Roche Applied Science). After developing, slices were rinsed in 1x NTM, washed twice in 1x PBS and stained with 1µl/ml Hoechst 34580 (nuclear dye) in 1x TBS for visualization of nuclei for 5 minutes at 4°C. Then slices were rinsed in water and mounted in Mowiol.

4.6 Immunohistochemistry

4.6.1 Diaminobenzidine immunohistochemistry

Sections were postfixed in an ice-cold solution of 4% formaldehyde/HBSS for 20 minutes and then washed in 1x TBS. To block endogenous peroxidase activity, sections were treated with 0.3% H_2O_2 in methanol for 30 minutes. After three additional washing steps for 5 minutes in 1x TBS, non-specific binding of antibodies was blocked by incubating the sections with 5% skim milk in 1x TBS ("blocking solution") for 30 minutes. Rat monoclonal antibody against anti-neural cell adhesion molecule L1 was appropriately diluted (1:1000) in blocking solution. The primary antibody was applied overnight at 4°C, followed by three washings in 1x TBS and incubation of the sections with biotinylated goat anti-rat secondary antibody, dissolved in blocking solution (1:300) for 30 minutes at room temperature. Sections were washed three times in 1x TBS for 5 minutes and incubated with the avidin-biotin horseradish peroxidase complex (Vectastain Elite ABC Kit), dissolved in blocking solution for 30 minutes at room temperature. To visualize antibodies, sections were washed in 1x TBS for 5 minutes and treated with a solution of 0.03% 3,3-diaminobenzidine tetrahydrochloride, 0.04% nickel chloride, and 0.01% hydrogen peroxide in 1x TBS as substrate. After enough color precipitate had formed, the sections were dehydrated in an ascending ethanol series (10 minutes in 70% ethanol, 2 minutes in 96% ethanol, 1 minute in 100% ethanol), cleared in xylenes, and mounted in Entellan (Merck, Darmstadt, Germany).

4.6.2 Nissl staining

To allocate the staining patterns of the *in situ* hybridization and the immunohistochemistry results to neuroanatomical structures, one adjacent slice of each series of sections was stained with thionin. This staining is specific for DNA and ribosomal RNA (Nissl substance) and therefore visualizes neuronal perikarya.

Slices were removed from the -80°C freezer and dried at 50°C for 1 hour. Sections were fixed for 10 minutes in 4% formaldehyde in 1x HBS at 4°C. After 10 minutes washing in H_2O and 10 minutes degreasing in 70% ethanol, sections were equilibrated twice in H_2O for 5 minutes. Then sections were incubated in 0.1% thionin solution for a minimum of 10 seconds or a maximum of 1 minute under microscopic control. After rinsing in H_2O to remove excessive thionin, slices were dehydrated and differentiated in an ascending ethanol series (5 minutes in 50% ethanol, 10 minutes in

70% in ethanol, 10 minutes in 95% ethanol, 10 minutes in 100% ethanol, 5 minutes in isopropanol), cleared in xylenes and mounted in Entellan.

4.7 Photomicrograph production

Digital photomicrographs of the sections were taken either with a light transmission microscope (BX40, Olympus, Hamburg, Germany) and a digital camera (DP70, Olympus) or under a confocal laser scanning microscope (SP5, Leica Microsystems, Wetzlar, Germany). Images were adjusted in contrast and brightness for optimal display of the staining patterns by using the Photoshop software (Adobe Systems, Mountain View, CA). To produce the merged images, the staining patterns were pseudo-color coded. The NBT/BCIP *in situ* hybridization signal was digitized and converted to green color by a computer.

For the identification of the different areas of the brain, atlases of the adult mouse and rat brain were consulted (Paxinos and Franklin, 2001; Paxinos and Watson, 1998). The nomenclature and the abbreviations were used according to the atlas by Paxinos and Watson (1998).

5. RESULTS

The Results chapter is divided in two parts. First, the expression patterns of cadherins are described for the cerebral cortex of wild-type and Reeler mutant mice. The focus is on the primary somatosensory, motor and cingulate cortex. This part has already been published (Hertel and Redies, 2011). Here, additionally, a comparison of the neocortical findings with expression patterns of the cadherins in the hippocampal region, a phylogenetic old cortical area, is carried out. Some representative examples of cadherin stainings for this area in wild-type and Reeler mutants are shown. Second, cadherin expression within the amygdala in wild-type and Reeler mice is described. The heterogeneity and the complexity of the amygdala can, at least in part, be explained by its multiple developmental origins in the ventrolateral pallium and the subpallium (Puelles et al., 2000; Puelles and Rubenstein, 2003; Medina et al., 2004). The combinatory expression mapping of the members of the cadherin superfamily allows the distinction of multiple molecular subdivisions. The results from this mapping study may provide a basis for understanding the functional organization of the amydgala. They also serve to identify altered brain histogenesis in the Reeler mutant mice.

5.1 Cerebral cortex

An overview of the expression patterns of 13 cadherins in the primary somatosensory cortex (S1) of the adult mouse is provided in Figure 5.1. As previously shown for the ferret visual cortex (Krishna-K. et al., 2009), each layer of the cerebral cortex in the adult mouse is characterized by the expression of a subset of cadherins. Vice versa, expression of each cadherin is more or less restricted to specific cortical layers. Cdh11 (Fig. 5.1F) and Pcdh10 (Fig. 5.1K) exhibit a ubiquitous expression pattern in all layers. Pcdh19 and Pcdh11 are expressed in layers II, V and VI (Fig. 5.1L, N). Cdh7 is expressed in a subpopulation of scattered cells in all layers (Fig. 5.1D), whereas Cdh4 (Fig. 5.1B) and Pcdh8 message (Fig. 5.1I) is found in most cells of layer II but only in subpopulations of cells in the other layers. A characteristic feature of SI in rodents is the barrel field in layer IV, which shows strong signal for several cadherins (Gil et al., 2002). For example, Figure 5.1F, G shows that the barrel septa are marked by the expression of Cdh11 and Pcdh1. Therefore, cadherins can be used as markers for the different layers and regions of the cerebral cortex (see also Krishna-K et al., 2009) and

are helpful for studying corticogenesis. In the Reeler mutant, a model for cortical development, the extent to which cortical layering is altered, remains unclear.

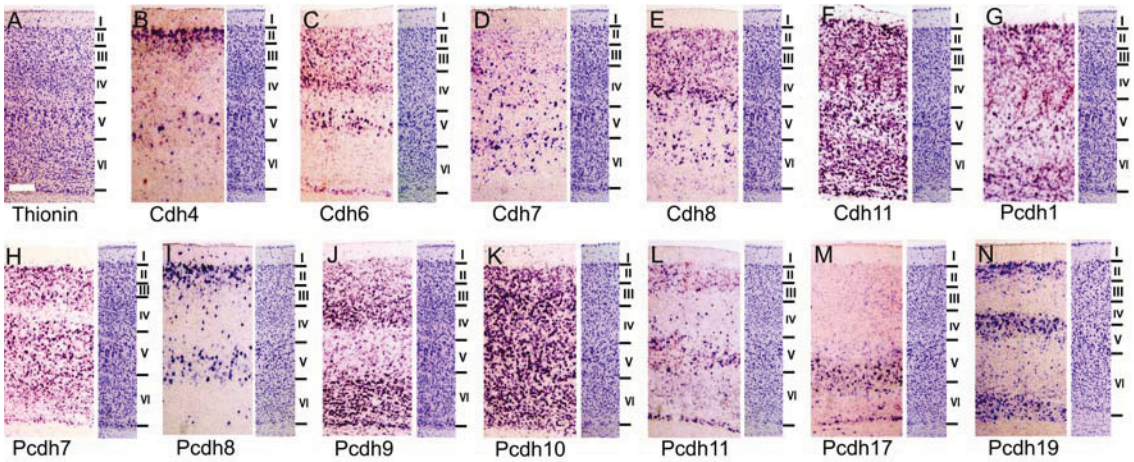

Figure 5.1. Expression mapping of multiple cadherins in the adult mouse primary somatosensory cortex. Cadherin-specific cRNA probes were used by *in situ* hybridization. The cadherin probes are indicated at the bottom of each panel. To facilitate neuroanatomical orientation, cortical layers are indicated for a thionin stain of an adjacent section to the right of each panel. A thionin stain of an adjacent section is shown also in panel A. Scale bar in A = 100µm (applies to A-N).

In general, this layer-specific expression pattern is largely abrogated in the cerebral cortex of the Reeler mutant mouse; instead, cells that express a given cadherin are rather ubiquitously distributed across the radial dimension. In the following sections, I will describe the expression patterns of the classic cadherins and the δ-protocadherins in detail for three neocortical areas (primary somatosensory, motor and cingulate) in wild-type mice and compare them to Reeler mutant mice.

To confirm that the Reeler mutant mice studied here display a cerebral cortical phenotype that is comparable to that of earlier studies, the expression of three well-established layer-specific markers was mapped (Figs. 5.2, 5.3). The expression patterns obtained are identical to results published previously for ER81 (compare to Suppl. Fig. S1A in Hack et al., 2007; Fig. 2 in Dekimoto et al., 2010), Tbr-1 (compare to Fig. 6 in Hevner et al., 2003; Fig. 2 in Dekimoto et al., 2010) and Cux-2 (compare to Suppl. Fig. S1B in Hack et al., 2007; Fig. 5B, D in Ferrere et al., 2006).

Results of the cadherin expression patterns for the mature brain are depicted in Figures 5.4 and 5.5 and are summarized in a schematic diagram in Figure 5.6. Figures 5.7-5.10 show results for postnatal day 5 (P5) and Figure 5.11 for embryonic day 18

(E18). In the figures, cadherin signals are shown side-by-side for wild-type mice (wt) and Reeler mice (reln).

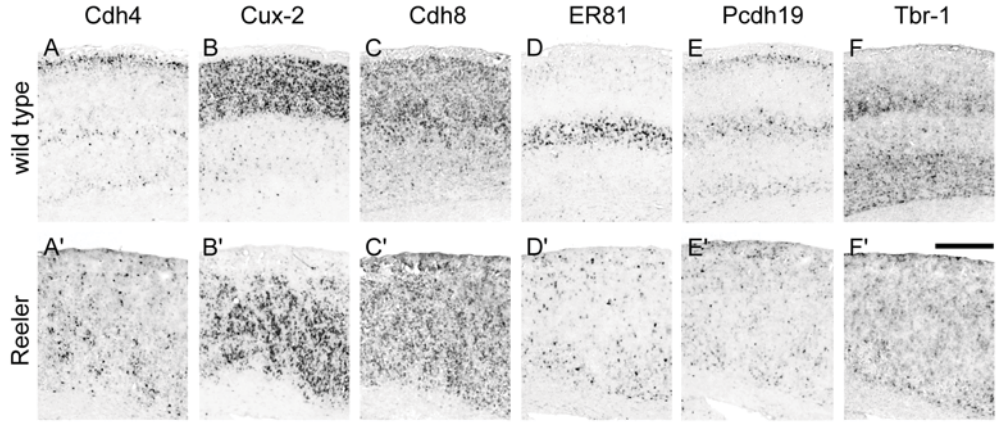

Figure 5.2. Expression mapping of cadherins and well-established layer markers in mature primary somatosensory cortex of wild-type (**A-F**) and Reeler (**A'-F'**) mice in a series of adjacent frontal sections. Results of *in situ* hybridization were obtained with mRNA probes for Cdh4 (**A, A'**), Cux-2 (**B**, **B'**), Cdh8 (**C**, **C'**), ER81 (**D**, **D'**), Pcdh19 (**E**, **E'**) and Tbr-1 (**F**, **F'**). Scale bar in F' = 500µm (applies to A-F').

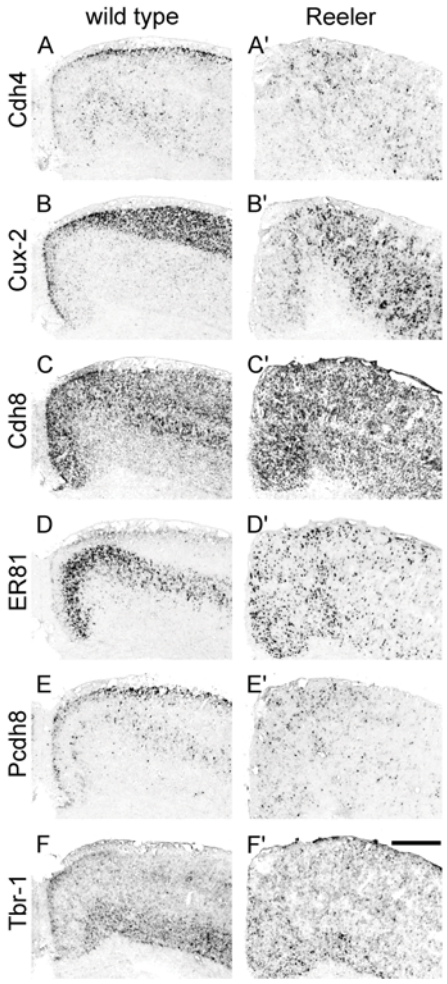

Figure 5.3. Expression mapping of cadherins and well-established layer markers in mature cingulate cortex and motor cortex of wild-type (**A-F**) and Reeler (**A'-F'**) mice in a series of adjacent frontal sections. Results of *in situ* hybridization were obtained with mRNA probes for Cdh4 (**A**, **A'**), Cux-2 (**B, B'**), Cdh8 (**C**, **C'**), ER81 (**D**, **D'**), Pcdh8 (**E**, **E'**) and Tbr-1 (**F**, **F'**). Scale bar in F' = 500µm (applies to A-F').

5.1.1 Layer-specific expression in wild-type primary somatosensory cortex contrasts with scattered expression in Reeler cortex of adult mice

The primary somatosensory cortex (SI) consists of the six layers typical of neocortex. In wild-type littermates, each layer of the adult cortex displays cadherin expression, except for layer I, which lacks neuronal perikarya in the mature brain. Most cadherins are expressed in layers II and III, for example Cdh6 (Fig. 5.4C), Cdh8 (Fig. 5.4E), and Pcdh8 (Fig. 5.4F). Although the border between layers II and III is poorly demarcated in Nissl stains (Fig. 5.4A), layer II can be discerned by its more prominent expression of Cdh4 and Pcdh19 (Fig. 5.4B, I). The barrel field in layer IV is positive for Cdh8 (arrowheads in Fig. 5.4E) in the adult SI and for Pcdh9 (arrowheads in Fig. 5.7G) in the P5 SI. The signal is more prominent in the septa than in the barrels for these cadherins.

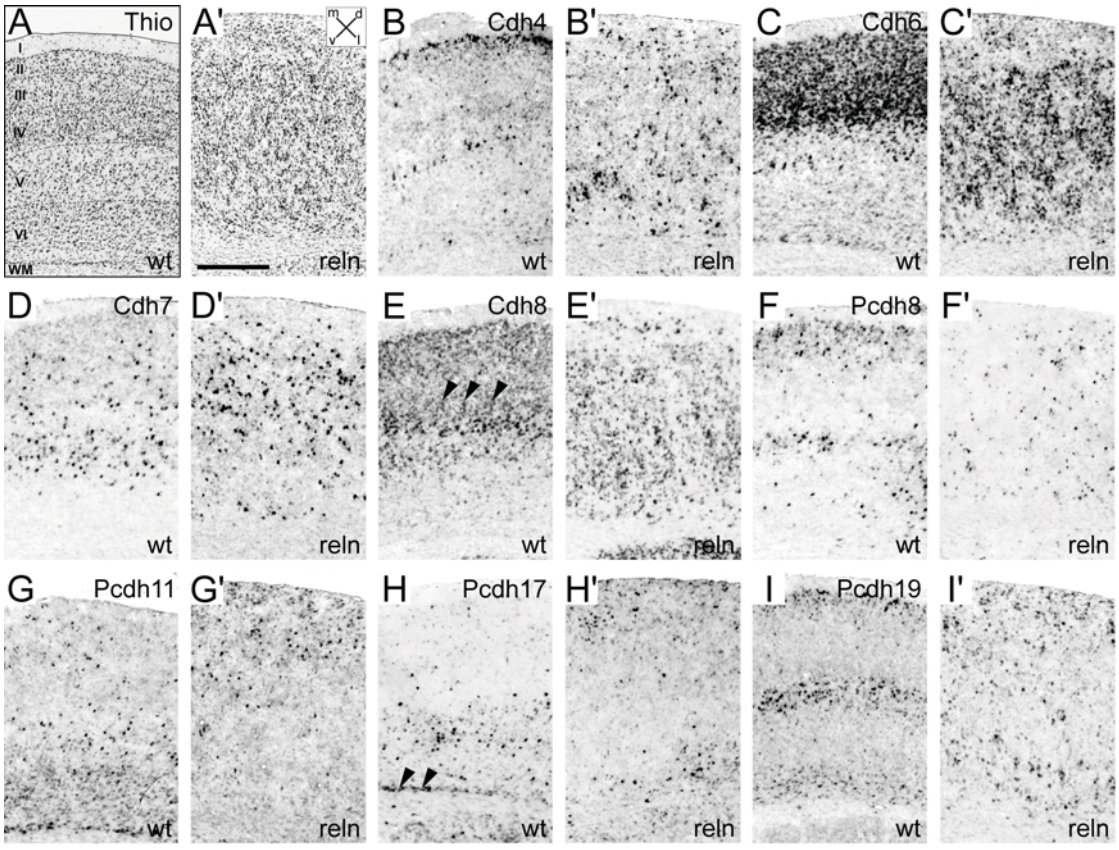

Figure 5.4. Expression mapping of cadherins in the adult primary somatosensory cortex of wild-type mice (wt; **A-I**) and of homozygous Reeler mice (reln; **A'-I'**) in series of adjacent sections. Results were obtained with mRNA probes for Cdh4 (**B** and **B'**), Cdh6 (**C** and **C'**), Cdh7 (**D** and **D'**), Cdh8 (**E** and **E'**), Pcdh8 (**F** and **F'**), Pcdh11 (**G** and **G'**), Pcdh17 (**H** and **H'**) and Pcdh19 (**I** and **I'**). To facilitate the identification of cortical layers, a thionin (Nissl) stain of an adjacent section is shown for wild-type (**A**) and homozygous Reeler mice (**A'**), including a

schematic diagram of the layers of wild-type primary somatosensory cortex in **A**. The arrowheads in E point to the Cdh8-positive septa between the barrels in layer IV. Arrowheads in H point to Pcdh17-positive perikarya adjacent to the white matter. Scale bar in A' = 500µm (applies to A-I').

The deep part of layer IV is positive for Pcdh19 (Fig. 5.4I). Most of the investigated δ-protocadherins are expressed in layer V, except for Pcdh19. Pcdh8 (Fig. 5.4F) is only expressed in neurons of the superficial part. Few perikarya of the deeper part of layer V are positive for Pcdh11 (Fig. 5.4G) and Pcdh17 (Fig. 5.4H). Cdh7 (Fig. 5.4D) is the only classic cadherin that is expressed in layer V. Cadherin expression in layer VI is similar to that in layer V. All the δ-protocadherins are expressed in this layer. Neurons in the deep part of layer VI express Pcdh19 (Fig. 5.4I). Perikarya directly adjacent to the white matter (WM in Fig. 5.4A) show moderate signal for Cdh6 (Fig. 5.4C) and strong signal for Pcdh11 (Fig. 5.4G) and Pcdh17 (arrowheads in Fig. 5.4H).

In homozygous adult Reeler mice, cadherin-expressing cells do not form layers in SI (Fig. 5.4A'-I'). For example, Cdh4 (Fig. 5.4B'), Cdh7 (Fig. 5.4D'), Pcdh8 (Fig. 5.4F') and Pcdh19 (Fig. 5.4I'), which are restricted to particular layers in the wild-type mice, are scattered between white matter and the pial surface. Only Pcdh11 shows a preferential distribution of positive cells in the upper cortical layers (Fig. 5.4G'). Most cadherins are not expressed in perikarya directly beneath the pial surface, except for Cdh6, Pcdh11, Pcdh17 and Pcdh19 (Fig. 5.4C', G', H', I'), which are expressed in deep layer VI in wild-type mice (see above).

5.1.2 Expression in motor and cingulate cortex of the mature brain

The motor cortex and the cingulate cortex also show a layer-specific expression profile in wild-type mice (Fig. 5.5B-K). In both cortical areas, the expression profiles roughly resemble those observed in SI. For example, Pcdh8 (Fig. 5.5G) and Pcdh19 (Fig. 5.5K) are markers for layer II neurons. Neurons in layers IV and V are positive for Cdh8 (Fig. 5.5F). Subsets of perikarya in layer V show signal for Cdh6 (Fig. 5.5D), Cdh7 (Fig. 5.5E) and Pcdh8 (Fig. 5.5G), respectively. The deep parts of layers IV and VI show signal for Pcdh19 (Fig. 5.5K). Mainly in the deep part of layer V, Pcdh17 expression is detectable in both areas (Fig. 5.5J). Cdh4 (Fig. 5.5C) is expressed in layer VI.

A closer inspection reveals differences in the expression profiles between motor and cingulate cortex. For example, Cdh4 and Cdh8 display a mediolateral gradient of

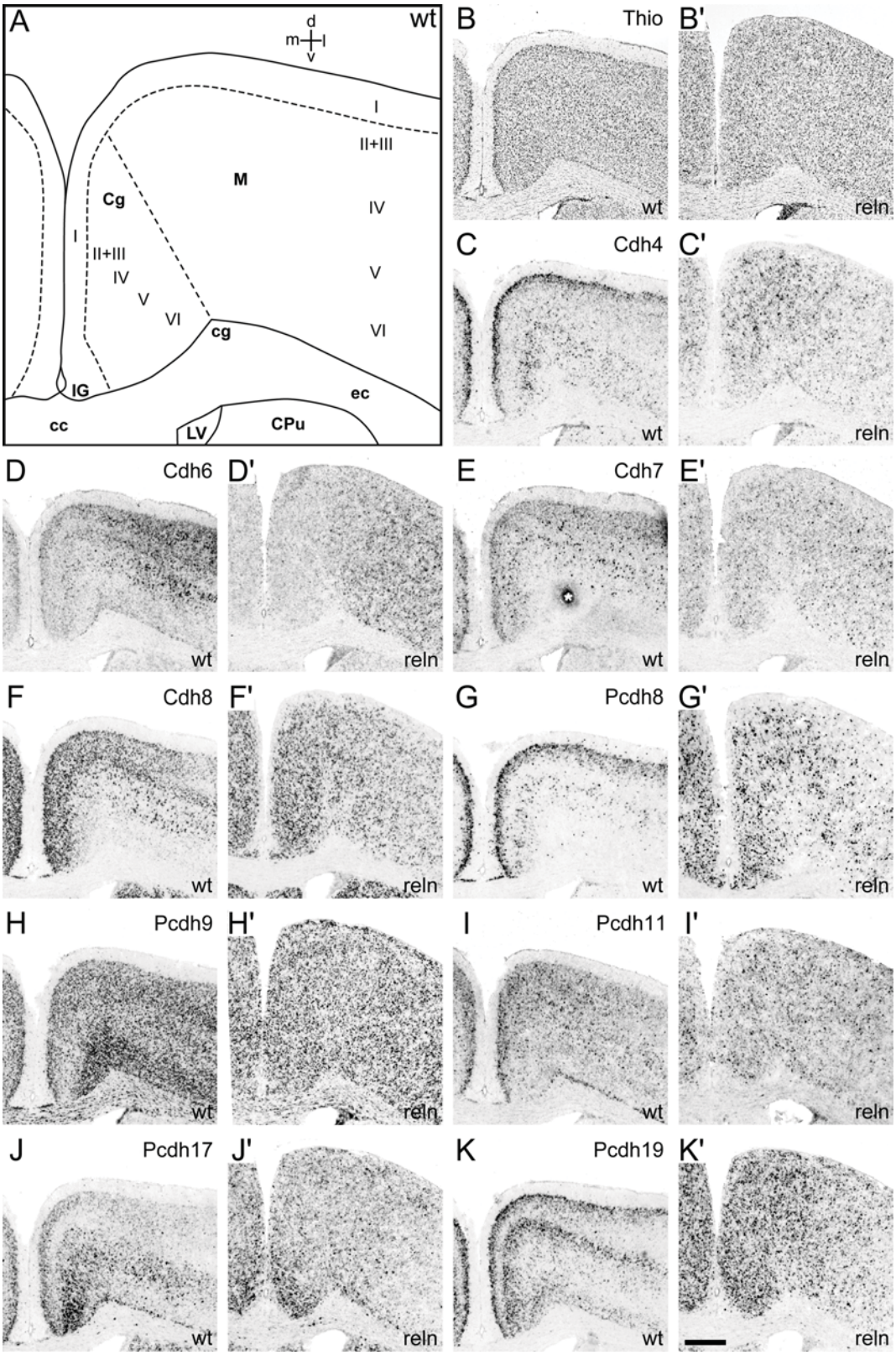

Figure 5.5. Adjacent frontal sections through adult cingulate and motor cortex are shown for wild-type (wt; **C**-**K**) and Reeler (reln; **C'**-**K'**) mice. Results are shown for in situ hybridization with mRNA probes for Cdh4 (**C** and **C'**), Cdh6 (**D** and **D'**), Cdh7 (**E** and **E'**), Cdh8 (**F** and **F'**), Pcdh8 (**G** and **G'**), Pcdh9 (**H** and **H'**), Pcdh11 (**I** and **I'**), Pcdh17 (**J** and **J'**) and Pcdh19 (**K** and

K'). A schematic overview of the anatomical structures present at this section level is given for wild-type in **A**. To identify the different anatomical parts and the cortical layers, a thionin stain of an adjacent section is shown for wild-type and for Reeler mice in **B** and **B'** respectively. The asterisk in E indicates an artefact. Scale bar in K' = 500µm (applies to B-K').

expression in layer V and layers II-IV, respectively (Fig. 5.5C, F). Cdh6 signal is weak in layer II perikarya of cingulate cortex but stronger in both layers II and III in the motor cortex (Fig. 5.5D). Pcdh17 shows signal in layer II and III of cingulate cortex but not of motor cortex (Fig. 5.5J). For Pcdh19, there is a mediolateral expression gradient in layers II, IV and VI (Fig. 5.5K).

Like in SI, cadherin-expressing cells are distributed across the entire radial dimension in motor and cingulate cortex of adult Reeler mice. Expression gradients that are similar to the ones described above for wild-type mice are also observed in the mutants (Fig. 5.5C', D', F', J', K').

The schematic summary diagram (Fig. 5.6) of the various cadherin expression patterns in wild-type and Reeler adult dorsolateral cortex confirms that the layer-specific cadherin expression profiles observed in wild-type cortex are replaced by cadherin expression that is scattered across the radial dimension in the Reeler cortex.

5.1.3 Expression patterns in the developing cerebral cortex

To study whether the radial dispersion of cadherin-expressing cells in Reeler mice occurs after cortical layers have formed or during corticogenesis, the cortical expression of the same cadherins was next analyzed at a postnatal stage (P5; Figs. 5.7-5.10), when cortical layer formation has just been completed in wild-type mice, and at an embryonic stage (E18; Fig. 5.11), when layer formation is still incomplete.

Postnatal day 5. Figures 5.7 and 5.8 show cadherin expression in SI, cingulate cortex and motor cortex of wild-type and Reeler mice. In general, the layer-specific expression profiles of all cadherins are conserved between P5 and the adult stage in all three cortical areas, with the exception of Pcdh8 (Fig. 5.7F) and Pcdh19 (Figs. 5.7I; 5.8H). Pcdh8 expression in the P5 wild-type somatosensory cortex is denser in layers II/III (Fig. 5.7F) compared to the scattered expression pattern in adult (Figs. 5.4F, 5.6C). In the mutant SI cortex, Pcdh8-positive perikarya are more numerous at P5 (Fig. 5.7F') than in the adult (Figs. 5.4F', 5.6C). Finally, layer IV in motor cortex shows strong expression for Pcdh19 at P5 (Fig. 5.8H). A distribution of these Pcdh19-positive

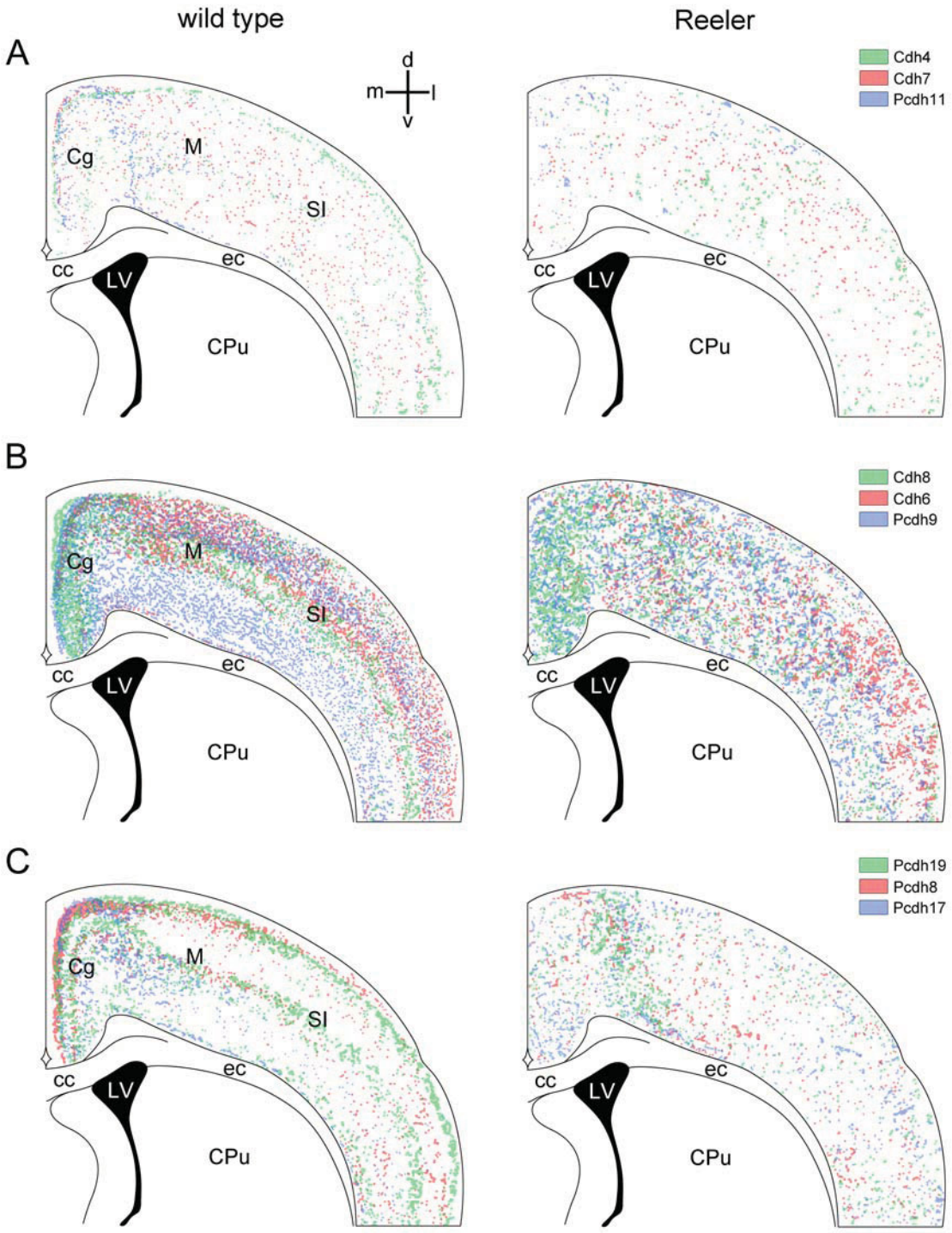

Figure 5.6. Summary diagram for the cadherin expression patterns of the mature cortex in wild-type and Reeler mutant mice. Each scheme shows the expression patterns for three cadherins in different colors. **A.** Cdh4, Cdh7 and Pcdh11. **B.** Cdh8, Cdh6 and Pcdh9. **C.** Pcdh19, Pcdh8 and Pcdh17. For color-coding, see right edge of each scheme. Every colored dot stands for a stained perikaryon.

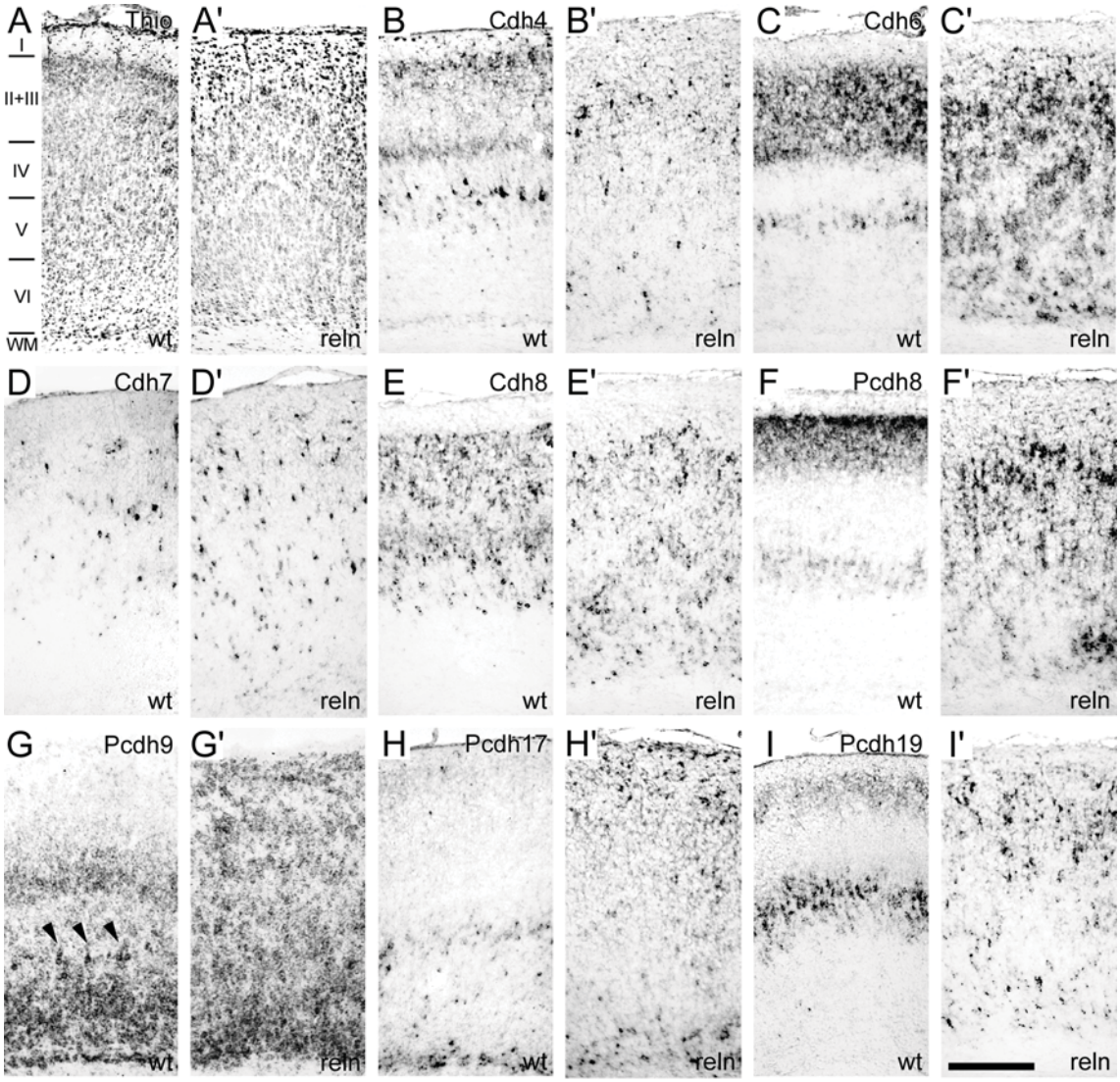

Figure 5.7. Expression mapping of cadherins in the primary somatosensory cortex of wild-type mice (wt; **A-I**) and of homozygous Reeler mice (reln; **A'-I'**) in series of adjacent sections at P5. Results were obtained with mRNA probes for Cdh4 (**B** and **B'**), Cdh6 (**C** and **C'**), Cdh7 (**D** and **D'**), Cdh8 (**E** and **E'**), Pcdh8 (**F** and **F'**), Pcdh9 (**G** and **G'**), Pcdh17 (**H** and **H'**) and Pcdh19 (**I** and **I'**). To facilitate the identification of cortical layers, a thionin (Nissl) stain of an adjacent section is shown for wild-type (**A**) and homozygous Reeler mice (**A'**). In G, the arrowheads indicate the septa between the barrels. Scale bar in I' = 250µm (applies to A-I').

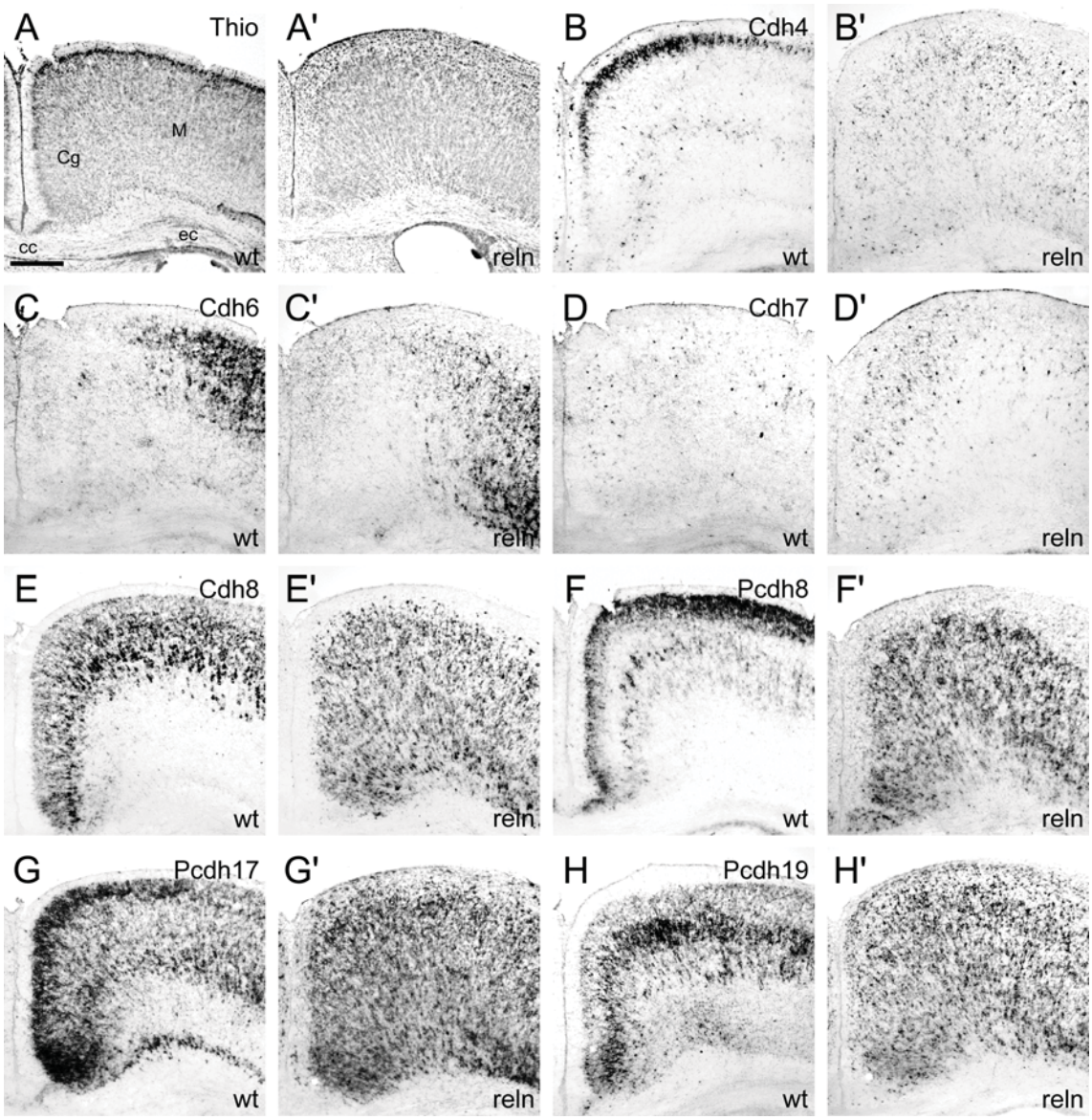

Figure 5.8. Expression mapping of cadherins in the cingulated and motor cortex of wild-type mice (wt; **B-H**) and of homozygous Reeler mice (reln; **B'-H'**) in series of adjacent sections at P5. Results were obtained with mRNA probes for Cdh4 (**B** and **B'**), Cdh6 (**C** and **C'**), Cdh7 (**D** and **D'**), Cdh8 (**E** and **E'**), Pcdh8 (**F** and **F'**), Pcdh17 (**G** and **G'**) and Pcdh19 (**H** and **H'**). To facilitate the identification of cortical layers, a thionin (Nissl) stain of an adjacent section is shown for wild-type (**A**) and homozygous Reeler mice (**A'**). Scale bar in A = 250µm (applies to A-H').

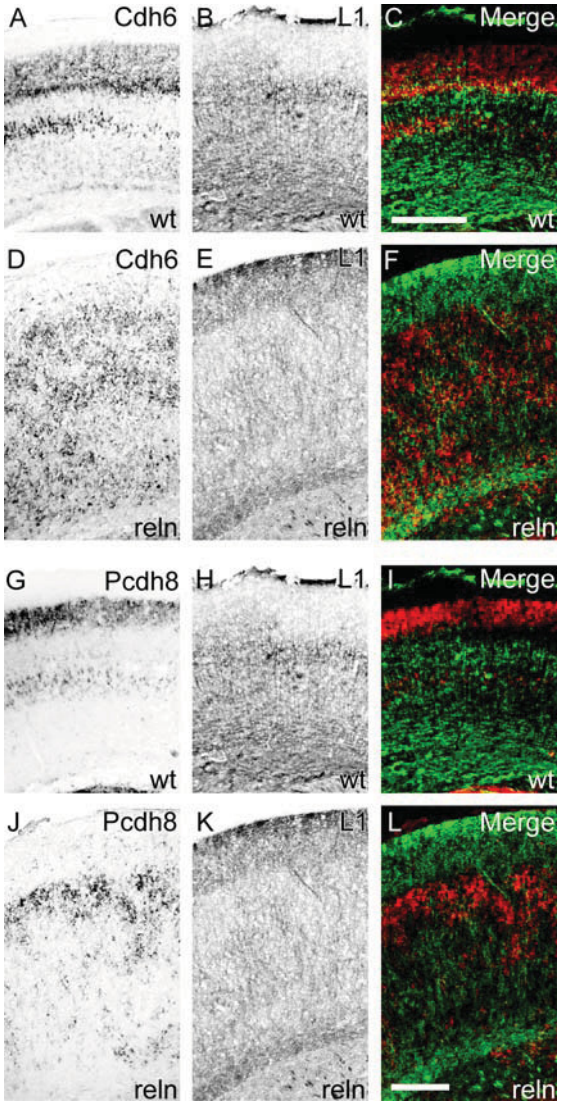

Figure 5.9. Comparison of layered (wild-type, wt) and patchy (Reeler, reln) cadherin expression to immunohistochemistry for the anti-neural cell adhesion molecule L1 at P5. Adjacent frontal sections were hybridized *in situ* with probes for Cdh6 (**A, D**) and Pcdh8 (**G, J**) and compared to adjacent sections stained with L1 antibody (**B, E, H, K**). Combined results of this analysis are shown in pseudocolor-coded overlays (**C, F, I, L**). Colors represent cadherin staining (red) or L1 staining (green). Scale bars, 500µm in C (applies to A-C and G-I), and 250µm in L (applies to D-F and J-L).

perikarya in layers II and IV, as observed in the adult (Fig. 5.5K), is not found postnatally. For Pcdh8 and Pcdh9, positive cells show stronger signal and/or are more numerous at particular radial positions in P5 Reeler cortex compared to adult mutant cortex. However, this stratification is not compatible with an inversion of cortical layers at P5. Pcdh8 is strongly expressed in layers II/III of wild-type SI cortex at P5, and in the superficial half of cortex in Reeler mice (Fig. 5.7F, F'). Pcdh9 is more prominently expressed in the deeper strata of SI cortex both in wild-type mice and in Reeler mice (Fig. 5.7G, G').

Patch-like gray matter architecture in Reeler cerebral cortex. In SI cortex, neurons positive for some cadherins are not evenly distributed but form patchy aggregates of various sizes. In the figures, this is most evident for Cdh6 at P5 and in the adult (Figs. 5.4C'; 5.7C'), for Pcdh8 at P5 (Fig. 5.7F') and for Pcdh19 at P5 (Fig. 5.7I'). Similar patches of cadherin-positive cells are found in the motor and cingulate cortex of

Reeler mice, for example for Pcdh8 at P5 (Fig. 5.8F') and in the adult (Fig. 5.5G'). To check whether the patches or the spaces between the patches can be attributed to fiber fascicles, we compared cadherin expression profiles with immunostaining results for a marker of fiber fascicles (L1; Fig. 5.9; Godfraind et al., 1988; Chung et al., 1991). L1 immunostaining is especially prominent in layer IV, which receives thalamic afferents (Fig. 5.9B, H). Cdh6 shows strong expression in layer III and in the deeper part of layer IV in wild-type cortex (Fig. 5.9A, C). In Reeler cortex, there are Cdh6-positive patches that express L1, and Cdh6-positive patches that do not express L1 (Fig. 5.9D-F). The Pcdh8 staining is complementary to the L1 immunostaining in both wild-type cortex and Reeler cortex (Fig. 5.9G-L). In wild-type, layers II/III and V are Pcdh8-positive (Fig. 5.9G, I) while L1 labels mainly layer IV and VI (Fig. 5.9H, I). In Reeler mice, patches positive for Pcdh8 are not co-localized with the L1 immunostaining (Fig. 5.9J-L).

To visualize the spatial relationship between the cadherin expression patterns, double-label in situ hybridization was performed (Fig. 5.10). Interestingly, the pair Cdh6/Cdh8, which exhibits a roughly complementary distribution pattern in wild-type cortex, shows a complementary expression profile also in mutant cortical aggregates (Fig. 5.10A-F). Pcdh8 and Pcdh19 display complementary staining patterns in wild-type SI, also in layer V (Fig. 5.10G-I). Likewise in the Reeler cortex, there are no overlapping patches (Fig. 5.10J-L). Regionalization in the cingulate and motor cortex is not affected in Reeler cortex for Cdh6/Cdh8 (Fig. 5.10M-R). Complementarity of expression and regional expression gradients are also preserved for Pcdh8/Pcdh19 in homozygous cingulate cortex (Fig. 5.10S-X). The minor differences in the expression patterns between conventional and fluorescent double-labeling results are likely caused by the lower sensitivity of the fluorescent double-labeling procedure (e.g., compare Pcdh19 expression in upper cortical layers; Figs. 5.7I, 5.10H).

Embryonic day 18. Figure 5.11 displays cadherin expression patterns in the developing cortex at E18. Cdh4 is expressed in the ventricular and subventricular zone in wild-type and Reeler mice (Fig. 5.11B, B'). Noteworthy, Cdh4 demarcates the border between cortex and the caudoputamen in wild-type and Reeler mice (arrowheads in Fig. 5.11B, B'). Cdh6 (Fig. 5.11C, C'), Cdh8 (Fig. 5.11D, D') and Pcdh8 (Fig. 5.11E, E') are also expressed in the cortical plate. The compact expression pattern of Cdh6 in wild-type mice (Fig. 5.11C) is disrupted in the Reeler cortical plate (Fig. 5.11C') at positions where fiber fascicles traverse the cortical plate. Similar results are obtained for Cdh8

(Fig. 5.11D') and Pcdh8 (Fig. 5.11E'). For Pcdh8, staining intensity is more prominent in Reeler than in wild-type mice (Fig. 5.11 E, E').

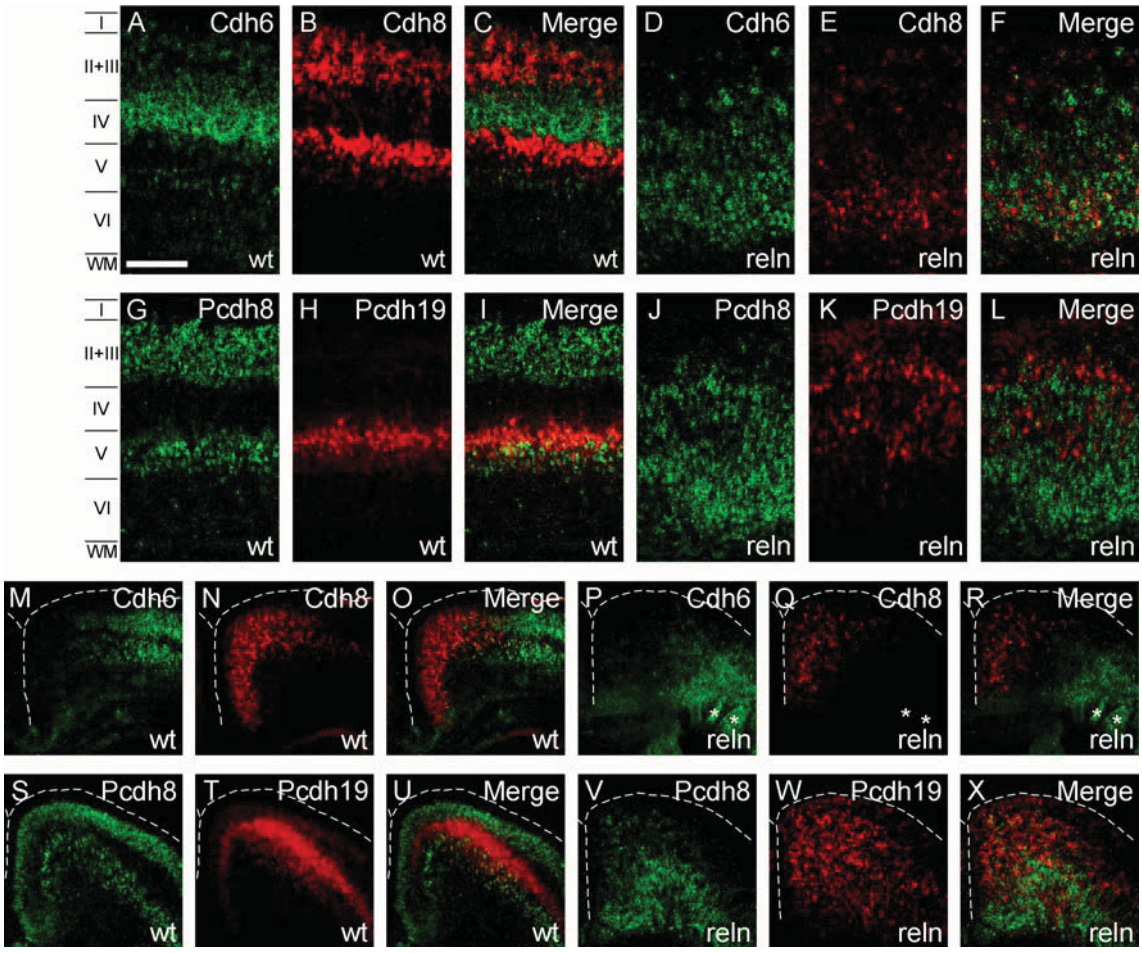

Figure 5.10. Layer-specific cadherin expression in P5 wild-type (wt) somatosensory and cingulate cortex compared to patchy cadherin expression in P5 Reeler (reln) cortex. Frontal sections were hybridized with probes for Cdh6 **(A, D, M, P)**, Cdh8 (**B, E, N, Q**), Pcdh8 (**G, J, S, V**) and Pcdh19 (**H, K, T, W**). Two pairs of cadherins (Cdh6/Cdh8 [**A-F and M-R**] and Pcdh8/Pcdh19 [**G-L and S-X**]) were analyzed. Combined results of this analysis are summarized in pseudocolor-coded overlays (**C, F, I, L, O, R, U and X**). Colors represent cadherin staining. The dashed lines indicate the cortical surface in M to X. The asterisks in P-R indicate artefacts. Scale bar, 250µm in A (applies to A-X).

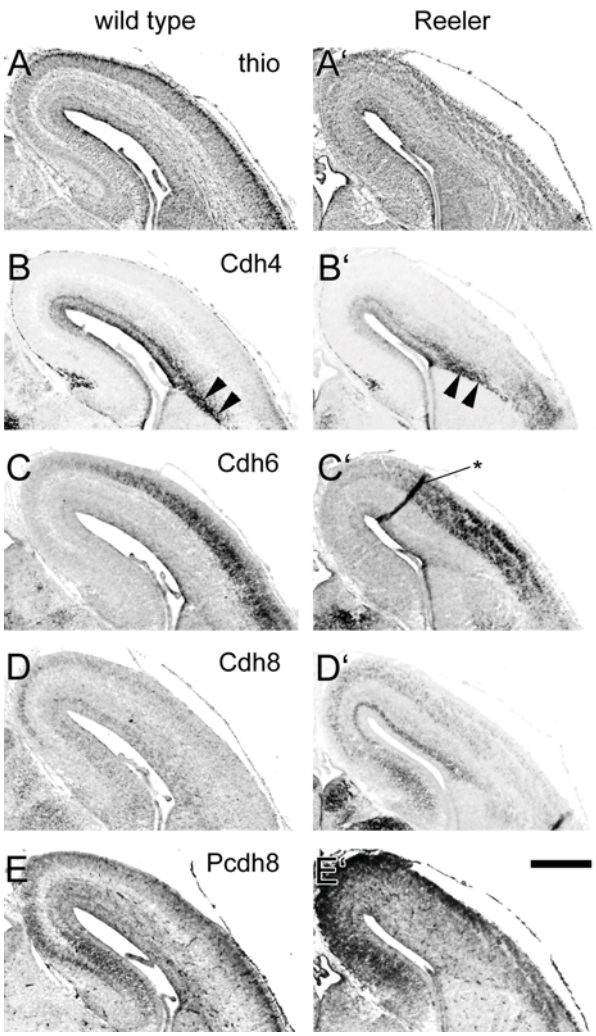

Figure 5.11. Expression mapping of cadherins in the neocortical anlage of wild-type (**A-E**) and Reeler (**A'-E'**) mice in series of adjacent sections at embryonic day 18. Results were obtained with mRNA probes for Cdh4 (**B** and **B'**), Cdh6 (**C** and **C'**), Cdh8 (**D** and **D'**) and Pcdh8 (**E** and **E'**). To facilitate the identification of layers, a thionin (Nissl) stain of an adjacent section is shown for wild-type (**A**) and homozygous Reeler mice (**A'**). Arrowheads in B and B' point to the border between the cortex and the caudoputamen. The asterisk in C' indicates an artefact. Scale bar in E' = 500µm (applies to A-E').

5.1.4 Expression patterns in the phylogenetically older allocortex

The hippocampal region is a phylogenetically older cortical area that is characterized by its laminated organization in wild-type mice. To compare the neocortical findings with cadherin expression in this allocortical area, the expression patterns of 13 different cadherins in the hippocampal region were examined by *in situ* hybridization in adult wild-type mice and Reeler mice. All the cadherins investigated exhibit a differential, locally restricted expression pattern in wild-type mice. Figure 5.12 shows representative examples of expression patterns of cadherins for the hippocampal region. This work was carried out in collaboration with my colleague, Dr. G. Stoya, with the following contributions by myself: allocation of the mice (wild type and mutant), assistance in the *in situ* hybridization procedure and in the analysis of the results, photomicrograph production and preparation of Figure 5.12.

The dentate gyrus shows moderate to strong expression for Cdh11 (Fig. 5.12B), Pcdh17 (Fig. 5.12C) and Pcdh19 (Fig. 5.12D). A spatially restricted expression pattern

can be observed in the hippocampus. Cdh11 shows a strong signal in all the three fields of the Ammon´s horn (CA1-3; Fig. 5.12B), whereas Pcdh17 and Pcdh19 are expressed in a gradient-like fashion. Pcdh17 shows a moderate signal in the distal CA1 region and in the CA3 region (Fig. 5.12C), and strong signal in the CA2 region (arrowheads in Fig. 5.12C). Pcdh19 exhibits a strong expression in the CA1 and CA2 regions and moderate signal in the distal CA3 region (Fig. 5.12D). The subiculum displays a gradient of cadherin expression. Cdh11 shows moderate signal in the apical part of the subiculum that becomes stronger in the basal part (Fig. 5.12B). Pcdh17 and Pcdh19 are expressed moderately by the proximal subiculum (Fig. 5.12C, D). These expression patterns may reflect the topographical organization of the subicular connections. The distal CA1 region is connected with the proximal subiculum. Pcdh17 (Fig. 5.12C) and Cdh4 (data not shown), both positive within these regions, are examples for this transverse topography. The periallocortical regions show differential expression patterns also. The superficial cortical layers II and III of the presubiculum, the parasubiculum and the entorhinal cortex exhibit moderate to weak expression for Cdh11, Pcdh17 and Pcdh19 (Fig. 5.12B, C, D). However, perikarya of the deep layers V and VI of the entorhinal cortex express strongly Cdh11 (arrowheads in Fig. 5.12B) and Pcdh19 (arrowheads in Fig. 5.12D), whereas Pcdh17 shows only weak expression (Fig. 5.12C).

In the Reeler mutant, the cortical layers of the hippocampal formation are disorganized (Fig. 5.12A'). In parallel, a disruption of the cadherin expression can be seen. The strong expression of Cdh11 in the CA1 region is split into two seperate layers (Fig. 5.12B'). Pcdh17-positive perikarya in the CA2 region show a two-layered appearance (arrowheads in Fig. 5.12C'). The borders of the subiculum are hard to define, but the gradient-like expression of Pcdh19 (weak/distal to moderate/proximal) seems to be unaffected (Fig. 5.12D'). Like in neocortical regions, the cells of the periallocortical region do not form layers in the Reeler mutant. Perikarya positive for Cdh11 (Fig. 5.12B'), Pcdh17 (Fig. 5.12C') and Pcdh19 (Fif. 5.12D') are scattered throughout the entire radial dimension. Only deep layers V and VI seem to be inverted. Cdh11 (arrowheads in Fig. 5.12B') and Pcdh19 (arrowheads in Fig. 5.12D') that are expressed in deep layers in wild-type mice, show expression directly beneath the pial surface. These findings are compatible to the results in neocortex (see above).

In summary, every area of the hippocampal region shows expression for several cadherins. These expression profiles are altered in the radial dimension in the Reeler mutants, resulting in a dispersion of cadherin-expressing cells. Layer formation differs

in the allocortex and disappears in the periallocortex. Regionalized cadherin expression (in the CA regions, subiculum etc.) is preserved in the Reeler mutant.

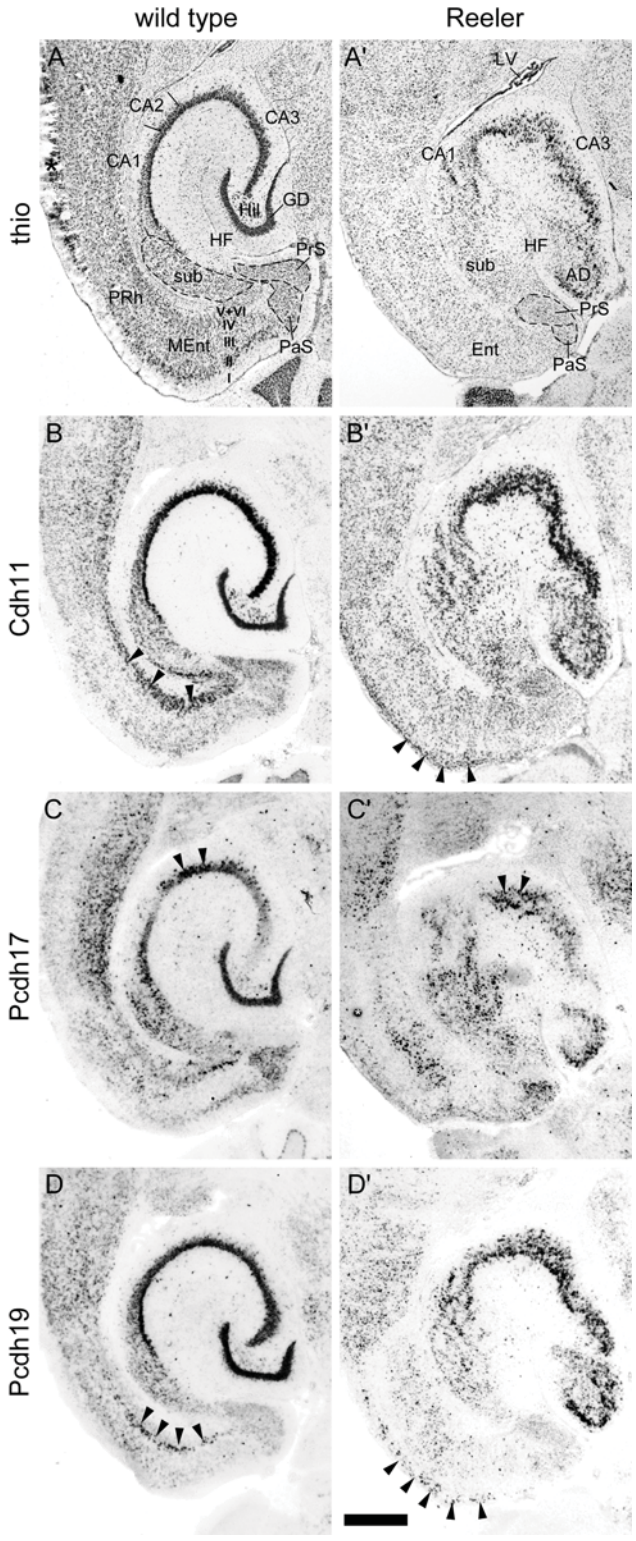

Figure 5.12. Cadherin expression in the adult hippocampal region of wild-type (**A-D**) and Reeler (**A'-D'**) mice in a series of adjacent sections. Results were obtained with mRNA probes for Cdh11 (**B** and **B'**), Pcdh17 (**C** and **C'**) and Pcdh19 (**D** and **D'**). To facilitate the

identification of the different areas within the hippocampal region, a thionin (Nissl) stain of an adjacent section is shown for wild-type (**A**) and homozygous Reeler mice (**A'**). Arrowheads in B and D point to positive perikarya in the deep layer of wild-type entorhinal cortex. Positive cells are found subpially in the Reeler mutant (arrowheads in B' and D'). The arrowheads in C and C' indicate the CA2 region. The asterisk in A indicates an artefact. Scale bar in D' = 500μm (applies to A-D').

5.2 Amygdala

The expression patterns of five classic cadherins and eight protocadherins in the postnatal and adult amygdala of wild-type mice were analyzed. The results for the postnatal animals (P5) are presented in Table 5.1 and Figures 5.13-5.25. In each Figure, the expression of a specific (proto-) cadherin is shown in frontal sections at six different rostrocaudal levels through the amygdala. Whenever possible, a similar section level (namely L1-L6, with L1 being the most rostral level) is shown for each (proto-) cadherin. Next, examples of the expression in the amygdala of adult animals (Figs. 5.26 and 5.27) are presented to show the continuity in the cadherin staining, followed by a comparison of the expression profiles of specific pairs of (proto-) cadherins for double-labeled sections (Fig. 5.28). Each (proto-) cadherin shows a specific expression pattern that will be described in the following paragraphs. The combinatory expression of the thirteen (proto-) cadherins in the amygdala allows the distinction of multiple molecular subdivisions that appear related to distinct cell subpopulations.

Additionally, the (proto-) cadherins are used as markers to analyze the amygdala of the Reeler mutant mouse (Figs. 5.29 and 5.30). This study reveals that cortical amygdaloid areas are affected by the loss of Reelin. Cortical amygdaloid areas fail to migrate to their destination point. However, deep pallial and subpallial nuclei appear to be unaffected by the mutation.

Table 5.1. Expression profiles of cadherins in the murine wild-type amygdala at P5

	Cdh4	Cdh6	Cdh7	Cdh8	Cdh11	Pcdh1	Pcdh7	Pcdh8	Pcdh9	Pcdh10	Pcdh11	Pcdh17	Pcdh19
AAD	+/++*	+/-	+	+	++	++	+	+/++*	+/-	+/-	+/++*	+	++
AAV	+/++*	-	+	+/-	++	++	+	+	-	+	++	++	++
ACo	+	+	+	+	++	++/+++*	+/++*	+	+/-	+	++/+++*	++	++
AHip	++	-	-	++	++	+/++*	++	+++		+/-	+++	+++	
AStr	+/-	++	+/++*	-	++	++	-	+/-	+	+/-	+	++	++/+++*
BAOT	++	-	+/-	+/-	+	+/-	+/++*	+	-		-	-	+/-
BLA	++	-	+/-	+++	+++	+++	++/+++*	+/-	+	+++	-	-	+/++*
BLP	++	+/-	+++	++	+++	+++	++/+++*	+/++*	+++	++	-	+	++
BLV	++	-	+++	++	+++	++	+	+	-	++	+/-	+	+
BMA	++	+	++	-/++*	++/+++*	++/+++*	+++	++/+++*	+*	+/++*	+	+	++
BMP	+++	-	+++	-	+++	+/++*	++	++	+*	++	-	+++	++
CeC	+/-	+	+	-	++	+/++*	-	++/+++*	-	+/-	+	+	++/+++*
CeL	++	+/-	+	-	++	++	+/++*	+++	+	+/-	-	-	++
CeM	++	-	++	+/-	++	+/++*	+/+++*	+	+	+	+	+	++
CxA	+++	-	++	-	+++	+++	+	++	++	++/+++*	+/-	+++	++/+++*
IM	+++	+	-	-	++/+++*	++/+++*	+	+++	++	+/-	+	+	+++
LaDL	++	+	++/+++*	+/-	++	+++	+++	+++	+/-	++/+++*	-	++	++/+++*
LaVL	++	-	+++	+/-	++	+	++	+++	+++	++	-	++	++
LaVM	++	-	+++	+/-	++/+++*	+++	++	+++	+/-	+++	-	++	++
LOT1	-	-	+/-	+	-	+++	-	+/-	-	+/-	+/-	-	-
LOT2	+++	-	+/-	-	+++	+++	+/++*	++/+++*	+++	+++	-	-	+/-
LOT3	+	-	-	+	+++	+++	+	+/++*	+	+	+/-	+	+
MeA	+++	+	++	+	++	++	+	+	++	+/++*	++/+++*	+/+++*	++/+++*
MePD	++	-	+/-	+/-	++	++	+++	++/+++*	++	++	+++	+++	++/+++*
MePV	+++	+/-	+/-	+	++	++	++	++	+++	+/-	++/+++*	++/+++*	++/+++*
PLCo	+++	-	+/++*	++	+++	+++	+	++	+	++/+++*	+++	+++	++/+++*
PMCo	++	+/-	-	+/-	++	+/++*	+++	+/++*	+	++	+++	++/+++*	++

Legend for Table 5.1. The following abbreviations are used in the table: -, no expression; +/-, expression in scattered perikarya; +, low expression; ++, moderate expression; +++, high expression; *, regional differences within the nucleus or area

5.2.1 Cadherin-4

As shown in Figure 5.13 and summarized in Table 5.1, Cdh4 is highly expressed in the amygdala in general, being particularly strong in a subset of specific areas and nuclei.

Anterior, central, medial, and intercalated cell groups of the amygdala. The expression of Cdh4 is particularly strong in abundant cells of the intercalated masses and the medial amygdala (Fig. 5.13B-E). In the medial amygdala, the expression is prominent in the anterior and posteroventral nuclei (MeA, Fig. 5.13B, C; MePV, Fig. 5.13D). Nevertheless, the labelling is not uniformly distributed throughout the nuclei, but it is more abundant in the cortical part of MeA (usually named anteroventral amygdaloid nucleus or MeAV), and in the deeper and central part of MePV. Weak to moderate expression is also observed in the anterior and central amygdala (Fig. 5.13D). In the central amygdala, the expression is generally moderate with patches of strong expression in the medial part; it is less intense in the capsular part (Fig. 5.13C).

Basal amygdalar complex. The lateral, basolateral and basomedial nuclei of the amygdala show moderate to strong expression of Cdh4. The expression in the lateral nucleus changes from rostral to caudal levels: it shows patches of strong expression at rostral levels and, in particular, at caudal levels (Fig. 5.13C, E); however, at intermediate levels, the expression is moderate in the dorsolateral and ventromedial parts, and strong in the ventrolateral part (LaVL, Fig. 5.13D). The expression in the basolateral (BL) and basomedial (BM) nuclei also shows variations, with patches of strong expression in the anterior and posterior parts (BLA, BMA, Fig. 5.13B, C; BLP, BMP, Fig. 5.13D-F).

Cortical amygdalar areas. Cdh4 is strongly expressed in abundant cells of the nucleus of the lateral olfactory tract (LOT, Fig. 5.13A) and in the posterolateral cortical amygdalar area (PLCo, Fig. 5.13F). The expression in the cortical areas is patchy. There also is weak to moderate expression in subpopulations of cells in the anterior and posteromedial cortical amygdalar areas (ACo, Fig. 5.13A-C; PLCo, Fig. 5.13F), and in the nucleus of the accessory olfactory tract (BAOT, Fig. 5.13B).

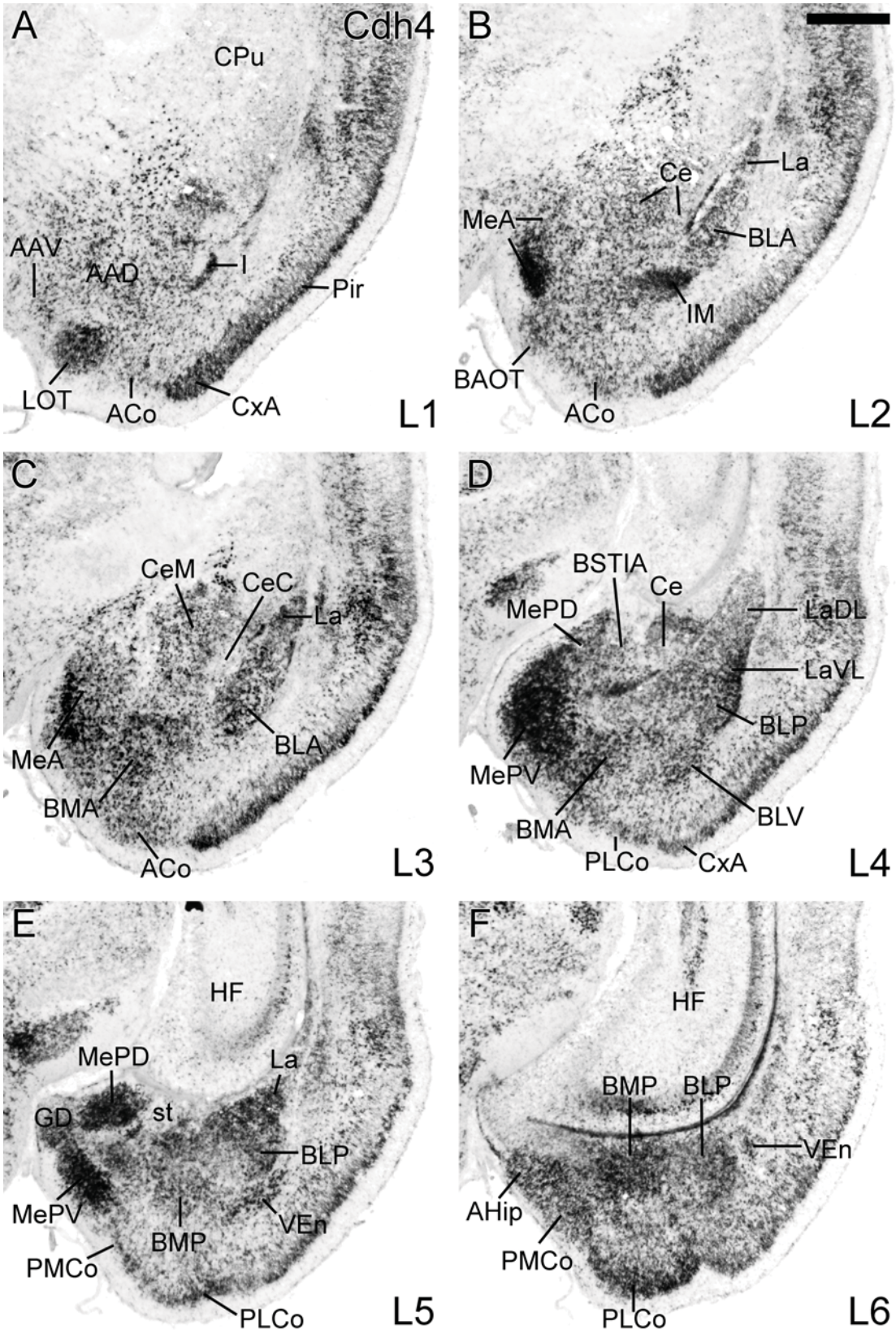

Figure 5.13. Expression mapping of cadherin-4 (Cdh4) in the wild-type amygdaloid complex in a series of adjacent frontal sections at postnatal day 5. Six different levels (L1-L6) are shown in a rostral-to-caudal sequence. Results were obtained by *in situ* hybridization with an mRNA probe for Cdh4. Scale bar in B = 500µm (applies to A-F).

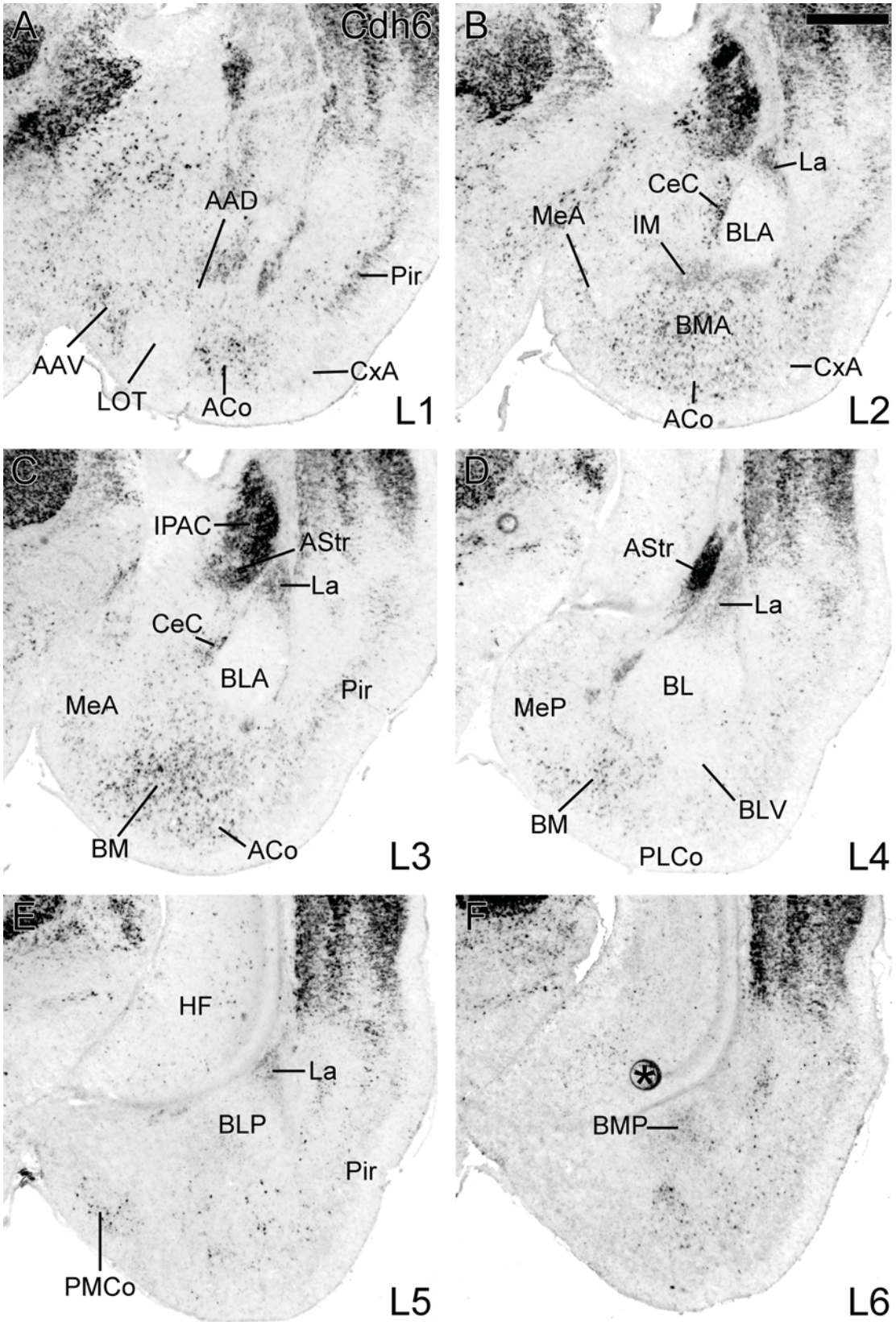

Figure 5.14. Expression mapping of cadherin-6 (Cdh6) in the wild-type amygdaloid complex in a series of adjacent frontal sections at postnatal day 5. Six different levels (l1-L6) are shown in a rostral-to-caudal sequence. Results were obtained by *in situ* hybridization with an mRNA probe for Cdh6. The asterisk in F indicates an artefact. Scale bar in B = 500µm (applies to A-F).

5.2.2 Cadherin-6

In contrast to the previous classic cadherin, Cdh6 shows only moderate expression by scattered subpopulations of cells in specific amygdalar nuclei and areas (Fig. 5.14; Table 5.1).

Anterior, central, medial, and intercalated cell groups of the amygdala. Scattered cells showing Cdh6 expresssion are present in the lateral/capsular part of the central amygdala, in the intercalated masses and in the anterior amygdala (CeC, AAD, AAV, IM, Fig. 5.14A, B). A few Cdh6-expressing cells are also scattered in the anterior medial amygdala (MeA, Fig. 5.14B), but they are extremely rare in the posterior medial amygdala (MeP, Fig. 5.14D).

Basal amygdalar complex. The lateral and basomedial amygdalar nuclei contain a number of cells showing moderate Cdh6 expression at all rostrocaudal levels (La, BM, Fig. 5.14B-E). In contrast, the basolateral nucleus is free of Cdh6 expression.

Cortical amygdalar areas. The anterior and posteromedial cortical amygdalar areas contain scattered cells expressing Cdh6 (ACo, PMCo, Fig. 5.14A, B, E). In contrast, the nucleus of the lateral olfactory tract (LOT) and the posterolateral cortical amygdalar area (PLCo) do not show Cdh6 expression in any of their layers (Fig. 5.14A, D).

5.2.3 Cadherin-7

Cdh7 is strongly expressed in numerous cells of specific amygdalar nuclei and areas, but its expression becomes even stronger and much more abundant at caudal levels of the basal amygdalar complex (Fig. 5.15; Table 5.1).

Anterior, central, medial, and intercalated cell groups of the amygdala. The anterior and central amygdala contain cells expressing Cdh7; signal is stronger and positive cells are more numerous in the rostral and medial parts of central amygdala (Ce, CeM, Fig. 5.15B-D) and in the ventral part of the anterior amygdala (AAV, Fig. 5.15A). Cdh7 expression also occurs in a large subpopulation of cells in the anterior and posteroventral parts of the medial amygdala (MeA, MePV, Fig. 5.15C, D).

Basal amygdalar complex. At rostral and intermediate levels, the basal amygdalar complex shows Cdh7 expression in a large subpopulation of cells of the lateral nucleus, anterior basomedial nucleus and posterior basolateral nucleus (La, BMA, BLP, Fig. 5.15C, D). More caudally, signal becomes strong to very strong and

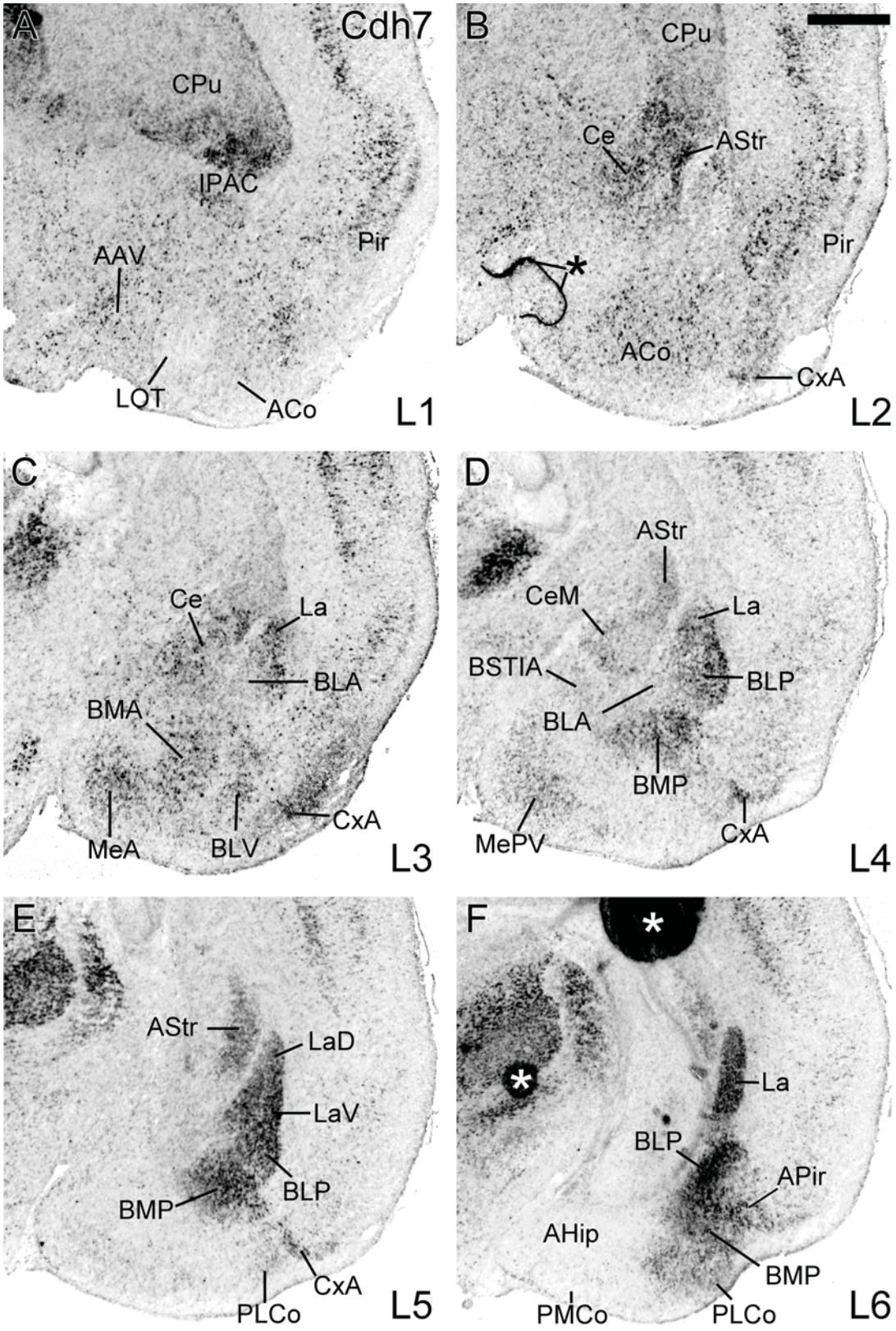

Figure 5.15. Expression mapping of cadherin-7 (Cdh7) in the wild-type amygdaloid complex in a series of adjacent frontal sections at postnatal day 5. Six different levels (L1-L6) are shown in a rostral-to-caudal sequence. Results were obtained by *in situ* hybridization with an mRNA probe for Cdh7. The asterisks in B and F indicate artefacts. Scale bar in B = 500µm (applies to A-F).

abundant, being present in most (if not all) cells of the most posterior parts of the three nuclei (Fig. 5.15E, F). Cdh7 signal in the basal complex is not uniformly distributed, but shows some patches of stronger expression.

Cortical amygdalar areas. Cdh7 is expressed in a number of cells of the anterior cortical amygdalar area (ACo, Fig. 5.15B), and in a lateral part of the posterolateral cortical amygdalar area (PLCo, Fig. 5.15E, F). Extremely few (if any) Cdh7-positive cells were observed in the nucleus of the lateral olfactory tract (LOT, Fig. 5.15A) or in the posteromedial cortical amygdalar area (PMCo, Fig. 5.15F).

5.2.4 Cadherin-8

Cdh8 signal is prominent in specific subnuclei of the basal amygdalar complex, while only minor cell subpopulations are positive in other amygdalar areas and nuclei (Fig. 5.16; Table 5.1).

Anterior, central, medial, and intercalated cell groups of the amygdala. Cdh8 is moderately expressed in a subpopulation of cells in the anterior and medial amygdala (AAV, MeA, Fig. 5.16A, B). In the medial amygdala, Cdh8-positive cells are uniformly distributed in the anterior part (MeA, Fig. 5.16B), but tend to be located superficially in the posteroventral part (MePV, Fig. 5.16C). In contrast, the central and intercalated masses of the amygdala show only weak Cdh8 expression by extremely few, scattered cells (Ce, Fig. 5.16B-D).

Basal amygdalar complex. A high number of cells that show strong expression of Cdh8 is observed mainly in the lateral amygdalar nucleus at rostral levels (La, Fig. 5.16B-D), and in the basolateral amygdalar nucleus at all levels (BLA, BLV, BLP, Fig. 5.16B-F). The expression in La, BLA and BLP is patchy, showing areas of strong expession adjacent to other areas with moderate expression (Fig. 5.16B-F). In contrast, the posterior parts of the lateral nucleus show very weak or no expression of Cdh8 (Fig. 5.16E, F). The basomedial amygdalar nucleus contains only a few scattered cells positive for Cdh8 in its anterior part (BMA, Fig. 5.16C), but appears to be free of expression at caudal levels (BMP, Fig. 5.16F).

Cortical amygdalar areas. Subpopulations of Cdh8-expressing cells are observed in layers 1 and 3 of the nucleus of the lateral olfactory tract (LOT, Fig. 5.16A), in the anterior pole of the anterior cortical amygdalar area (ACo, Fig. 5.16A) and in the posteromedial cortical amygdalar area (PMCo, Fig. 5.16F). In contrast, only very few

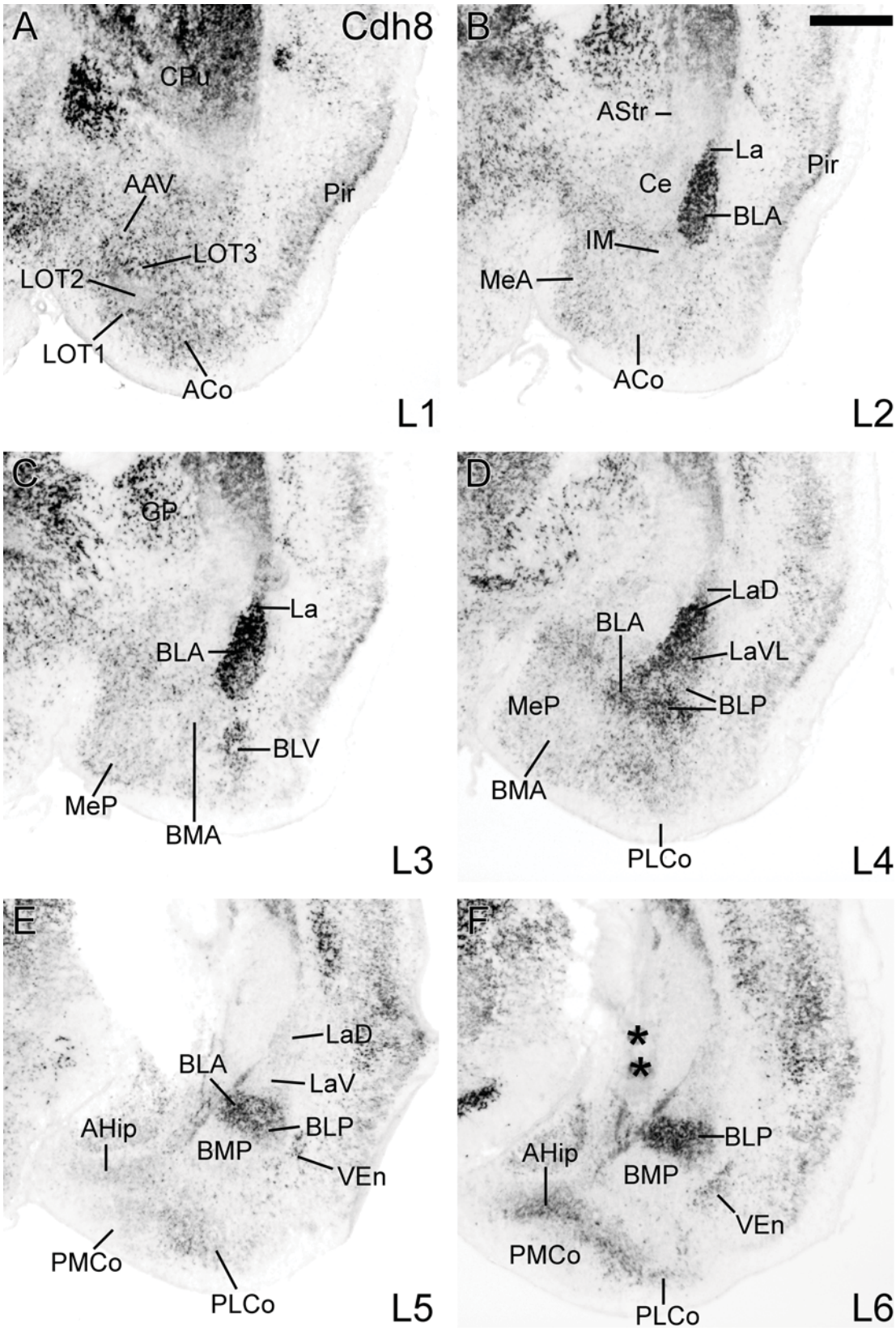

Figure 5.16. Expression mapping of cadherin-8 (Cdh8) in the wild-type amygdaloid complex in a series of adjacent frontal sections at postnatal day 5. Six different levels (L1-L6) are shown in a rostral-to-caudal sequence. Results were obtained by *in situ* hybridization with an mRNA probe for Cdh8. The asterisk in F indicate artefacts. Scale bar in B = 500µm (applies to A-F).

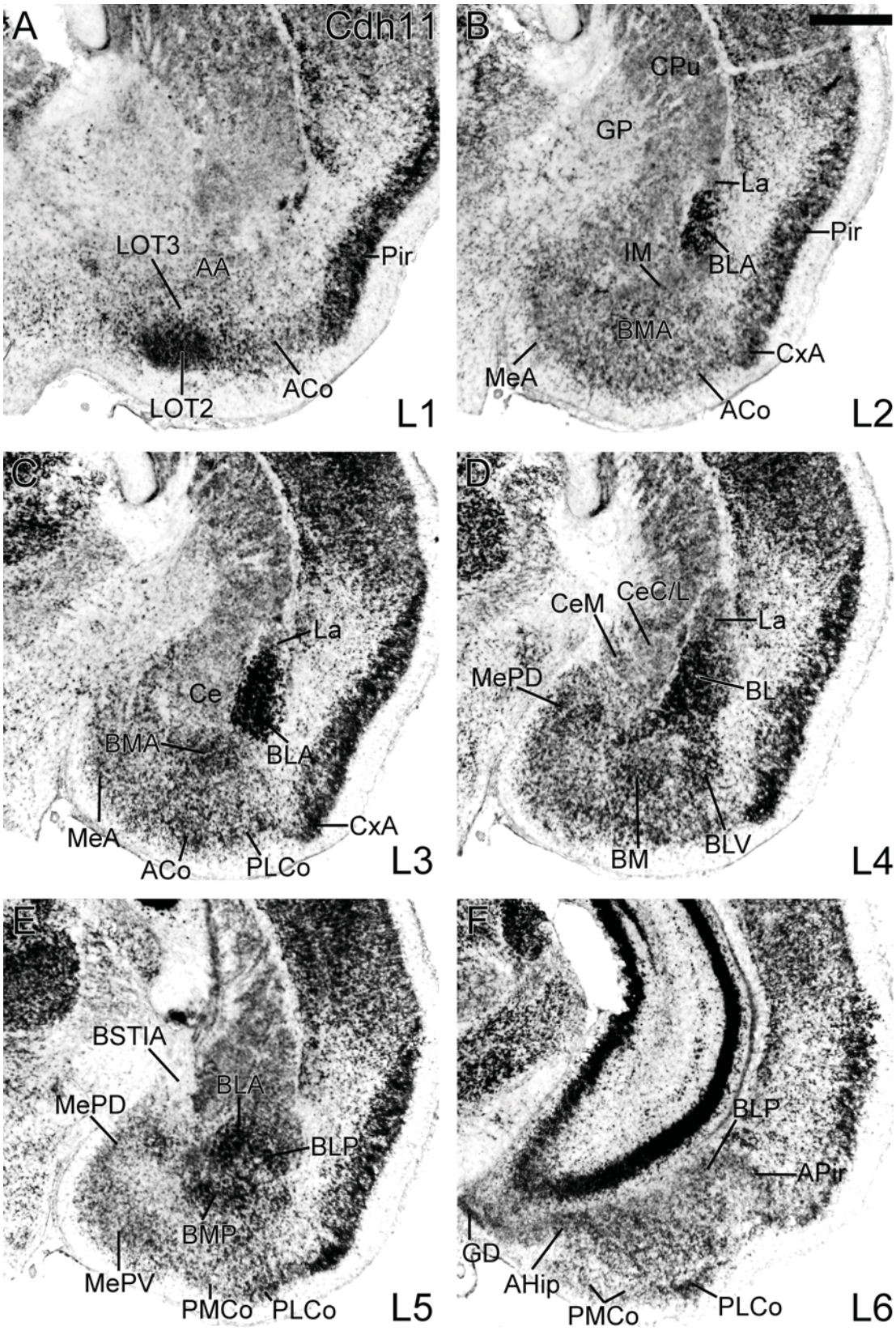

Figure 5.17. Expression mapping of cadherin-11 (Cdh11) in the wild-type amygdaloid complex in a series of adjacent frontal sections at postnatal day 5. Six different levels (L1-L6) are shown in a rostral-to-caudal sequence. Results were obtained by *in situ* hybridization with an mRNA probe for Cdh11. Scale bar in B = 500µm (applies to A-F).

Cdh8-positive cells are observed at the medial edge of the posterolateral cortical amygdalar area (PLCo, Fig. 5.16F).

5.2.5 Cadherin-11

Cdh11 exhibits strong to very strong expression in most of the amygdalar complex (Fig. 5.17; Table 5.1).

Anterior, central, medial, and intercalated cell groups of the amygdala. Expression levels for Cdh11 are moderate in most cells of the anterior, central and intercalated masses of the amygdala (AA, Ce, IM, Fig. 5.17A-D). In the medial amygdala, the expression of Cdh11 is moderate to strong and displays a non-uniform pattern: in the anterior nucleus, the superficial part of the cortical subnucleus (AAV) shows stronger Cdh11 expression (MeA, Fig. 5.17B), whereas in the posterodorsal nucleus, there are cell patches that are more strongly positive for Cdh11 (MePD, Fig. 5.17D).

Basal amygdalar complex. The entire complex shows strong to very strong signal for Cdh11 in most (if not all) of its cells (Fig. 5.17B-E). This is particularly evident at rostral and intermediate levels of the basolateral nucleus (BLA, BLV, BLP, Fig. 5.17B-E). At some levels of the basolateral and basomedial nuclei, the expression is patchy (Fig. 5.17B, D, E).

Cortical amygdalar areas. Cdh11 expression is strong to very strong in most cells of layers 2-3 of the nucleus of the lateral olfactory tract (LOT2, LOT3, Fig. 5.17A). Strong signal with a patchy distribution was observed in layer 2 of the posterolateral cortical amygdalar area (PLCo, Fig. 5.17E, F). The rest of the amygdalar cortical areas generally show moderate Cdh11 expression, with patches of stronger expression (ACo, PMCo, Fig. 5.17A, B, E, F).

5.2.6 Protocadherin-1

This protocadherin shows a moderate to strong, patchy expression in many nuclei and areas of the amygdala (Fig. 5.18, Table 5.1).

Anterior, central, medial, and intercalated cell groups of the amygdala. Signal for Pcdh1 is generally moderate with patches of stronger expression in the anterior (AA, Fig. 5.18A), central (Ce, Fig. 5.18B-D), medial (MeA, MePD, MePV, Fig. 5.18B-E) and intercalated masses (IM, Fig. 5.18B) of the amygdala.

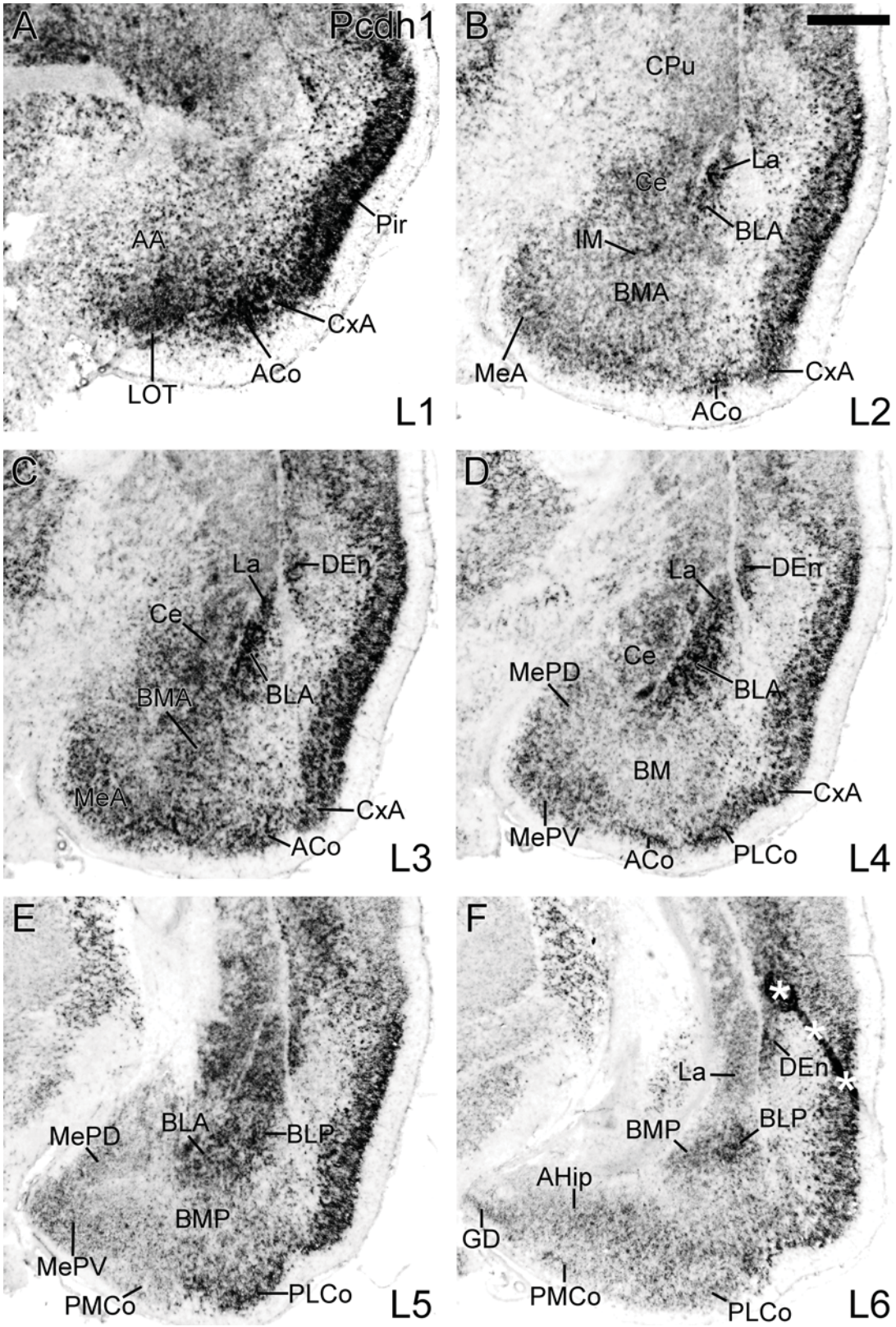

Figure 5.18. Expression mapping of protocadherin-1 (Pcdh1) in the wild-type amygdaloid complex in a series of adjacent frontal sections at postnatal day 5. Six different levels (L1-L6) are shown in a rostral-to-caudal sequence. Results were obtained by *in situ* hybridization with an mRNA probe for Pcdh1. Asterisks in F indicate an artefact. Scale bar in B = 500µm (applies to A-F).

Basal amygdalar complex. The lateral and basolateral amygdalar nuclei show a strong to very strong, patchy expression of Pcdh1 at rostral and intermediate levels (La, BLA, BLP, Fig. 5.18B-E). Caudally, the expression becomes moderate in general, but continues to show patches of stronger expression (Fig. 5.18F). In contrast, the expression of Pcdh1 in the basomedial nucleus is moderate from rostral to caudal levels, although there are patches of stronger expression at intermediate levels (BMA, BMP, Fig. 5.18B-F).

Cortical amygdalar areas. Pcdh1 is expressed strongly to very strongly (in some patches) throughout the nucleus of the lateral olfactory tract (LOT, Fig. 5.18A). In the anterior and posterolateral cortical amygdalar areas (ACo, PLCo, Fig. 5.18A-F), expression is patchy and ranges from moderate to very strong. In contrast, expression levels are generally low in the posteromedial cortical amygdalar area (PMCo, Fig. 5.18E, F).

5.2.7 Protocadherin-7

Pcdh7 shows a moderate to strong, patchy expression in specific nuclei and areas of the amygdala, such as in some subdivisions of the centromedial amygdala and the basal amygdalar complex (Fig. 5.19, Table 5.1).

Anterior, central, medial, and intercalated cell groups of the amygdala. In the medial part of the central amygdala (CeM, Fig. 5.19B, C), Pcdh7 signal is prominent with patches of very strong expression, while it is absent or extremely weak in the capsular and lateral parts of the central amygdala (CeC, CeL, Fig. 5.19B, C). In the medial amygdala, Pcdh7 expression shows subnuclear variations also: it is moderate to strong (in specific patches) in the anterior and posteroventral parts (MeA, MePV, Fig. 5.19B-D), while it is generally strong, with patches of very strong expression, in the posterodorsal subnucleus (MePD, Fig. 5.19D). Pcdh7 staining is moderate in the anterior and intercalated masses of the amygdala, which comprises scattered cells with stronger expression in the anterior amygdala (AAD, AAV, Fig. 5.19A). Expression is uniformly distributed in the intercalated masses (IM, Fig. 5.19A, B).

Basal amygdalar complex. The expression of Pcdh7 in the basal complex varies between nuclear and subnuclear divisions. At all rostrocaudal levels, it is very strong in the dorsal part of the lateral nucleus, but generally moderate in the ventral part (LaD, LaV, Fig. 5.19B-E). In the basolateral nucleus, Pcdh7 shows moderate expression with patches of strong expression in the anterior and posterior subnuclei (BLA, BLP, Fig.

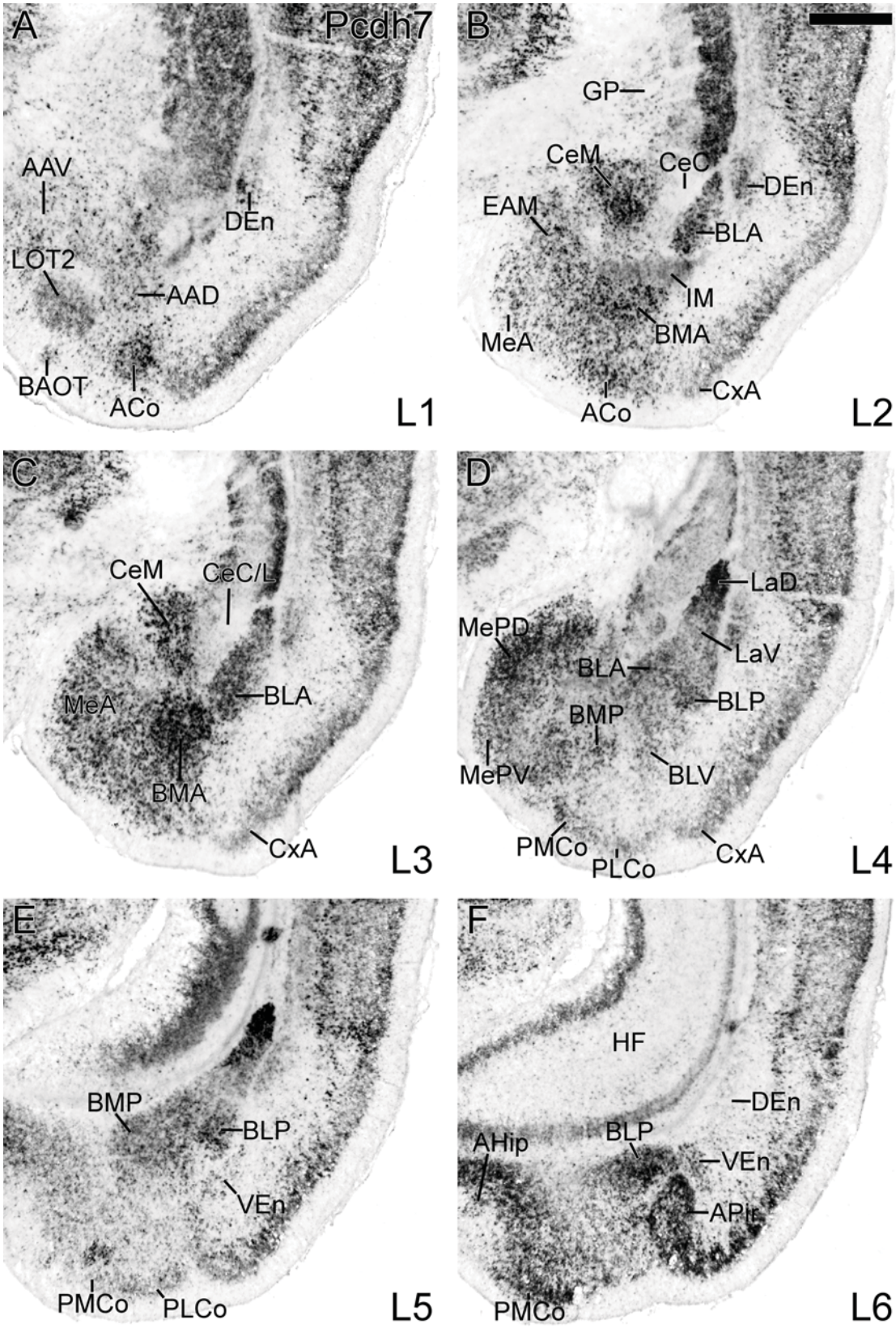

Figure 5.19. Expression mapping of protocadherin-7 (Pcdh7) in the wild-type amygdaloid complex in a series of adjacent frontal sections at postnatal day 5. Six different levels (L1-L6) are shown in a rostral-to-caudal sequence. Results were obtained by *in situ* hybridization with an mRNA probe for Pcdh7. Scale bar in B = 500µm (applies to A-F).

5.19B-F). In the ventral subnucleus (BLV, Fig. 5.19D), expression is generally weak. In the basomedial nucleus, Pcdh7 staining is patchy and ranges from moderate to very strong in the anterior part (BMA, Fig. 5.19B-D); it becomes moderate in the caudal subnucleus (BMP, Fig. 5.19E).

Cortical amygdalar areas. In general, Pcdh7 shows moderate to strong expression in layer 2 of the nucleus of the lateral olfactory tract (LOT2, Fig. 5.19A), and in the anterior and posteromedial cortical amygdalar areas (ACo, PMCo, Fig. 5.19A, B, D-F). The expression of the posterolateral cortical amygdalar area is generally weak (PLCo, Fig. 5.19D, E).

5.2.8 Protocadherin-8

Similarly to the previous protocadherin, Pcdh8 exhibits moderate to strong, patchy expression in specific nuclei and areas of the amygdala, such as some subdivisions of the centromedial amygdala and the basal amygdalar complex (Fig. 5.20, Table 5.1).

Anterior, central, medial, and intercalated cell groups of the amygdala. Pcdh8 staining is very strong in the intercalated masses of the amygdala (I, IM, Fig. 5.20A-E), and in patches of the central and medial amygdala (Ce, Me, Fig. 5.20B, C). Pcdh8 staining is especially strong in the central amygdala where it assumes a patchy appearance in the lateral and capsular parts (CeC, CeL, Fig. 5.20B-D). In contrast, it is weak to moderate in the medial part (CeM, Fig. 5.20B, C). In the medial amygdala, Pcdh8 expression is generally moderate in the anterior and posteroventral subnuclei (MeA, MePV, Fig. 5.20B-E), with some patches of stronger expression. However, Pcdh8 shows very strong and patchy expresion in the ventral aspect of the posterodorsal medial amygdala, while the expression is moderate in the rest of this subnucleus (MePD, Fig. 5.20C, E). The anterior amygdala, in which Pcdh8 signal is weak to moderate, contains scattered cells that are strongly Pcdh8 positive (AAD, AAV, Fig. 5.20A).

Basal amygdalar complex. The lateral nucleus shows strong to very strong, patchy expression throughout its rostrocaudal extension (LaD, LaV, Fig. 5.20B-E). In contrast, the basolateral nucleus contains weakly Pcdh8-positive cells that are scattered in its anterior part (BLA, Fig. 5.20B-D), and moderate, patchy signal in the posterior subnucleus (BLP, Fig. 5.20D-F). In the basomedial nucleus, Pcdh8 expression is moderate to strong and patchy at all rostrocaudal levels (BMA, BMP, Fig. 5.20B-F).

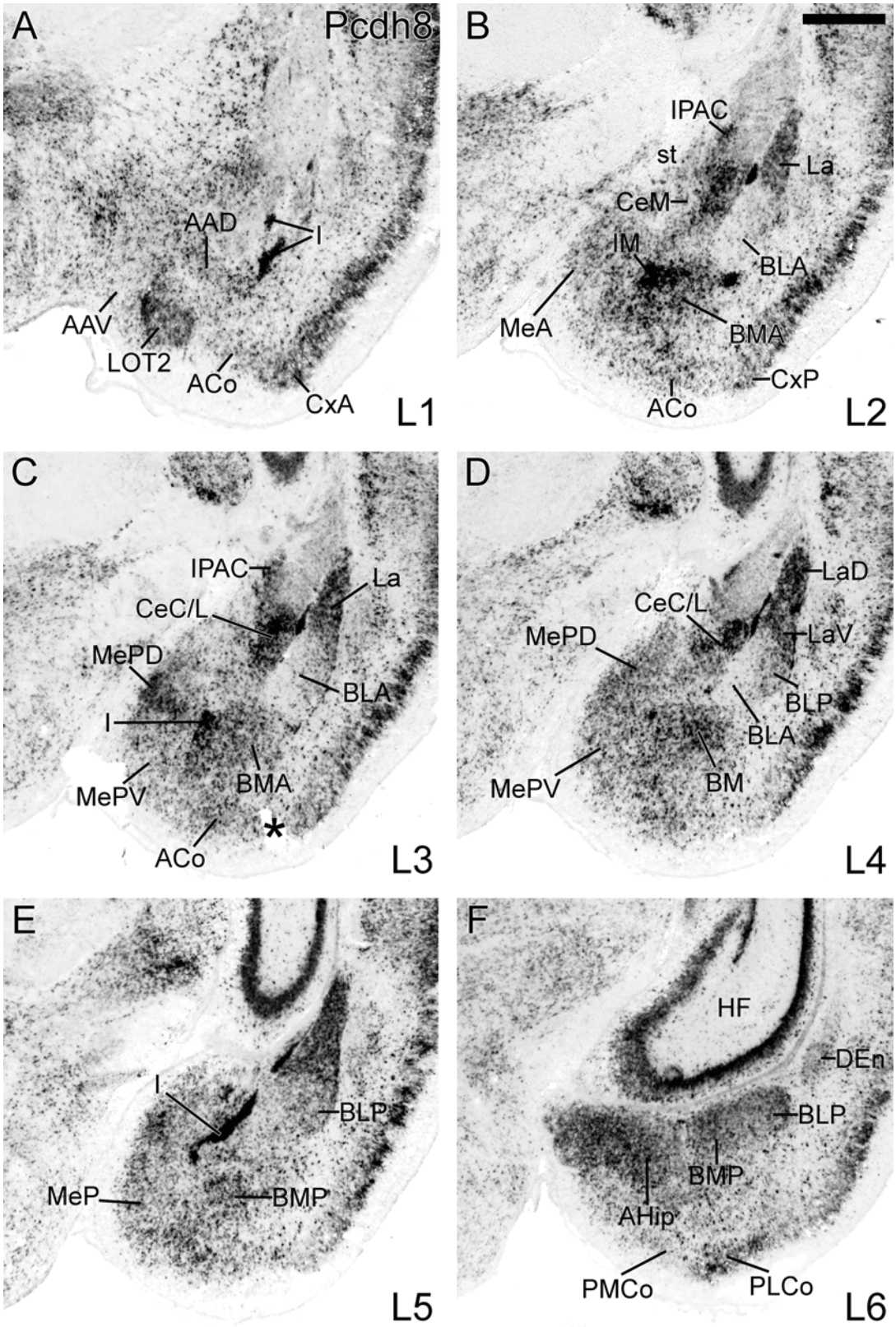

Figure 5.20. Expression mapping of protocadherin-8 (Pcdh8) in the wild-type amygdaloid complex in a series of adjacent frontal sections at postnatal day 5. Six different levels (L1-L6) are shown in a rostral-to-caudal sequence. Results were obtained by *in situ* hybridization with an mRNA probe for Pcdh8. The asterisk in C indicates an artefact. Scale bar in B = 500µm (applies to A-F).

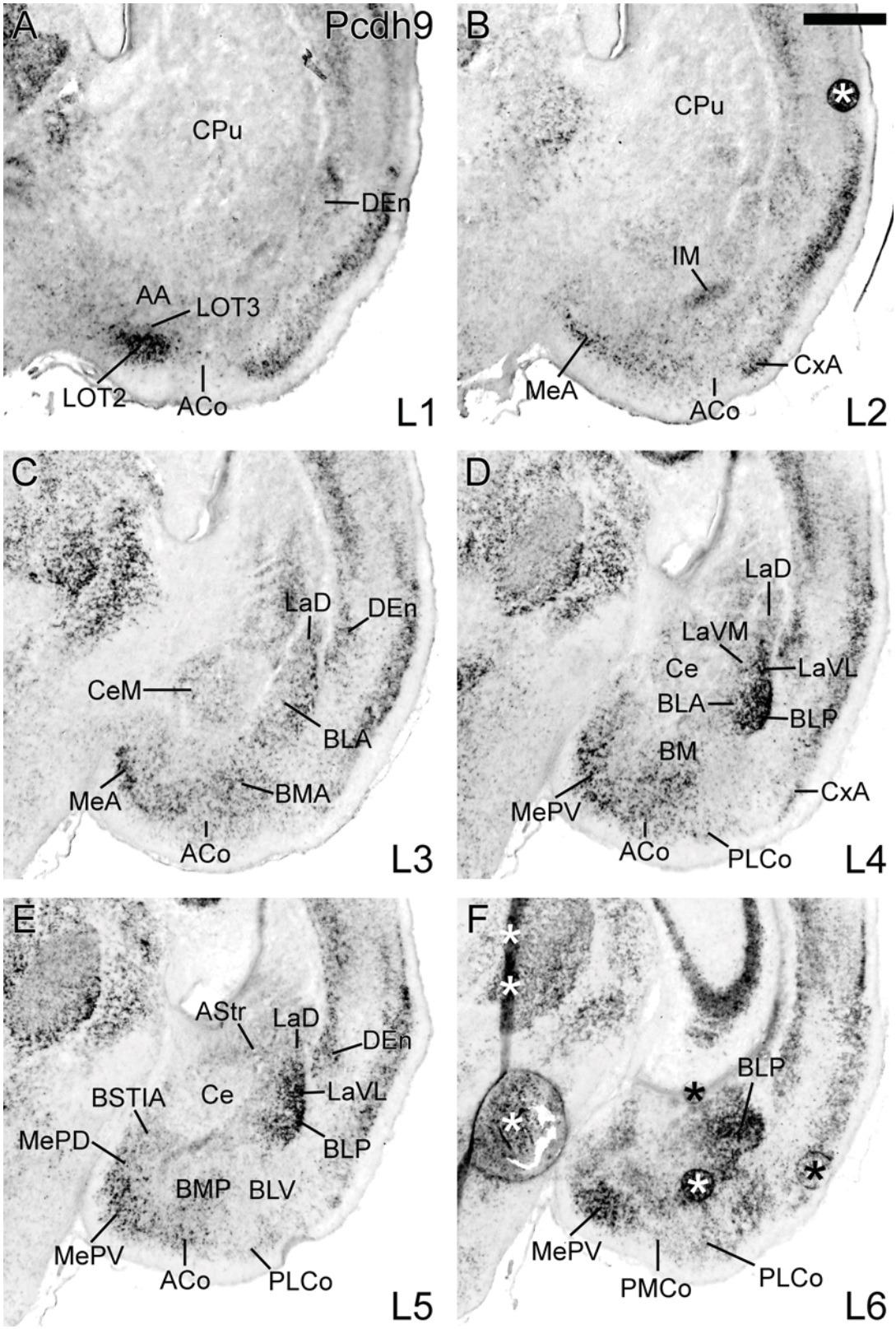

Figure 5.21. Expression mapping of protocadherin-9 (Pcdh9) in the wild-type amygdaloid complex in a series of adjacent frontal sections at postnatal day 5. Six different levels (L1-L6) are shown in a rostral-to-caudal sequence. Results were obtained by *in situ* hybridization with an mRNA probe for Pcdh9. Asterisks in B and F indicate artefacts. Scale bar in B = 500µm (applies to A-F).

Cortical amygdalar areas. The nucleus of the lateral olfactory tract (mainly its layer 2; LOT2, Fig. 5.20A) and the posterolateral cortical amygdala area (PLCo, Fig. 5.20F) show moderate to strong, patchy staining of Pcdh8. In contrast, Pcdh8 expression is weak to moderate in the anterior and posteromedial cortical amygdalar areas (ACo, PMCo, Fig. 5.20A, B, F).

5.2.9 Protocadherin-9

Compared to the previous protocadherins, the expression of Pcdh9 in the amygdala is much more restricted, and only few nuclei or areas show strong expression (Fig. 5.21, Table 5.1).

Anterior, central, medial, and intercalated cell groups of the amygdala. Staining for Pcdh9 in the anterior and central amygdala is generally weak, while it is moderate in the intercalated masses (AA, Ce, IM, Fig. 5.21A-D). In contrast, the medial amygdala contains some strongly Pcdh9-positive patches and scattered cells, mainly in the cortical part of the anterior nucleus (MeA, Fig. 5.21C), and in the deep and posterior parts of the posteroventral nucleus (MePV, Fig. 5.21E, F).

Basal amygdalar complex. Pcdh9 is expressed strongly and in a patchy pattern in the ventrolateral part of the lateral amygdalar nucleus (LaVL, Fig. 5.21D, E) and in the posterior part of the basolateral nucleus (BLP, Fig. 5.21D-F). The rest of the basal amygdalar complex shows weak Pcdh9 expression.

Cortical amygdalar areas. Pcdh9 is expressed strongly in the nucleus of the lateral olfactory tract (LOT, Fig. 5.21A), and weakly to moderately in the other cortical amygdalar areas (ACo, PLCo, PMCo, Fig. 5.21A-F).

5.2.10 Protocadherin-10

In general, Pcdh10 is expressed weakly to moderately in most nuclei and areas of the amygdala, except for the nucleus of the lateral olfactory tract and some parts of the basal amygdalar complex, in which the expression is strong or very strong (Fig. 5.22, Table 5.1).

Anterior, central, medial, and intercalated cell groups of the amygdala. Pcdh10 expression is weak or moderate in the anterior, central and intercalated masses of the amygdala (AAD, AAV, IM, Ce, Fig. 5.22A-D). In the central amygdala, signal is weak in the capsular and lateral parts (CeC, CeL, Fig. 5.22B, C), but moderate in the medial part (CeM, Fig. 5.22C). In the medial amygdala, Pcdh10 expression also ranges from

weak to moderate: the anterior nucleus is weakly positive, except for a large patch of staining that is related to (or deep to) the cortical part (MeA, Fig. 5.22B, C); the posteroventral medial amygdalar nucleus shows weak Pcdh10 expression (MePV, Fig. 5.22E), while the posterodorsal nucleus show moderate expression, with scattered cells that are more strongly positive (MePD, Fig. 5.22E).

Basal amygdalar complex. In general, the lateral and basolateral amygdalar nuclei show moderate to strong Pcdh10 expression, with some variations depending on the subnucleus. The expression is strong and patchy in the dorsal and ventromedial parts of the lateral nucleus (LaD, LaVM, Fig. 5.22B-E), and in the anterior part of the basolateral nucleus (BLA, Fig. 5.22B-D). The basomedial nucleus is weakly to moderately positive (BMA, BMP, Fig. 5.22B-D, F).

Cortical amygdalar areas. The nucleus of the lateral olfactory tract displays very strong Pcdh10 staining in its layer 2 (LOT2), while layers 1 and 3 are weakly to moderately positive, respectively (Fig. 5.22A). The cortical amygdalar areas are moderately stained (ACo, PLCo, PMCo, Fig. 5.22B-F).

5.2.11 Protocadherin-11

Pcdh11 signal is weak or absent in the basal complex and the central amygdala, but it is strong and patchy in the medial extended amygdala and many cortical areas of the amygdala (Fig. 5.23, Table 5.1).

Anterior, central, medial, and intercalated cell groups of the amygdala. The anterodorsal, central and intercalated masses of the amygdala only show weak or moderate Pcdh11 expression, which is mostly restricted to scattered cells (AAD, Ce, IM, Fig. 5.23A-C). Staining in the central amygdala is primarily located in its medial part (CeM, Fig. 5.23B). In contrast, the anteroventral amygdala and the medial amygdala (mostly its anterior and posterodorsal parts) contain abundant patches of strong or very strong Pcdh11 signal (AAV, MeA, MePD, Fig. 5.23B-D).

Basal amygdalar complex. The entire basal amygdalar complex is free of Pcdh11 expression throughout its rostrocaudal extent (La, BL, BM, Fig. 5.23B-F).

Cortical amygdalar areas. The anterior, posterolateral and posteromedial cortical amygdalar areas show patches of strong to very strong Pcdh11 expression, but there are some variations from rostral to caudal levels in each area (ACo, PLCo, PMCo, Fig. 5.23B-F). In contrast, the nucleus of the lateral olfactory tract is free of expression (LOT, Fig. 5.23A).

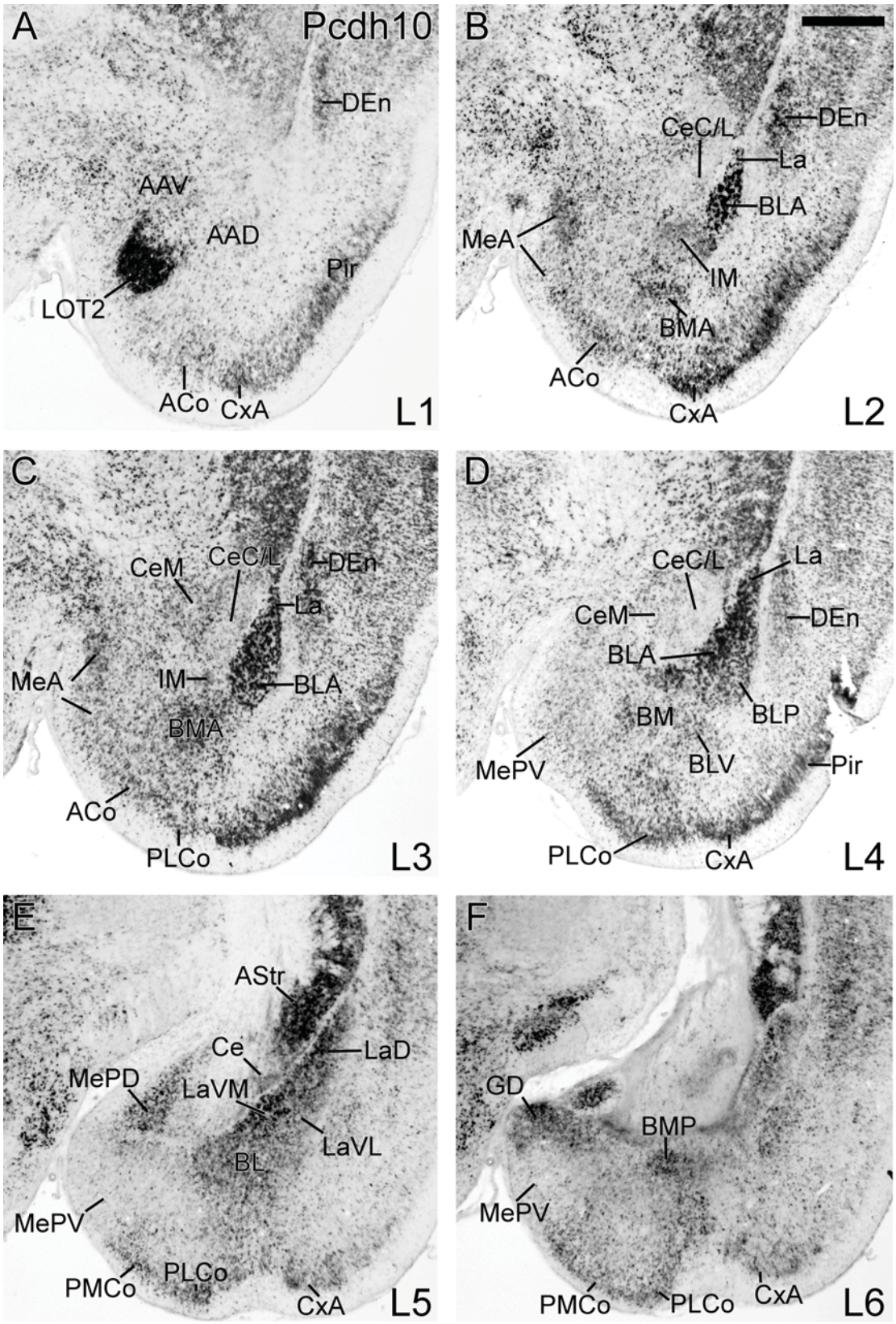

Figure 5.22. Expression mapping of protocadherin-10 (Pcdh10) in the wild-type amygdaloid complex in a series of adjacent frontal sections at postnatal day 5. Six different levels (L1-L6) are shown in a rostral-to-caudal sequence. Results were obtained by *in situ* hybridization with an mRNA probe for Pcdh10. Scale bar in B = 500µm (applies to A-F).

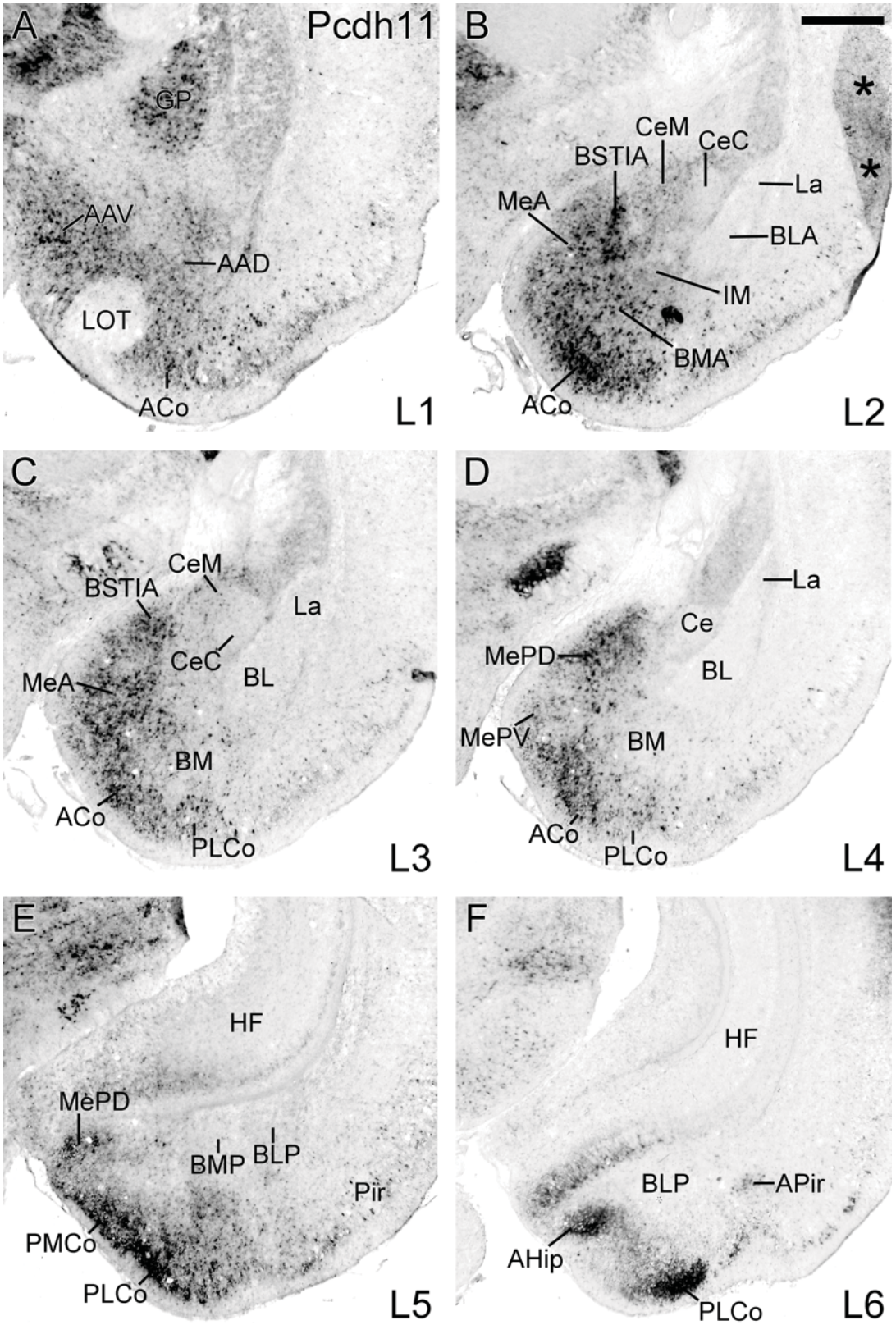

Figure 5.23. Expression mapping of protocadherin-11 (Pcdh11) in the wild-type amygdaloid complex in a series of adjacent frontal sections at postnatal day 5. Six different levels (L1-L6) are shown in a rostral-to-caudal sequence. Results were obtained by *in situ* hybridization with an mRNA probe for Pcdh11. Asterisks in B indicate an artefact. Scale bar in B = 500µm (applies to A-F).

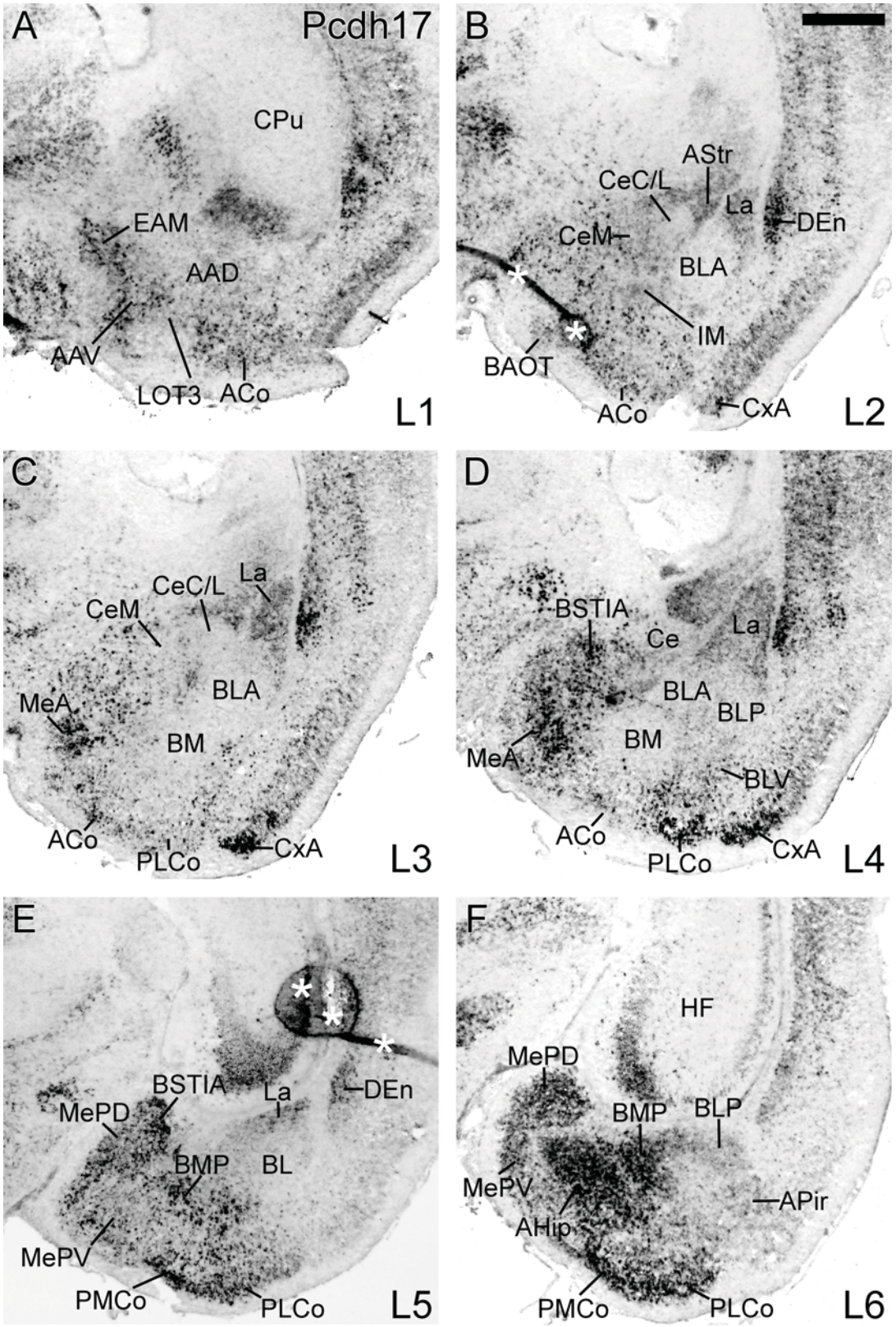

Figure 5.24. Expression mapping of protocadherin-17 (Pcdh17) in the wild-type amygdaloid complex in a series of adjacent frontal sections at postnatal day 5. Six different levels (L1-L6) are shown in a rostral-to-caudal sequence. Results were obtained by *in situ* hybridization with an mRNA probe for Pcdh17. The asterisks in B and E indicate artefacts. Scale bar in B = 500µm (applies to A-F).

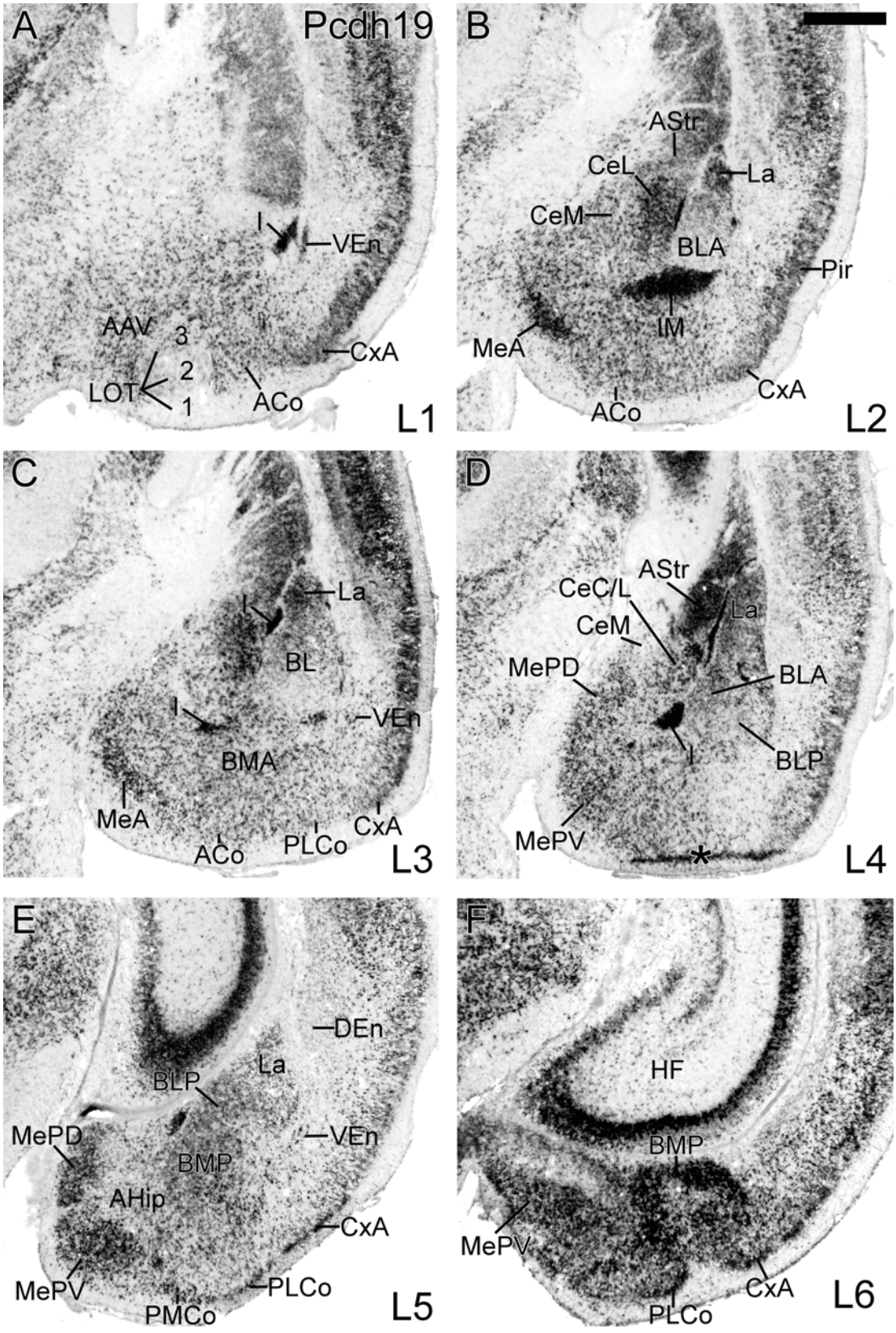

Figure 5.25. Expression mapping of protocadherin-19 (Pcdh19) in the wild-type amygdaloid complex in a series of adjacent frontal sections at postnatal day 5. Six different levels (L1-L6) are shown in a rostral-to-caudal sequence. Results were obtained by *in situ* hybridization with an mRNA probe for Pcdh19. Scale bar in B = 500µm (applies to A-F).

5.2.12 Protocadherin-17

The expression of Pcdh17 ranges from weak or moderate at rostral amygdalar levels, to strong or very strong at caudal levels (Fig. 5.24, Table 5.1).

Anterior, central, medial, and intercalated cell groups of the amygdala. Pcdh17 expression is weak or moderate in the anterior, central and intercalated masses of the amygdala, although some scattered cells exhibit strong signal in the anteroventral amygdala (AAD, AAV, Ce, IM, Fig. 5.24A-C). The medial amygdala displays a similar pattern at rostral levels, but Pcdh17 expression becomes stronger and patchy in the caudal part of the anterior subnucleus (MeA, Fig. 5.24C, D), and in the posterior subnuclei of the medial amygdala (MePD, MePV, Fig. 5.24E, F).

Basal amygdalar complex. The lateral amygdalar nucleus shows moderate Pcdh17 expression along its rostrocaudal extent (La, Fig. 5.24A-E). In contrast, the basolateral and basomedial nuclei are primarily free of signal at rostral levels (BLA, BMA, Fig. 5.24A-D), but the caudal parts of these nuclei present either moderate expression (BLP) or very strong and patchy expression (BMP, Fig. 5.24E, F).

Cortical amygdalar areas. Pcdh17 expression is weak or moderate in the nucleus of the lateral olfactory tract (layer 3, LOT3) and the anterior cortical amygdalar area (ACo, Fig. 5.24A, B). In contrast, the posterolateral and posteromedial cortical amygdalar areas show strong to very strong and patchy expression of Pcdh17 (PLCo, PMCo, Fig. 5.24D-F).

5.2.13 Protocadherin-19

Pcdh19 shows moderate to strong, patchy expression in many nuclei and areas of the amygdala (Fig. 5.25, Table 5.1).

Anterior, central, medial, and intercalated cell groups of the amygdala. Pcdh19 expression is moderate or strong and assumes a patchy appearance in the anterior, central and medial amygdala. It is very strong in the intercalated masses (AAD, AAV, Ce, Me, I, IM, Fig. 5.25A-E). In the central amygdala, the expression is strong with patches of very strong expression in the capsular and lateral parts (CeC, CeL, Fig. 5.25B, C), in the anterior, cortical part of the medial amygdala (MeA, Fig. 5.25B), and at the caudal poles of the posterodorsal and posteroventral subnuclei (MePD, MePV, Fig. 5.25E).

Basal amygdalar complex. Pcdh19 staining is strong and patchy in the rostral aspect of the lateral amygdalar nucleus. At caudal levels, signal becomes moderate and

is uniformly distributed (La, Fig. 5.25B-E). Expression is weak to moderate in the basolateral and basomedial amygdalar nuclei, although some patches of stronger staining are observed in the posterior part of the basomedial nucleus (BL, BM, Fig. 5.25B-E).

Cortical amygdalar areas. Pcdh19 staining is moderate in the anterior (ACo, Fig. 5.25A-C), posterolateral (PLCo, Fig. 5.25E) and posteromedial (PMCo, Fig. 5.25E) cortical amygdalar areas, although all of these regions contain strongly positive subpopulations of cells, which are scattered in ACo and more dense in the superficial layer 1 in PLCo and PMCo. Finally, the nucleus of the lateral olfactory tract shows low levels of Pcdh19 signal (LOT, Fig. 5.25A).

5.2.14 Cadherin expression in the amygdala of adult animals

To study the degree of similarity in cadherin expression between P5 brain and mature brain, we analyzed the expression of the thirteen cadherins and protocadherins in the amygdala of adult mice. Figures 5.26 and 5.27 show some examples of the expression profiles at a rostral and an intermediate amygdalar level. In general, the expression is highly conserved between P5 and the adult amygdala, with a few exceptions (Cdh8 and Pcdh8). Conserved expression profiles are observed, for example Cdh11, Pcdh7, Pcdh9, Pcdh11 and Pcdh19 in the LOT nucleus and in the anterior parts of the amygdala (Fig. 5.26). Other examples of conserved expression are presented in Fig. 5.27 for Cdh4, Cdh7, Cdh8, Pcdh7, Pcdh8 and Pcdh19 in the basal amygdalar complex at intermediate amygdalar levels. Cdh8 expression is less well conserved; in the adult amygdala, signal is found in regions that are positive at P5, but in addition, it is present in layer 2 of LOT (Fig. 5.26A), along the entire mediolateral extension of PLCo (not shown), and in scattered cells of the lateral and in basomedial amygdalar nuclei at caudal levels (not shown). Finally, the Pcdh8 staining in the adult amygdala is also highly similar to that at P5, except for an apparent downregulation of expression in the lateral nucleus (Fig. 5.27).

5.2.15 Double-labeling in situ hybridization for selected cadherin pairs

To visualize more clearly the multiple molecular subregions within the amygdala, double-label *in situ* hybridization was performed at P5 for selected cadherin pairs. The partially overlapping expression profiles for representative cadherin pairs (Fig. 5.28) allow a more complete delineation of the amygdaloid subregions and their boundaries.

For example, layer 2 of the nucleus of the lateral olfactory tract is positive for Cdh4 and Pcdh10 (LOT, Fig. 5.28A). Cdh4 signal is strong for the cortex-amygdala transition zone and delineates the boundary to the anterior cortical amygdaloid nucleus (CxA, ACo; Fig. 5.28A). This identification is also evident in the comparison between Cdh4 and Pcdh19: CxA and LOT2 are negative for Pcdh19 (Fig. 5.28B). The pair Cdh4/Pcdh8 defines the subdivisions within the central amygdalar nucleus. The capsular and the lateral part of the central nucleus express Cdh8, whereas only the medial part is positive for Cdh4 (CeM, CeC/L; Fig. 5.28C). Cdh8 is a marker for the basolateral amygdalar nucleus (Legaz et al., 2005, Medina et al., 2004). The pair Cdh8/Pcdh9 (Fig. 5.28D) defines the boundary between the basolateral nucleus and the lateral nucleus. Another cadherin pair to identify this boundary is Pcdh8/Pcdh19 (Fig. 5.28E). The lateral nucleus (La, Fig. 5.28E) is positive for Pcdh8 and the anterior basolateral nucleus (BLA, Fig. 5.28E) shows Pcdh19 expression. Subdivisions of the basolateral amygdalar nucleus can be distinguished with the pair Cdh4/Pcdh10. The posterior part and parts of the anterior basolateral nucleus are positive for Cdh4 (BLP, Fig. 5.28F), while only the anterior basolateral nucleus is positive for Pcdh10 (BLA, Fig. 5.28F).

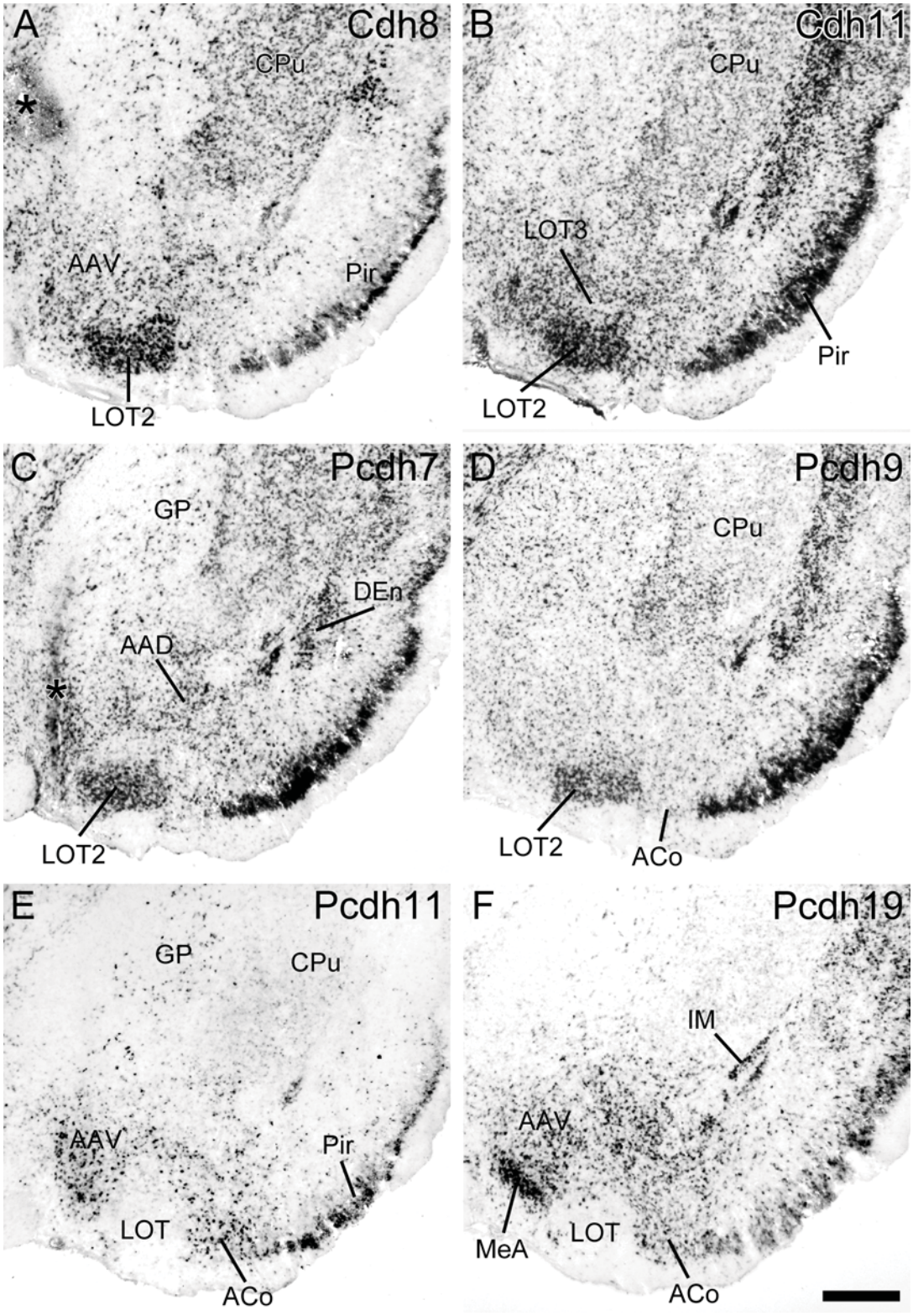

Figure 5.26. Cadherin expression in the wild-type adult mouse. *In situ* hybridization results obtained with cRNA probes for Cdh8 (**A**), Cdh11 (**B**), Pcdh7 (**C**), Pcdh9 (**D**), Pcdh11 (**E**) and Pcdh19 (**F**) are displayed for adjacent frontal sections through the amygdala at a rostral level. This level is compatible to level 1 in Figs. 5.13-5.25. Scale bar in F = 500µm (applies for A-F).

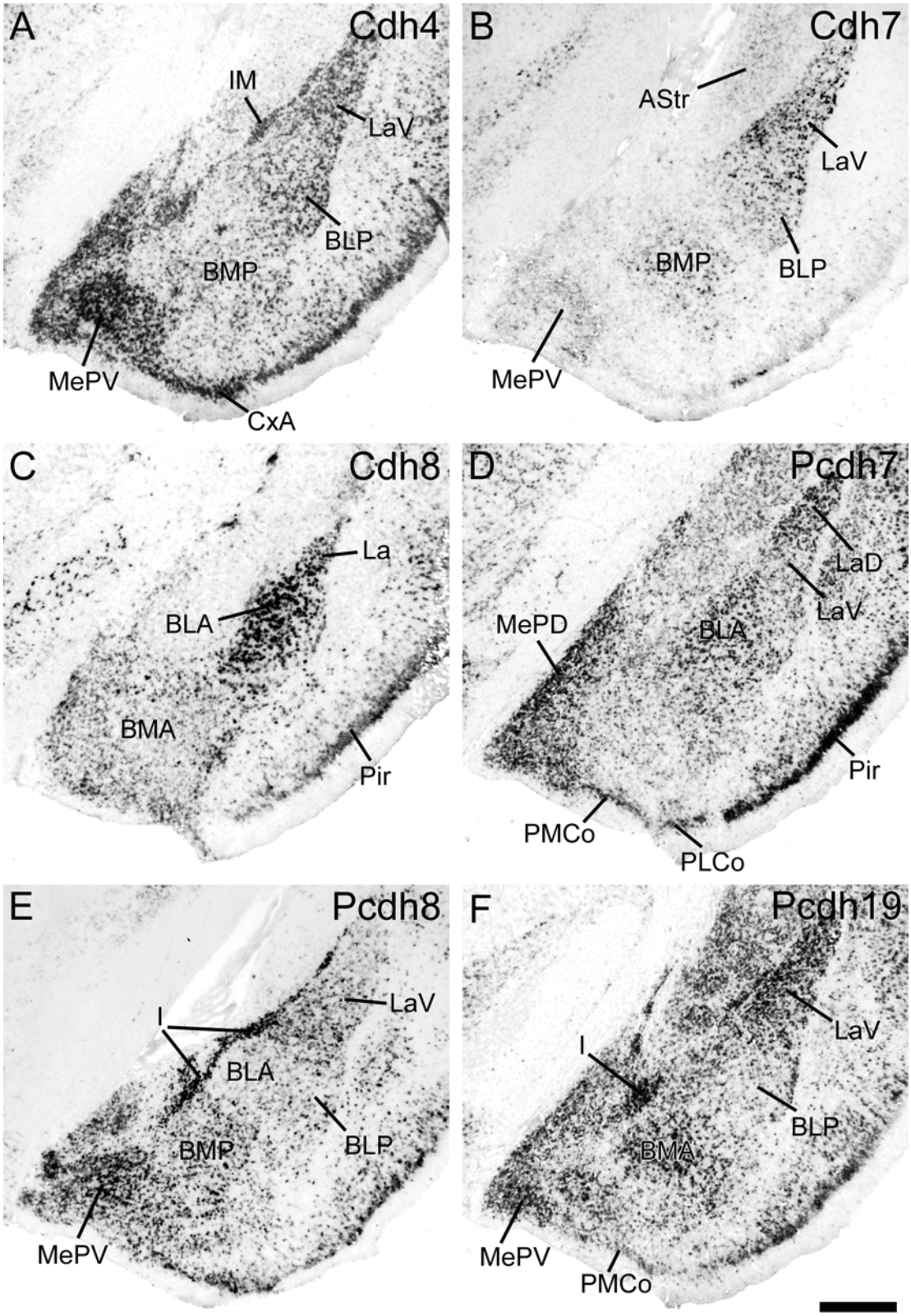

Figure 5.27. Cadherin expression in the wild-type adult mouse. *In situ* hybridization results obtained with cRNA probes for Cdh4 (**A**), Cdh7 (**B**), Cdh8 (**C**), Pcdh7 (**D**), Pcdh8 (**E**) and Pcdh19 (**F**) are displayed for adjacent frontal sections through the amygdala at a caudal level. This level is compatible to levels 3 and 4 in Figs. 5.13-5.25. Scale bar in F = 500µm (applies for A-F).

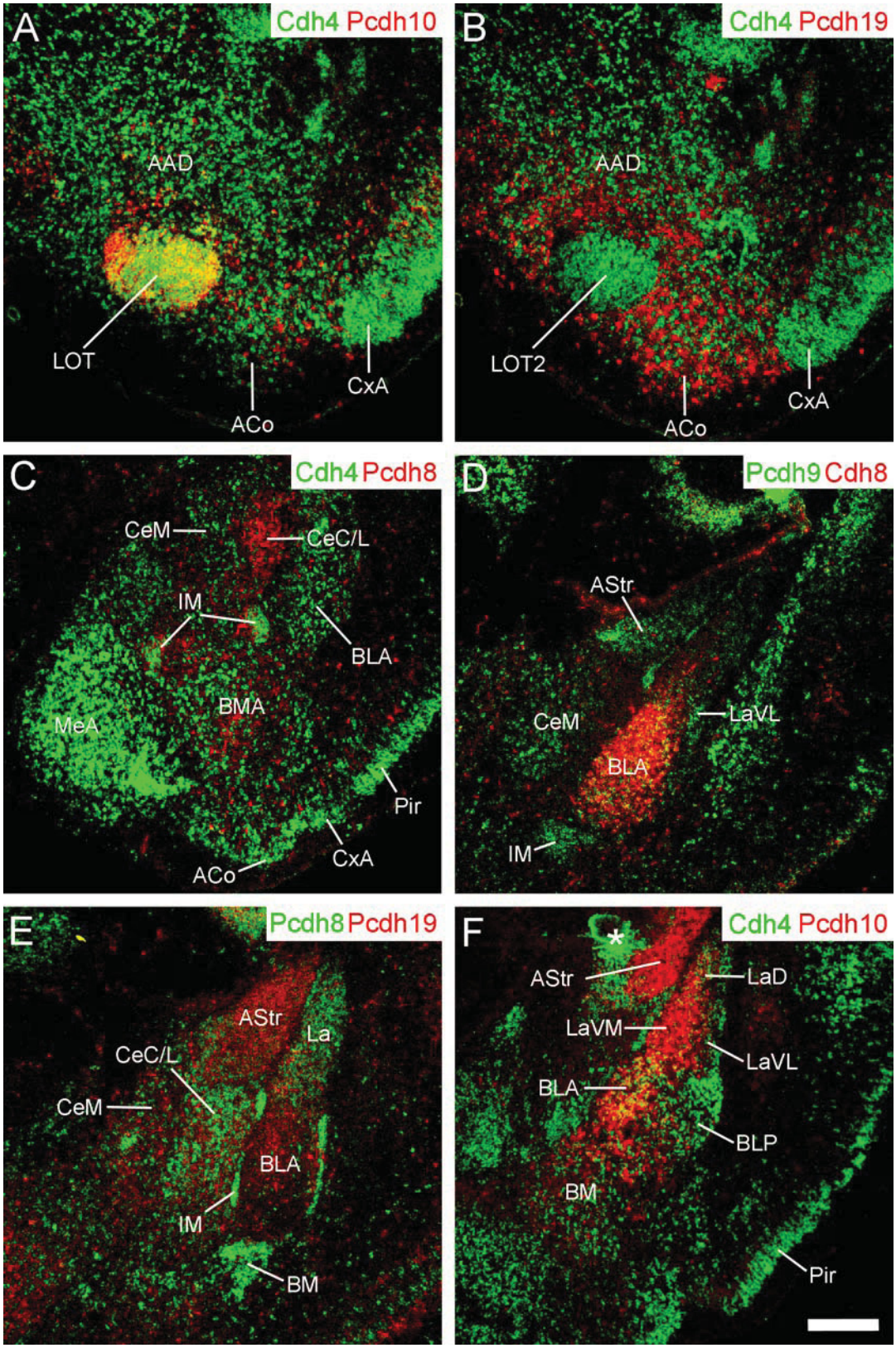

Figure 5.28. Combinatorial expression mapping of cadherins/protocadherins allows the distinction of multiple amygdalar subdivisions. Frontal sections of the entire amygdaloid area were double hybridized *in situ* with cRNA probes in wild-type P5 mice. Five pairs of cadherins (Cdh4/Pcdh10 [**A, F**], Cdh4/Pcdh19 [**B**], Cdh4/Pcdh8 [**C**], Pcdh9/Cdh8 [**D**] and Pcdh8/Pcdh19

[**E**]) were analyzed. In the pseudocolor-coded overlays, colors represent cadherin staining. The asterisk in F indicates an artefact. The level in panel A, B corresponds to level 1 in Figs. 5.13-5.25, in panel C-F to levels 3 and 4 in Figs. 5.13-5.25. Scale bar, 250µm in F (applies to A-F).

5.2.16 Cadherin expression in the amygdala of the Reeler mutant mouse

In this section, I studied the spatial arrangement of amygdalar regions in Reeler mutant mice based on the cadherin mapping results from wild-type mice. A particular focus was put on differences between pallial and subpallial subregions of the amygdala because it has been proposed that pallial brain regions are affected by the Reeler mutation while subpallial parts are not.

In addition to the cadherins, I used Tbr-1 as a general pallial marker (Puelles et al., 2000). Pallial parts of the amygdala are the cortical areas. Therefore, Tbr-1 was a good additional marker to identify pallial regions within the Reeler amygdaloid complex, for example the nucleus of the lateral olfactory tract (LOT), which has a three layered appearance in wild-type mice (Fig. 5.29B). The LOT cells originate at the caudalmost part of the telencephalic neuroepithelium and migrate a considerable distance to their final, superficial destination. In the Reeler amygdaloid complex, LOT can be identified by its characteristic expression of Tbr-1 (Fig. 5.29C), Pcdh10 (Fig. 5.29F) and, as a negative marker, by Pcdh19 (Fig. 5.29I). Strikingly, the LOT cells in the Reeler mutant form a circular aggregate at a deep position in the amygdala next to the basolateral complex, which is normally situated more caudally in wild-type mice (Fig. 5.29 C, F, I). Interestingly, the basolateral complex and other subpallial parts of the Reeler amygdala are located at positions similar to those in wild-type mice (Fig. 5.30). The anterior basolateral nucleus, a subpallial derivative, is characterized by strong expression for ER81 in wild-type mice (BLA; Fig. 5.30, B). Cdh8 is another marker for the basolateral nucleus (Medina et al., 2004). In the Reeler mutant, the two markers indicate that the basolateral nucleus can be found at positions typical for wild-type mice (Fig. 5.30 C, D). Moreover, Pcdh7 expression can be used to distinguish more strongly positive dorsal parts (LaD; Fig. 5.30 E, F) and more weakly positive ventral parts (LaV; Fig. 5.30 E, F) within the lateral amygdaloid nucleus (part of the deep pallium). Pcdh8 displays a gradient expression within LaV in wild-type (Fig. 5.30 G). A similar staining profile is also visible at about the same position in the Reeler mutant (Fig. 5.30H). The posterior part of the basomedial amygdaloid nucleus (BMP), part of the deep pallium, shows moderate expression for Pcdh8 in wild-type (Fig. 5.30G) and

Reeler (Fig. 5.30H) and seem to be unaffected in the mutant. However, the posteroventral part of the medial amygdaloid nucleus (MePV) that is a Pcdh8-positive cortical pallial part (Fig. 5.30G), is either more scattered so that expression seems less strong, or it is located more caudally because of the migration defects in the Reeler mutant (Fig. 5.30H).

In summary, my results provide evidence that the cortical pallial parts of the amygdaloid complex are disorganized in the Reeler mutant, but the deep pallial and subpallial nuclei seem to be unaffected.

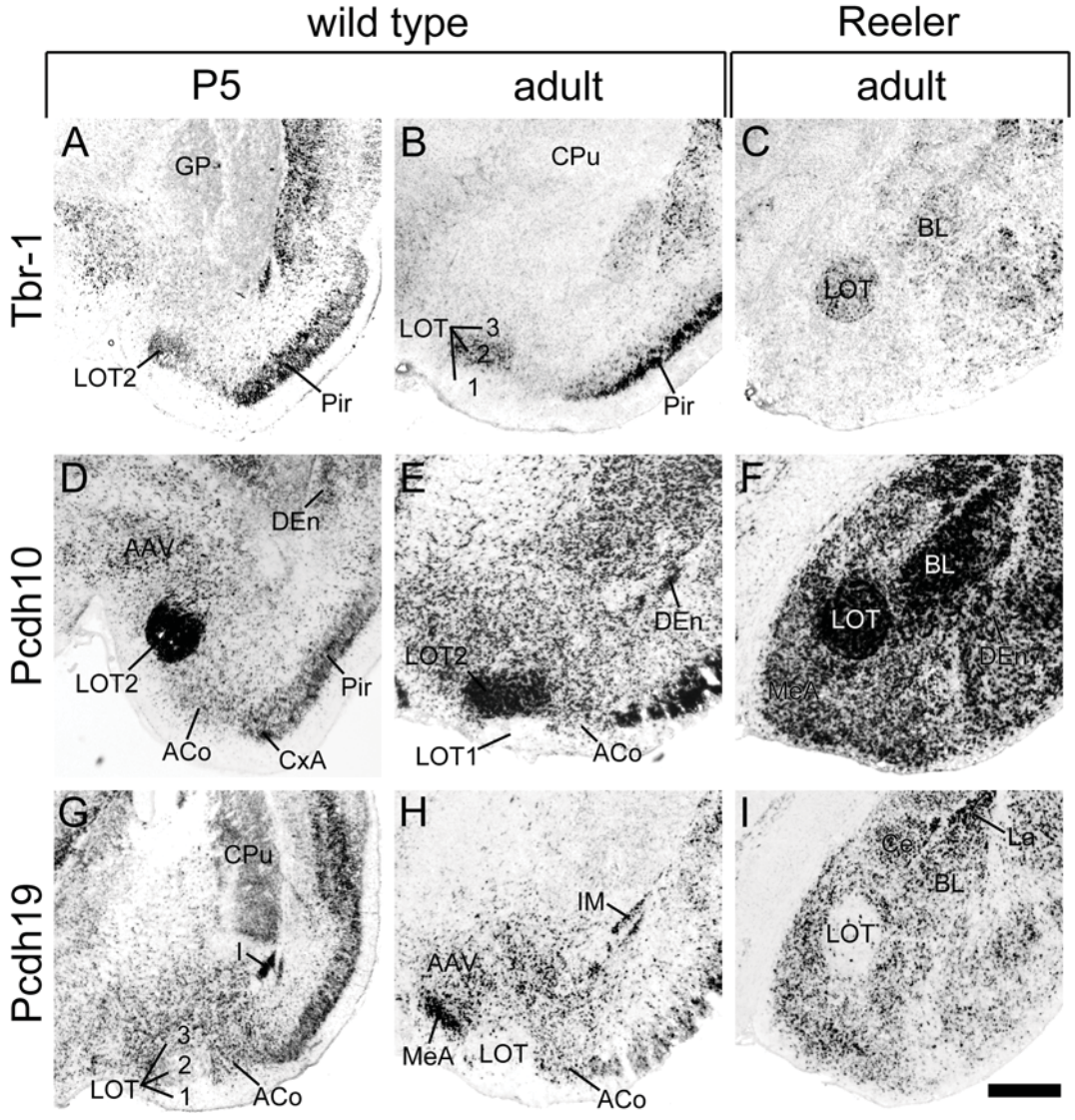

Figure 5.29. A comparison of gene expression patterns in the amygdala of wild-type mice and Reeler mutants at a rostral level. Cortical amygdaloid areas are shown. Representative results for *in situ* hybridization with mRNA probes for Tbr-1 (**A**, **B** and **C**), Pcdh10 (**D, E** and **F**) and Pcdh19 (**G**, **H** and **I**) are presented for adjacent frontal sections of the P5 and adult wild-type amygdala and the adult Reeler mutant amygdala as indicated on the top of the figure. Scale bar in I = 500µm (applies to A – I).

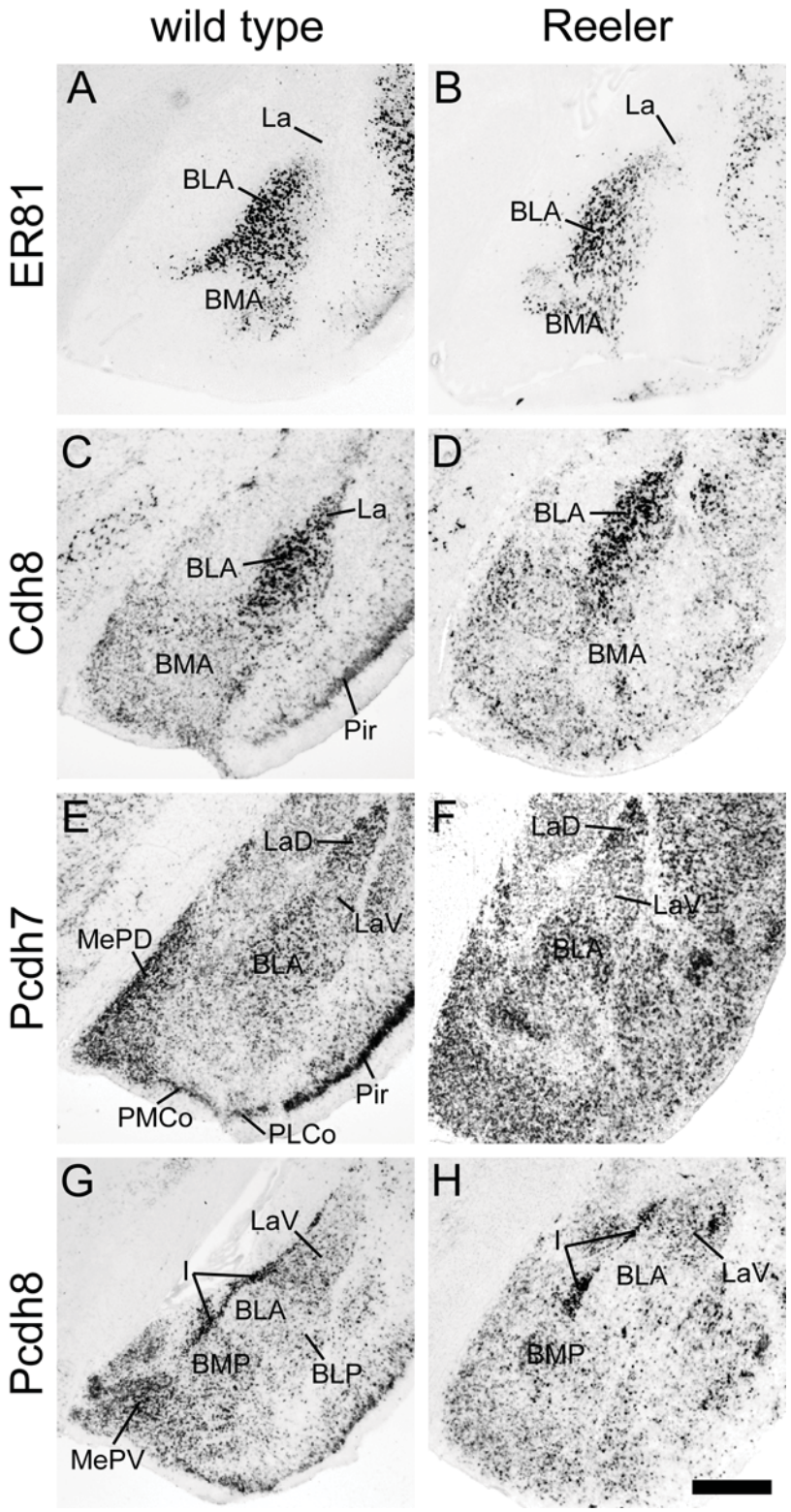

Figure 5.30. Comparison of gene expression patterns in the amygdala of wild-type mice and Reeler mutants at an intermediate level. Pallial and subpallial nuclei are shown. Representative results for *in situ* hybridization with mRNA probes for ER81 (**A** and **B**), Cdh8 (**C** and **D**), Pcdh7 (**E** and **F**) and Pcdh8 (**G** and **H**) are presented for adjacent frontal sections of the adult wild-type and Reeler mutant amygdala, as indicated on top of the figure. Scale bar in H = 500µm (applies to A – H).

6. DISCUSSION

In this thesis, I used cadherin expression mapping to study the histoarchitecture of the cerebral cortex and the amygdaloid complex in wild-type mice and Reeler mutants. By *in situ* hybridization, the expression of thirteen different cadherins in three neocortical regions (the cingulate cortex, the motor cortex and the primary somatosensory cortex), the allocortical hippocampal region and the amygdaloid complex was examined.

In the cerebral cortical regions, each cadherin shows a layer-specific expression profile in wild-type mice. In contrast, the Reeler mice exhibit a widespread distribution of cadherin-expressing cells throughout all cortical layers. A comparison between wild type and Reeler mice revealed no evidence for an "outside-in" layering in Reeler mice. Strikingly, the area-specific expression of the cadherins is preserved in the Reeler cortex.

To map the expression of the cadherins in the amygdala, the expression of classic cadherins and δ-protocadherins was studied in the postnatal (P5) and adult mouse amygdala. Each cadherin shows a specific expression pattern in the different amygdaloid subdivisions, which is highly similar between P5 and the adult mouse. However, at P5, neuropil is less differentiated so that cellular aggregates corresponding to amygdaloid subdivisions can be visualized more easily by *in situ* hybridization. The combinatory expression of the cadherins allows the distinction of multiple molecular subdivisions within the amygdala that go beyond the strict morphological divisions. Cadherins thus provide a descriptive molecular code for defining the functional organization of the amygdala. Additionally, the cadherins were used as markers to analyze the amygdala of the Reeler mutant mouse. Reelin, a molecule critical for neuronal migration in the neocortex, is expressed in cortical areas of the amygdala, but not in deep nuclei (Remedios et al., 2007). The results provide evidence that the cortical pallial parts of the amygdaloid complex are disorganized in the Reeler mutant, but the deep pallial and subpallial nuclei seem to be unaffected.

The Discussion chapter is divided into five parts. Parts 6.1-6.3 are contained, in modified form, in Hertel and Redies (2011).

6.1 A cadherin-based code of potentially adhesive cues for cerebral cortical layers and the regions of the amygdala in wild-type mice

It has been proposed previously that cadherins provide an adhesive code for developing brain structures, neural circuits and synapses (for reviews, see Redies, 2000; Hirano et al. 2003; Takeichi, 2007). In the present thesis, I show that each of the thirteen cadherins studied exhibits a unique, spatially restricted expression pattern in the cortical layers (neo- and allocortex) of the adult mouse as well as in the postnatal and mature amygdaloid complex, although partial overlap between the cadherins is observed. Vice versa, each layer of cerebral cortex and each nucleus of the amygdala are characterized by the expression of a subset of cadherins. The cadherin-based code for specifying neo- and allocortical layers and amygdaloid subdivisions is probably a combinatorial one because each layer/area is characterized by the expression of multiple cadherins. Although I show results only for three neocortical regions (somatosensory, motor and cingulate cortex) and the allocortical hippocampal region (see also Kim et al., 2010), similar results were obtained for other cortical regions in the mouse (Redies and Takeichi, 1993; Suzuki et al., 1997; Korematsu et al., 1997b; Kim et al., 2007), in ferret visual cortex (Krishna-K. et al., 2009), in the cerebellum (Neudert et al., 2008; Neudert and Redies, 2008; Redies et al., 2010) and in other layered central nervous system structures, for example, in the vertebrate retina (Wöhrn et al., 1998; Faulkner-Jones et al., 1999a, b; Honjo et al., 2000; Etzrodt et al., 2009) and in the chicken tectum (Wöhrn et al., 1999). A region-specific expression of cadherins in non-layered (roundish) nerve cell aggregates, like that observed throughout the amygdaloid complex, has been described before for brain nuclei (Redies et al. 1993; Suzuki et al. 1997; Hirano et al. 1999; Redies et al. 2000, 2005; Bekirov et al. 2002; Vanhalst et al. 2005; Kim et al. 2007) and in patch/matrix type of gray matter architecture (Heyers et al., 2003; Hertel et al., 2008) of the vertebrate brain. Furthermore, it has been shown that the classic cadherins Cdh4, Cdh6, Cdh7, Cdh8 and Cdh11 and the δ-protocadherin Pcdh-10 are expressed at the synapse (Arndt et al., 1998; Hirano et al., 1999; Tang et al., 1998; Yamagata et al., 1999; Manabe et al., 2000; Wang et al., 2002). Their expression both at the critical (postnatal) stage of synapse formation and in the adult brain suggests that at least some of the investigated cadherins play roles during synapse formation as well as in the maintanance of synaptic connections.

Other members of the δ-protocadherin subfamiliy might also play roles in the formation and stabilization of neural connections. For example, the δ2-protocadherin

Pcdh18 has been shown to interact directly with the intracellular adaptor protein disabled-1 (Dab-1) that regulates axon outgrowth in the developing nervous system (Homayouni et al., 2001). Dab-1 is a downstream component of the Reelin signaling pathway, which controls neural positioning in the vertebrate brain (Bar et al., 2000). Another family of protocadherins, the α-protocadherins or CNRs, interacts intracellularly with the tyrosine kinase Fyn, a key regulator of synaptic plasticity and LTP (Kohmura et al., 1998). The proposal that the CNRs are receptors for Reelin (Senzaki et al., 1999) has been questioned by Jossin et al. (2004). Last but not least, the δ1-protocadherins Pcdh1, Pcdh7, Pcdh9 and Pcdh11 possess an intracellular motif that binds to protein phosphate 1α (PP1α; Yoshida et al., 1999; Redies et al., 2005; Vanhalst et al., 2005). This molecule regulates synaptic plasticity (Terry-Lorenzo et al., 2002), and isoform C of Pcdh7 was shown to inhibit the activitiy of PP1α (Yoshida et al., 1999).

6.2 Loss of layer-specific cadherin expression in Reeler cortex and cortical amygdaloid areas

In the cerebral/amygdaloid cortex of Reeler mutants, the expression of each cadherin is not restricted to specific layers, but positive cells are more widely scattered across the entire cortical thickness or form clusters of cells within the mature brain and P5 brain. These results suggest that the disorganization of the cortical layers in Reeler mouse leads to a disruption of the cadherin expression. In parallel, the histoarchitecture of the neo- and allocortical parts are also rather homogenous (Figs. 5.4A', 5.5B', 5.7A', 5.8A', 5.12A'). Similarly scattered expression patterns in Reeler neocortex were reported previously for Fez1 (Inoue et al., 2004) and for Cux2 (Ferrere et al., 2006; Figs. 5.2, 5.3) that are markers of layer V projection neurons and layer II/III neurons, respectively, in wild-type cortex. Moreover, several tracing studies have demonstrated that layer V pyramidal neurons are scattered along the radial axis in Reeler mutant mice and rat (for a review, see Katsuyama and Terashima, 2009). Despite the scattering of neurons across the radial dimension, we obtained evidence that regionalization is not affected in Reeler cortex and amygdaloid areas because the regional prevalence of cells expressing particular cadherins is similar to that observed in wild-type mice (Figs. 5.5, 5.8, 5.10, 5.12, 5.29, 5.30). These results confirm previous studies that showed a preservation of regional specificity in the Reeler cortex (Polleux et al., 1998, 2001). Also, the areal targeting of the superplate by thalamocortical axons in Reeler mutants is

indistinguishable from that in wild-type mice (Molnar et al., 1998).

Previous findings demonstrated that the subplate markers ER81, Foxp2 and Tbr-1 are found beneath the surface of the Reeler and Scrambler cortex (Hoerder-Suabedissen et al., 2009; Dekimoto et al., 2010; for ER81 and Tbr-1, see also Figs. 5.2 and 5.3). Our results for cadherins are compatible with this finding because cadherin subtypes that are expressed in the deep part of layer VI (adjacent to the white matter) in wild-type mice are found at subpial positions in Reeler cortex (see Fig. 5.4C, C' for Cdh6; Fig. 5.4G, G' for Pcdh11; Fig. 5.4H, H' for Pcdh17; and Fig. 5.4I, I' for Pcdh19).

The disruption of layer-specific expression of cadherins and other molecular markers in Reeler cortex (see above) is surprising because it is generally believed that Reeler cortex displays a reverse, outside-in layering (Caviness and Sideman, 1973; Caviness, 1982). This hypothesis is based on a [^{3}H] thymidine birthdating study by Caviness (1982) who showed that early and late born neurons were unable to ascend through the zone occupied by the preceeding cohorts during cortical development. This defect is thought to result in a lamination pattern of the Reeler cortex that is inverted in terms of the birthdate of the cohorts of neurons. Later studies described the Reeler cortex as nearly inverted with not well differentiated layers (Kubo and Nakajima, 2003; Tissir and Goffinet, 2003). This idea was extended by the notion that early radially migrating neurons are not able to split the preplate due to the lack of Reelin (D'Arcangelo et al., 1995; Ogawa et al., 1995, D'Arcangelo et al., 1997). Our results on cadherin expression are compatible with an inversion of deep layer VI, but not with an inversion of other cortical layers. One possible explanation for this discprepancy is that early cortical neurons change their expression of layer-specific molecular markers after their displacement in Reeler cortex, as was observed for early branchiomotor neurons after their migration across the alar/basal plate boundary (Ju et al., 2004). However, cadherin expression is relatively stable throughout development in most other brain regions (Redies, 2000). Furthermore, Dekimoto et al. (2010) published results similar to mine with other molecular markers (ER81, Tbr-1, mSorLa and ROR-beta). Future studies will have to address some of these discrepancies by combining birthdating studies with the mapping of layer-specific genes.

A comparison of cadherin expression in developing and adult neocortex does not provide evidence for an initially inverted lamination that is lost later in development. Rather, the observed defect in layering is compatible with an abnormal migration pattern. The processes of radial glial cells, which are crucial for migration of early

cortical neurons, are significantly reduced in number and length in Reeler cortex (Hartfuss et al., 2003). Schaefer et al. (2008) demonstrated that Reelin contributes to the elongation of radial glial cells and is essential for neuronal positioning in neonatal ferret cortex. It is therefore conceivable that the scattered distribution pattern of cadherin-expressing neurons results from radial glial malfunction or an abnormal interaction of migrating neuroblast with radial glia. The absence of layer-specific cadherin expression profiles in Reeler cortex coincides with a misorientation of the dendritic processes of cortical neurons, which point in various directions (for reviews, see Katsuyama and Terashima, 2009; Frotscher et al., 2009, 2010). In contrast, wild-type apical processes are arranged in regular arrays that are oriented with respect to the radial dimension. The misdirection of dendritic processes in the Reeler cortex may be a consequence of loss of lamination of cadherin-based adhesive cues. Supporting these ideas, N-cadherin was shown to play a role in layer-specific growth cone movement in chicken and Drosophila (Inoue and Sanes, 1997; Nern et al., 2008). Other classic cadherins (for example, Cdh4, Cdh6 and Cdh7) are involved in the migration of axons (Treubert-Zimmermann et al., 2002) and in the extension of the leading axon of neuroblasts (Luo et al., 2004; Taniguchi et al., 2006).

6.3 Cadherin-mediated adhesive properties and patch formation

Although cells positive for each cadherin are found throughout all neocortical layers and cortical amygdaloid areas that are affected in the Reeler mutant brains, there is evidence for type-specific cell sorting that is typical for cadherin expression: cells that express specific cadherins are often found in clusters. This result suggests that cadherin-mediated adhesion and sorting of early neurons in the cortical plate and the pallial/subpallial origins is not completely abolished, as also indicated by previous studies (Ichinohe et al., 2008). Interestingly, in the neocortex there is a relation between the molecular marker L1, which labels afferent fiber fascicles in wild-type layer IV (Chung et al., 1991), and Pcdh8-expressing cell clusters. Pcdh8, which is not expressed in layer IV, labels L1-negative cell clusters in Reeler cortex. Pcdh19, which is expressed in layer IV, labels patches complementary to the Pcdh8 patches (Fig. 5.9G-L). Whether the cadherin-expressing cell clusters in Reeler cortex retain other properties of wild-type cortical layers remains to be studied in the future.

In several nuclei/areas of the wild-type amygdala, cadherin-expressing patches or cell aggregates can be observed. Such clusters are observed at P5, but also in the

adult amygdala, and appear to represent a previously unknown feature of amygdalar organization. Based on data from other areas, it is possible that these amygdalar cell aggregates or patches relate to cells of similar embryonic origins, birth date and/or similar connectivity patterns. Cadherins are differentially expressed also in other brain structures of the chicken telencephalon and mouse basal ganglia that display patch-like gray matter architecture (Heyers et al., 2003; Hertel et al., 2008). The striosomes and the surrounding matrix in the mouse basal ganglia are an example of this type of gray matter architecture (Redies et al., 2002). In both structures, as well as in cerebral cortex, there is a relation between adhesive properties and the birthdate of neurons. Interestingly, in mixed cultures of cells from basal ganglia and neocortex, early-born neurons but not late-born neurons selectively aggregate (Krushel and van der Kooy, 1993). This result indicates that similar adhesive mechanisms act throughout the telencephalon. It has been proposed that the action of Reelin in the cortical plate plays a crucial role in layer formation (for comprehensive reviews Rice and Curran, 2001; D'Arcangelo, 2006). It is therefore noteworthy that, in the absence of Reelin, cortical gray matter contains patchy aggregates of cells that express cadherins differentially.

6.4 Do the cadherin-expressing subdivisions and regions reflect the functional organization within the amygdaloid complex?

The combinatory expression of the thirteen cadherins studied in the amygdala allows the distinction of multiple molecular subdivisions that appear to be related to cell populations with different connectivity patterns. In fact, it has been proposed that the amygdala is neither anatomically nor functionally a single unit but should be divided, with its parts included in various other functional systems (Swanson and Petrovich, 1998; Pitkänen et al., 1998; Pitkänen, 2001). It is not feasible to analyze the cadherin profile of each amygdalar pathway with the scope of this discussion, but I will mention a few representative connections below.

Most of the cadherins exhibit regionalized expression within the different nuclei of the amygdala. For example, Pcdh1 shows strong expression in the medial part of the anterior basolateral nucleus (BLA; Fig. 5.18D), but weak staining in the lateral portion of this nucleus. The dorsal part of the lateral nucleus (LaD) shows strong expression for Pcdh7, whereas the ventral part (LaV) is more weakly stained (Fig. 5.19D). The medial amygdala exhibits strong Pcdh9-positive patches in the posteroventral part (MePV; Fig. 5.21 E, F) but the posterodorsal part (MePD) shows almost no Pcdh9 expression. This

regionalization may reflect the functional differentiation and the establishment of interconnections with other amygdaloid nuclei or brain areas, as previously shown for other brain regions (for reviews, see Redies, 2000; Hirano et al., 2003). The input from other brain areas reaches the amygdala via different amygdaloid nuclei. The information becomes processed within these nuclei or may be delivered into one or more amygdaloid regions via intra-amygdaloid circuitry. Therefore, information becomes processed in parallel at several amygdaloid locations. The resulting behavioral response is the sum of the modulated signal representations. The input and output of the amygdala is often organized in a topographic manner. For example, different parts of the cerebral cortex, including the parietal cortical areas, insular cortex and temporal cortex, project to the different divisions of the lateral nucleus (McDonald, 1998; Shi and Cassell, 1999). Gustatory, visceral and somatosensory cortical areas provide input to the rostral portion of the dorsolateral and the medial divisions, whereas the auditory and visual cortical areas provide input to the caudal portion of these divisions. All these regions exhibit a combinatorial cadherin expression pattern. Cdh7, Pcdh8 and Pcdh19, for example, are expressed strongly in the different divisions of the lateral nucleus (Figs. 5.15E, 5.20D, and 5.25D) and are also expressed in different layers of the somatosensory cortex (Fig. 5.6). Moreover, Pcdh11 shows no expression in the lateral amygdaloid nucleus (Fig. 5.23C, D) and it is largely absent in the somatosensory cortical areas (Fig. 5.6A).

Another example is the projection from the basal nucleus to the basal ganglia. The BLA division (magnocellular) projects to the caudolateral caudate putamen, and the posterior and lateral (parvicellular) divisions (BLP and BLV) project to the rostromedial caudate putamen (Wright et al., 1996). Cdh7 is strongly expressed in the BLP and BLV (Figs. 5.15D, E; 5.27B), but shows no expression in the BLA (Fig. 5.15C, D). Correspondingly, in the caudate putamen, Cdh7 expression is limited to the rostral part of the matrix, including its rostromedial portion (see Figs. 3, 5 in Hertel et al., 2008) in P5 and adult mice. Pcdh19, as another example, shows moderate expression in the BLA, but only light expression in the BLV and moderate signal in BLP (Figs. 5.25B, D, E; 5.27F). In the caudate putamen, there is a general increase of Pcdh19 expression from rostral to caudal resulting in a strong expression of the entire caudal striatum, including the caudolateral part (see Fig. 7M-P in Hertel et al., 2008). These data suggest that the amygdala is a component of the cortico-striato-pallidal output circuit that is involved in

control of neuroendocrine and autonomic systems (Swanson, 2000; Garcia-Lopez et al., 2008).

The amygdaloid complex includes pallial/cortical, striatal, pallidal, peduncular and subpallial derivatives (Puelles et al., 2000; Medina et al., 2004; Garcia-Lopez et al., 2008). The medial amygdala, for example, consists of a peduncular (MePD) derivative and a subpallial (MePV) derivative (Petrovich et al., 2001, Choi et al., 2005). The medial amygdala is one of the main centers projecting throughout the stria terminalis, and targets the ventromedial hypothalamic nucleus, among other areas. A previous publication using both immunohistochemistry and *in situ* hybridization reported the expression of R-cadherin (Cdh4) in the anterior commissure and the stria terminalis (Obst-Pernberg et al., 2001). The stria terminalis constitutes one of the major ouput fiber tracts with descending projections of the amygdala to the hypothalamus and brainstem (Alheid and Heimer, 1988; de Olmos et al., 2004). In the rat, the projections of the dorsal and ventral posterior parts of the medial amygdala (MePD, MePV) to the ventromedial hypothalamic nucleus are segregated, targeting distinct parts of the nucleus involved in either reproduction or defense (Choi et al., 2005). The data presented in my thesis indicate that the two parts of the posterior medial amygdala (MePD and MePV) express different combinations of cadherins: for example, MePD expresses high levels of Pcdh7 (Fig. 5.19D), Pcdh8 (Fig. 5.20C), Pcdh10 (Fig. 5.22E) and Pcdh11 (Fig. 5.23D). In contrast, MePV shows no expression for Pcdh10 (Fig. 5.22D-F) and Pcdh11 (Fig. 5.23D). Additionally, MePV shows moderate expression of Pcdh7 (Fig. 5.19D) and Pcdh8 (Fig. 5.20C, D), and is strongly Pcdh9 positive (Fig. 5.21 E, F). Cadherins are also expressed in different patterns and subdomains in the ventromedial hypothalamic nucleus of the mouse (Vanhalst et al., 2005), although the relation to the specific target areas in the medial amygdala is not clear. This point requires further investigations.

Another interesting example is the point-to-point, non-overlapping projection of the medial amygdala as well as the medial division of the lateral nucleus and the parvocellular part of the basomedial nucleus to the entorhinal cortex of the hippocampal region (McDonald, 1998; Pikkarainen et al., 1999; Petrovich et al., 2001). These projections terminate in different layers (layers III and V), respectively. The amygdalar projection and its entorhinal target layers display, at least in part, corresponding cadherin expression profiles. For example, Cdh7 and Cdh11 show strong expression in the medial division of the lateral nucleus and in the basomedial nucleus (Figs. 5.15,

5.17, Table 5.1) of the amygdala. In the entorhinal cortex of the hippocampal region, the layers III and V show moderate to strong expression for Cdh11 (see Fig. 5.12B) and Cdh7 (data not shown). Similarly, Pcdh19 is moderately expressed in the basomedial nucleus of the amygdala and the deep layers of the entorhinal cortex (Figs. 5.12D; 5.25; see also Kim et al., 2010). Vice versa, Cdh6 and Pcdh11 show almost no expression in the medial subdivision of the lateral amygdaloid nucleus (Figs. 5.14; 5.23D, E) and also no expression in the upper layers II and III of the entorhinal cortex (data not shown). This leads me to the suggestion that cadherins possibly play a role in functional connectivity between the amygdala and the hippocampal region within the medial temporal lobe memory system.

Cadherins have been suggested to contribute to the formation of the olfactory networks (Akins et al., 2007). Mitral and tufted cells of the main and accessory olfactory bulbs express Cdh4, Cdh6 and Cdh11 in their cell bodies and/or axons (Akins et al., 2007). Moreover, axons in the lateral olfactory tract express Cdh4 and Cdh11 (Obst-Pernberg et al., 2001; Akins et al., 2007). Cdh4 and Cdh11 are strongly expressed in the amygdala (Figs. 5.13, 5.17), including all olfactory targets (cortical amygdalar areas, nucleus of the lateral olfactory tract, nucleus of the accessory olfactory tract, and medial amygdala; Martínez-Marcos, 2009). Therefore, it is possible that cadherins play also a role in the formation of olfactory projections to the amygdala. Interestingly, Cdh6 expression appears to be restricted to subpopulations of mitral cells of the olfactory bulbs (Akins et al., 2007). This expression profile is correlated with the observation that Cdh6 is expressed only in scattered subpopulations of cells in some olfactory targets in the amygdala (Fig. 5.14A, B, E; for olfactory connections, see Martínez-Marcos, 2009). Cdh4, Cdh6 and Cdh11 expression in the mitral and tufted cells was investigated during embryonic development (E15) and during the first postnatal week (P0, P7) (Akins et al., 2007). In this thesis, the expression of these cadherins was observed during the first postnatal week (P5) and in the adult. The above findings suggest that cadherins may play roles in the olfactory projection to the amygdala, by regulating axonal pathfinding, synaptogenesis, and later in development, synaptic stabilization and plasticity.

In summary, the above examples suggest that cadherins might play an important role in the morphogenesis of the different subdivisions of the amygdala, the regionalization within the different nuclei, and the formation of their functional connectivities. Consequently, we identified a cadherin-based code for the functional architecture of amygdala. This code may be relevant for understanding the functional

organization of the amygdala as well as the subdivisions of amygdala-associated brain nuclei, cortical layers and neural circuits.

6.5 Reelin-dependent migration of the caudal amygdaloid stream

An interesting proposal of the origin of the nucleus of the lateral olfactory tract (LOT) was published by Remedios et al. (2007). LOT has been described as a three-layered structure that is connected with the olfactory bulb and the piriform cortex (Luskin and Price, 1983; Santiago and Shammah-Lagnado, 2004). Pax6, a developmental transcription factor, exhibits a differential expression within the three layers of this nucleus. Layer 1 of LOT (LOT1) and other surrounding amygdaloid structures are Pax6-negative whereas LOT2 and the deep nuclei La, BL and BM express Pax6 (Tole et al., 2005). This differential expression corresponds to differences in the origins of these nuclei. Remedios and co-workers (2007) provided evidence that LOT2 originates in the dorsal pallium (which also generates the neocortex) at a caudalmost position within the telencephalic neuroepithelium. From here, cells migrate rostrally, forming the caudal amygdaloid stream that finally reaches LOT2. This migration requires Reelin and Cdk5, two molecules critical for radial glial migration in the neocortex (Ohshima et al., 1996; Chae et al., 1997). However, mutants in Cdk5 (an intracellular kinase) that also affect cortical migration, differ from the Reeler phenotype. In contrast to the situation in Reeler mutants, preplate splitting does occur in Cdk5 mutants (Ohshima et al., 1996; Chae et al., 1997), although the splitting is abnormal (Rakic et al., 2006). Layers with the late-born neurons have a disrupted migration in the Cdk5 mutants (Gilmore et al., 1998). This difference may be attributed to the different modes of migration of early-born cells and late-born cells (Nadarajah et al., 2001). The cells of the caudal amygdaloid stream are born at early stages and require Cdk5 for their migration. In contrast, in the Reeler mutant, the cells of the LOT2 seem to be misdirected. LOT2 appears at more caudal levels than in wild type, but the positioning only, not the specification of the cells, seems perturbed (Fig. 5.29C, F, I). This finding can be explained by the expression of Dab-1, the key mediator of the Reelin signaling pathway (Remedios et al., 2007), in LOT2 and the anterior amygdala. However, the lateral, the basolateral and basomedial amygdala nuclei (lateral and ventral pallial derivatives) are negative for Dab-1 (Rice et al., 1998; Remedios et al., 2007). This finding suggests that only those components of the amygdala that derive from the dorsal pallium, especially cells of the caudal amygdaloid stream, are affected by the Reeler mutation. Consistent

with this interpretation, the deep caudal nuclei seem to be unaffected in the Reeler mutant (see Fig. 5.30). Interestingly, Cdk5 and its activator p35 are associated with the β-catenin/N-Cdh(Cdh2) complex in the murine cortex (Kwon et al., 2000). It has been hypothesized that N-Cdh is down-regulated during migration of neuroblasts by the activity of p35/Cdk5 and that neuroblast migration is terminated with the downregulation of p35/Cdk5 by Reelin (Homayouni and Curran, 2000). These results provide a possible explanation of how N-Cdh-mediated adhesion of migrating neurons may be regulated by the Reelin signaling pathway.

6.6 General conclusion and future directions

In conclusion, the spatially restricted expression of individual cadherins in the cerebral cortex and the amygdala in wild-type mice suggest that cadherins might provide an adhesive code for the formation, differentiation and connectivity of these brain structures (Redies et al., 1993; Neudert and Redies, 2008). The latter suggestion requires more definite confirmation by neuroanatomical tracing studies. Also, the precise functional role of cadherins in contributing to the development of the cerebral cortex and the amygdala remains to be studied by genetic or other experimental approaches, such as loss of function and/or gain of function analyses in transgenic mouse models. Such future studies may possibly result in the elucidation of novel genetic mechanisms involved in CNS patterning.

In the Reeler mutant mouse, an animal model used for studying corticogenesis, cadherin-expressing cells are distributed widely across the radial dimension in cerebral cortex, and cortical pallial parts of the amygdaloid complex are disorganized. This disorganization may possibly coincide with changes in the establishment of neural circuits caused by the lack of Reelin. The multiple structural deficits in the Reeler brain have lead to the suggestion that the Reelin glycoprotein may be involved in several neurodevelopmental disorders, e.g. schizophrenia (Impagnatiello et al., 1998; Fatemi et al., 2000; Guidotti et al., 2000), bipolar disorder (Fatemi et al., 2000; Guidotti et al., 2000), lissencephaly (Hong et al., 2000) and autism (Persico et al., 2001; Fatemi et al., 2005). A human equivalent of the homozygous Reeler mutant apparently exists, but affected individuals are extremely rare. Affected individuals have severe lissencephaly and cerebellar atrophy (Hong et al., 2000; Chang et al., 2007). It is possible that the homozygous mutant genotype is more prevalent but that fetuses die early due to low viability.

The finding that Reelin mRNA is down-regulated in psychotic post-mortem brains (Impagnatiello et al., 1998; Guidotti et al., 2000) resulted in a special interest in the heterozygous Reeler mouse as a possible animal model for psychoses (Tueting et al., 1999). Additionally, the heterozygous Reeler mouse shows a reduced cortical thickness, reduced spine density in layer III of frontal cortex and neuropil hypoplasia similar to that observed in schizophrenia postmortem brains (Garey et al., 1998; Selemon and Goldman-Rakic, 1999; Kalus et al., 2000; Liu et al., 2001). However, in schizophrenia, environmental factors are also known to be important variables. These aspects need to be considered also in any animal model for a role of Reelin in psychoses.

Apart from schizophrenia, cadherins were shown to be involved in other psychiatric diseases. For example, Cdh7 has been linked to bipolar disorder (Sklar et al., 2008; Soronen et al., 2010). Interestingly, Cdh7 is expressed in the developing eye and in the retina of mice and ferrets (Faulkner-Jones et al., 1999a; Etzrodt et al., 2009) and in the visual cortex of ferret (Krishna-K et al., 2009). The function of the visual system is also affected in bipolar disease that can manifest itself in disturbances of circadian rhythm, seasonal variation, visual attention and working memory. Further investigations are required to study the possible link between cadherins and psychotic disorders in humans in greater detail.

7. REFERENCES

Akins MR, Benson DL, Greer CA. 2007. Cadherin expression in the developing mouse olfactory system. J Comp Neurol. 501:483-497.

Alheid GF, Heimer L. 1988. New perspectieves in basal forebrain organization of special relevance for neuropsychiatric disorders: the striatopallidal, amygdaloid, and corticopetal components of substantia innominata. Neuroscience. 27:1-39.

Angevine, JB. 1965. Time of neuronal origin in the hippocampal region. Exp Neurol Suppl. 2: 1-70.

Angevine JB, Sidman RL. 1961. Autoradiography study of cell migration during histogenesis of cerebral cortex in the mouse. Nature. 192:766-768.

Arber S, Ladle D, Lin J, Frank E, Jessell TM. 2000. ETS gene Er81 controls the formation of functional connections between group Ia sensory afferents and motor neurons. Cell. 101:485-498.

Arnaud L, Ballif BA, Cooper JA. 2003a. Regulation of protein tyrosine kinase signaling by substrate degradation during brain development. Mol Cell Biol. 23: 9293-9302.

Arnaud L, Ballif BA, Forster E, Cooper JA. 2003b. Fyn tyrosine kinase is a critical regulator of disabled-1 during brain development. Curr Biol. 13:9-17.

Arndt K, Nakagawa S, Takeichi M, Redies C. 1998. Cadherin-defined segments and parasagittal cell ribbons in the developing chicken cerebellum. Mol Cell Neurosci. 10:211–228.

Bar I, Lambert de Rouvroit C, Goffinet AM. 2000. The Reelin signaling pathway in mouse cortical development. Eur J Morphol. 38:321-325.

Bayer SA. 1980. Development of the hippocampal region in the rat 1. Neurogenesis examined with 3H-thymidine autoradiography. J Comp Neurol. 190:87-114.

Beffert U, Morfini G, Bock HH, Reyna H, Brady ST, Herz J. 2002. Reelin-mediated signaling locally regulates protein kinase b/Akt and glycogen synthase kinase 3β. J Biol Chem. 51:49958-49964.

Bekirov IH, Needleman LA, Zhang W, Benson DL. 2002. Identification and localization of multiple classic cadherins in developing rat limbic system. Neuroscience. 115:213-227.

Bishop KM, Goudreau G, O'Leary DD. 2000. Regulation of area identity in the mammalian neocortex by Emx2 and Pax6. Science. 288:344-349.

Brose K, Tessier-Lavigne M. 2000. Slit proteins: key regulators of axon guidance, axonal branching, and cell migration. Curr Opin Neurobiol. 10:95-102.

Bulfone A, Smiga SM, Shimamura K, Peterson A, Puelles L, Rubenstein JL. 1995. T-brain-1: a homolog of Brachyury whose expression defines molecularly distinct domains within the cerebral cortex. Neuron 15:63-78.

Caviness VS.1982. Neocortical histogenesis in normal and Reeler mice: a developmental study based upon [3H]thymidine autoradiography. Brain Res. 256:293-302.

Caviness VS, Sidman RL. 1973. Time of origin or corresponding cell classes in the cerebral cortex of normal and Reeler mutant mice: an autoradiographic analysis. J Comp Neurol. 148:141-151.

Chae T, Kwon YT, Bronson R, Dikkes P, Li E, Tsai LH. 1997. Mice lacking p35, a neuronal specific activator of Cdk5, display cortical lamination defects, seizures, and adult lethality. Neuron. 18:29-42.

Chai X, Förster E, Zhao S, Bock HH, Frotscher M. 2009. Reelin acts as a stop signal for radially migrating neurons by inducing phosphorylation of n-cofilin at the leading edge. Commun Integr Biol. 2:375-377.

Chang BS, Duzcan F, Kim S, Cinbis M, Aggarwal A, Aspe KA, Ozdel O, Atmaca M, Zencir S, Bagci H, Walsh CA. 2007. The role of RELN in lissencephaly and neuropsychiatric disease. Am J Med Genet B Neuropsychiatr Genet. 144:58-63.

Choi GB, Dong H, Murphy AJ, Valenzuela DM, Yancopoulos GD, Swanson LW, Anderson DJ. 2005. Lhx6 delinates a pathway mediating innate reproductive behaviors from the amygdala to the hippocampus. Neuron. 46:647-660.

Chung WW, Lagenaur CF, Yan YM, Lund JS. 1991. Developmental expression of neural cell adhesion molecules in the mouse neocortex and olfactory bulb. J Comp Neurol. 314:290-305.

Cooper J, Howell BW. 1999. Lipoprotein receptors: signalling function in the brain? Cell. 97:671-674.

Curran T, D'Arcangelo G. 1998. Role of Reelin in the control of brain development. Brain Res Rev. 26:285-294.

D'Arcangelo G. 2006. Reelin mouse mutants as models of cortical development disorders. Epilepsy Behav. 8:81-90.

D'Arcangelo G, Miao GG, Chen SC, Soares HD, Morgan JI, Curran T. 1995. A protein related to extracellular matrix proteins deleted in the mouse mutant Reeler. Nature. 374:719-723.

D'Arcangelo G, Miao GG, Curran T. 1996. Detection of the Reelin breakpoint in Reeler mice. Brain Res Mol Brain Res. 39:234-236.

D'Arcangelo G, Nakajima K, Miyata T, Ogawa M, Mikoshiba K, Curran T. 1997. Reelin is a secreted glycoprotein recognized by the CR-50 monoclonal antibody. J Neurosci. 17:23-31.

D'Arcangelo G, Homayouni R, Keshvara L, Rice DS, Sheldon M, Curran T. 1999. Reelin is a ligand for lipoprotein receptors. Neuron. 24: 471-479.

Davis M. 2000. The role of the amygdala in conditioned and unconditioned fear and anxiety. In: Aggleton JP, editor. The Amygdala: a functional analysis. Oxford: Oxford University Press, 213–287.

Dekimoto H, Terashima T, Katsuyama Y. 2010. Dispersion of the neurons expressing layer specific markers in the reeler brain. Dev Growth Differ. 52:181-93.

de Olmos JS, Beltramino CA, Alheid GF. 2004. Amygdala and extended amygdala. In: Paxinos G, editor. The rat nervous system. San Diego: Academic Press, 443–493.

Dulabon L, Olson EC, Taglienti MG, Eisenhuth S, McGrath B, Walsh CA, Kreidberg JA, Anton ES. 2000. Reelin binds alpha3beta1 integrin and inhibits neuronal migration. Neuron. 27:33-44.

Etzrodt J, Krishna-K, Redies C. 2009. Expression of classic cadherins and delta-protocadherins in the developing ferret retina. BMC Neurosci. 10:153.

Fannon AM, Colman DR. 1996. A model for central synaptic junctional complex formation based on the differential adhesive specificities of the cadherins. Neuron. 17:423-434.

Fatemi SH. 2005. Reelin glycoprotein in autism and schizophrenia. Int Rev Neurobiol. 71: 179-187.

Fatemi SH. 2008. Reelin Glycoprotein. New York: Springer

Fatemi SH, Earle JA, McMenomy T. 2000. Reduction in Reelin immunoreactivity in hippocampus of subjects with schizophrenia, bipolar disorder and major depression. Mol Psychiatry. 5:654-663.

Fatemi SH, Snow AV, Stary JM, Araghi-Niknam M, Reutiman TJ, Lee S, Brooks AI, Pearce DA. 2005. Reelin signalling is impaired in autism. Biol Psychiatry. 57:777-787.

Faulkner-Jones BE, Godinho LN, Reese BE, Pasquini GF, Ruefli A, Tan SS. 1999a. Cloning and expression of mouse cadherin-7, a type-II cadherin isolated from the developing eye. Mol Cell Neurosci. 14:1-16.

Faulkner-Jones BE, Godinho LN, Tan SS. 1999b. Multiple cadherin mRNA expression and developmental regulation of a novel cadherin in the developing mouse eye. Exp Neurol. 156:316-325.

Ferrere A, Vitalis T, Gingras H, Gaspar P, Cases O. 2006. Expression of Cux-1 and Cux-2 in the developing somatosensory cortex of normal and barrel-defective mice. Anat Rec A Discov Mol Cell Evol Biol. 288:158–165.

Frotscher M. 1997. Dual role of Cajal-Retzius cells and Reelin in cortical development. Cell Tissue Res. 290:315-322.

Frotscher M. 2010. Role for Reelin in stabilizing cortical architecture. Trends Neurosci. 33:407-414.

Frotscher M, Chai X, Bock HH, Haas CA, Förster E, Zhao S. 2009. Role of Reelin in the development and maintenance of cortical lamination. J Neural Transm. 116:1451-1455.

Gaitan Y, Bouchard M. 2006. Expression of the delta-protocadherin gene Pcdh19 in the developing mouse embryo. Gene Expr Patterns. 6:893-899.

Garcia-Lopez M, Abellan A, Legaz I, Rubenstein JL, Puelles L, Medina L. 2008. Histogenetic compartments of the mouse centromedial and extended amygdala based on gene expression patterns during development. J Comp Neurol. 506:46-74.

Garey LJ, Ong WY, Patel TS, Kanani M, Davis A, Mortimer AM, Barnes TR, Hirsch SR. 1998. Reduced dendritic spine density on cerebral cortical pyramidal neurons in schizophrenia. J Neurol Neurosurg Psychiatry. 65:446-453.

Gil OD, Needleman L, Huntley GW. 2002. Developmental patterns of cadherin expression and localization in relation to compartmentalized thalamocortical terminations in rat barrel cortex. J Comp Neurol. 453:372-388.

Gilmore EC, Ohshima T, Goffinet AM, Kulkarni AB, Herrup K. 1998. Cyclindependent kinase 5–deficient mice demonstrate novel developmental arrest in cerebral cortex. J Neurosci. 18:6370–6377.

Gilmore EC, Herrup K. 2000. Cortical development: receiving reelin. Curr Biol. 10:162-166.

Godfraind C, Schachner M, Goffinet AM. 1988. Immunohistological localization of cell adhesion molecules L1, J1, N-CAM and their common carbohydrate L2 in the embryonic cortex of normal and reeler mice. Brain Res. 470:99-111.

Goffinet AM. 1979. An early developmental defect in the cerebral cortex of the Reeler mouse. Anat Embryol. 157:205-218.

Goffinet AM. 1984. Events governing organization of postmigratory neurons: studies on brain development in normal and reeler mice. Brain Res. 319:261-296.

Goichberg P, Geiger B. 1998. Direct involvement of N-cadherin-mediated signaling in muscle differentiation. Mol Biol Cell. 9:3119-3131.

Guidotti AR, Auta J, Davis J, Dwivedi Y, Grayson D, Impagnatiello F, Pandey G, Pesold C, Sharma R, Uzunov D, Costa E. 2000. Decrease in Reelin and glutamic acid decarboxylase 67 (GAD67) expression in schizophrenia and bipolar disorder: a post-mortem brain study. Arch Gen Psychiatry. 57:1061-1069.

Hack I, Bancila M, Loulier K, Carroll P, Cremer H. 2002. Reelin is a detachment signal in tangential chain-migration during postnatal neurogenesis. Nat Neurosci. 5:939-945.

Hack I, Hellwig S, Junghans D, Brunne B, Bock HH, Zhao S, Frotscher M. 2007. Divergent roles of ApoER2 and Vldlr in the migration of cortical neurons. Development. 134:3883-3891.

Hadj-Sahraoui N, Frederic F, Delhaye-Bouchaud N, Mariani J. 1996. Gender effect on Purkinje cell loss in the cerebellum of the heterozygous reeler mouse. J Neurogenet. 11:45-58.

Halbleib JM, Nelson WJ. 2006. Cadherins in development: cell adhesion, sorting, and tissue morphogenesis. Genes Dev. 20:3199-3214.

Hamburgh M. 1963. Analysis of the postnatal developmental effects of Reeler, a neurological mutation in mice. A study in developmental genetics. Dev Biol. 8:165-185.

Hartfuss E, Förster E, Bock HH, Hack MA, Leprince P, Luque JM, Herz J, Frotscher M, Götz M. 2003. Reelin signaling directly affects radial glia morphology and biochemical maturation. Development. 130:4597-4609.

Hertel N, Krishna-K, Nuernberger M, Redies C. 2008. A cadherin-based code for the divisions of the mouse basal ganglia. J Comp Neurol. 508:511-528.

Hertel N, Redies C. 2011. Absence of layer-specific cadherin expression profiles in the neocortex of the Reeler mutant mouse. Cereb Cortex. 21:1105-1117.

Hevner RF, Daza RAM, Rubenstein JLR, Stunnenberg H, Olavarria JF, Englund C. 2003. Beyond laminar fate: toward a molecular classification of cortical projection/pyramidal neurons. Dev Neurosci. 25:139-151.

Heyers D, Kovjanic D, Redies C. 2003. Cadherin expression coincides with birth dating patterns in patchy compartments of the developing chicken telencephalon. J Comp Neurol. 460:155-166.

Hiesberger T, Trommsdorff M, Howell BW, Goffinet A, Mumby MC, Cooper JA, Herz J. 1999. Direct binding of reelin to VLDL receptor and ApoE receptor 2 induces tyrosine phosphorylation of disabled-1 and modulates tau phosphorylation. Neuron. 24:481-489.

Hirano S, Kimoto N, Shimoyama Y, Hirohashi S, Takeichi M. 1992. Identification of a neural alpha-catenin as a key regulator of cadherin function and multicellular organization. Cell. 70:293-301.

Hirano S, Yan Q, Suzuki ST. 1999. Expression of a novel protocadherin, OL-protocadherin, in a subset of functional systems of the developing mouse brain. J Neurosci. 19:995-1005.

Hirano S, Suzuki ST, Redies C. 2003. The cadherin superfamily in neural development: diversity, function and interaction with other molecules. Front Biosci. 8:306-355.

Hirotsune S, Takahara T, Sasaki N, Hirose K, Yoshili A, Ohashi T, Kusakabe M, Murakami Y, Muramustu M, Watanabe S, Nakao K, Katsuki M, Hayashizaki. 1995. The reeler gene encodes a protein with an EGF-like motif expressed by pioneer nerons. Nat Genet. 10:77-83.

Hoerder-Suabedissen A, Wang WZ, Lee S, Davies KE, Goffinet AM, Rakić S, Parnavelas J, Reim K, Nicolić M, Paulsen O, Molnár Z. 2009. Novel markers reveal subpopulations of subplate neurons in the murine cerebral cortex. Cereb Cortex. 19:1738-1750.

Hoffarth RM, Johnston JG, Krushel LA, van der Kooy D. 1995. The mouse mutation reeler causes increased adhesion within a subpopulation of early postmitotic cortical neurons. J Neurosci. 15:4838-50.

Homayouni R, Curran T. 2000. Cortical development: Cdk5 gets into sticky situations. Curr Biol. 10: R331-334.

Homayouni R, Rice DS, Curran T. 2001. Disabled-1interacts with a novel developmentally regulated protocadherin. Biochem Biophys Res Commun. 289:539-547.

Hong SE, Shugart YY, Huang DT, Shawan SA, Grant PE, Hourihane JO, Martin ND, Walsh CA. 2000. Autosomal recessive lissencephaly with cerebellar hypoplasia is associated with human RELN mutations. Nature Genet. 26:93-96.

Honjo M, Tanihara H, Suzuki S, Tanaka T, Honda Y, Takeichi M. 2000. Differential expression of cadherin adhesion receptors in neural retina of the postnatal mouse. Invest Ophthalmol Vis Sci. 41:546-551.

Hulpiau P, van Roy F. 2009. Molecular evolution of the cadherin superfamily. Int J Biochem Cell Biol. 41:349-69.

Hulpiau P, van Roy F. 2011. New insights into the evolution of metazoan cadherins. Mol Biol Evol. 28:647-57.

Ichinohe N, Knight A, Ogawa M, Ohshima T, Mikoshiba K, Yoshihara Y, Terashima T, Rockland KS. 2008. Unusual patch-matrix organization in the retrosplenial cortex of the Reeler mouse and shaking rat Kawasaki. Cereb Cortex. 18:1125-1138.

Impagnatiello F, Guidotti A, Pesold C, Dwivedi Y, Caruncho H, Pisu MG, Smalheiser NR, Davis JM, Pandey GN, Pappas GD, Tueting P, Costa E. 1998. A decrease of reelin expression as a putative vulnerability factor in schizophrenia. Proc Natl Acad Sci USA. 95:15718-15723.

Inoue A, Sanes JR. 1997. Lamina-specific connectivity in the brain: regulation by N-cadherin, neurotrophins, and glycoconjugates. Science. 276:1428-1431.

Inoue T, Chisaka O, Matsunami H, Takeichi M. 1997. Cadherin-6 expression transiently delineates specific rhombomeres, other neural tube subdivisions, and neural crest subpopulations in mouse embryos. Dev Biol.183:183-194.

Inoue K, Terashima T, Nishikawa T, Takumi T. 2004. Fez1 is layer-specifically expressed in the adult mouse neocortex. Eur J Neurosci. 20:2909-2916.

Jossin Y, Ignatova N, Hiesberger T, Herz J, Lambert de Rouvroit C, Goffinet AM. 2004. The central fragment of reelin, generated by proteolytic processing in vivo, is critical to its function during cortical plate development. J Neurosci. 24:514-521.

Jossin Y, Goffinet AM. 2007. Reelin signals through PI3K and Akt to control cortical development and through mTor to regulate dendritic growth. Mol Cell Biol. 27:7113-7124.

Jossin Y, Gui L, Goffinet AM. 2007. Processing of Reelin by embryonic neurons is important for function in tissue but not in dissociated cultured neurons. J Neurosci. 27:4243-52.

Ju MJ, Aroca P, Luo J, Puelles L, Redies C. 2004. Molecular profiling indicates avian branchiomotor nuclei invade the hindbrain alar plate. Neuroscience. 128:785-796.

Kalus P, Müller TJ, Zuschratter W, Senitz D. 2000. The dendritic architecture of prefrontal pyramidal neurons in schizophrenic patients. Neuroreport. 11:1652-1659.

Kandel, Schwartz, Jessell. 2000. Principles of neural science. 4th edition. New York: McGraw-Hill, 1019-1040

Kaprielian Z, Imondi R, Runko E. 2000. Axon guidance at the midline of the developing CNS. Anat Record. 261:176-197.

Katayama S, Tomaru Y, Kasukawa T, Waki K, Nakanishi M, Nakamura M, Nishida H, Yap CC, Suzuki M, Kawai J, Suzuki H, Carninci P, Hayashizaki Y, Wells C, Frith M, Ravasi T, Pang KC, Hallinan J, Mattick J, Hume DA, Lipovich L, Batalov S, Engström PG, Mizuno Y, Faghihi MA, Sandelin A, Chalk AM, Mottagui-Tabar S, Liang Z, Lenhard B, Wahlestedt C; RIKEN Genome Exploration Research Group; Genome Science Group (Genome Network Project Core Group); FANTOM Consortium. 2005. Antisense transcription in the mammalian transcriptome. Science. 309:1564-1566.

Katsuyama Y, Terashima T. 2009. Developmental anatomy of Reeler mutant mouse. Dev Growth Differ. 51:271-286.

Keshvara L, Benhayon D, Magdaleno S, Curran T. 2001. Identification of reelin-induced sites of tyrosyl phosphorylation on disabled-1. J Biol Chem. 276:16008-16014.

Kim SY, Chung HS, Sun W, Kim H. 2007. Spatiotemporal expression pattern of non-clustered protocadherin family members in the developing rat brain. Neuroscience. 147:996-1021.

Kim SY, Mo JW, Han S, Choi SY, Han SB, Moon BH, Rhyu IJ, Sun W, Kim H. 2010. The expression of non-clustered protocadherins in adult rat hippocampal formation and the connecting brain regions. Neuroscience. 170:189-199.

Kimura Y, Matsunami H, Inoue T, Shimamura K, Uchida N, Ueno T, Miyazaki T, Takeichi M (1995) Cadherin-11 expressed in association with mesenchymal morphogenesis in the head, somite, and limb bud of early mouse embryos. Dev Biol 169:347-358.

Kohmura N, Senzaki K, Hamada S, Kai N, Yasuda R, Watanabe M, Ishii H, Yasuda M, Mishina M, Yagi T. 1998. Diversity revealed by a novel family of cadherins expressed in neurons at a synaptic complex. Neuron. 20:1137-1151.

Kojima T, Nakajima K, Mikoshiba K. 2000. The disabled 1 gene is disrupted by a replacement with L1 fragment in yotari mice. Brain Res Mol Brain Res. 75:121-127.

Korematsu K, Redies C. 1997a. Restricted expression of cadherin-8 in segmental and functional subdivisions of the embryonic mouse brain. Dev Dyn. 208:178-189.

Korematsu K, Redies C. 1997b. Expression of cadherin-8 mRNA in the developing mouse central nervous system. J Comp Neurol. 387:291-306.

Krishna-K, Nuernberger M, Weth F, Redies C. 2009. Layer-specific expression of multiple cadherins in the developing visual cortex (V1) of the ferret. Cereb Cortex. 19:388-401.

Krushel LA, van der Kooy D. 1993. Pattern formation in the developing mammalian forebrain: selective adhesion of early but not late postmitotic cortical and striatal neurons within forebrain reaggregate cultures. Dev Biol. 158:145-162.

Kubo K, Nakajima K. 2003. Cell and molecular mechanisms that control cortical layer formation in the brain. Keio J Med. 52:8-20.

Kwon YT, Gupta A, Zhou Y, Nikolic M, Tsai LH. 2000. Regulation of N-cadherin-mediated adhesion by the p35-Cdk5 kinase. Curr Biol. 10:363-372.

Lambert de Rouvroit C, Goffinet AM. 1998. The Reeler mouse as a model of brain development. Adv Anat Embryol Cell Biol. 150:1-106.

Lambert de Rouvroit C, de Bergeyck V, Cortfrindt C, Bar I, Eeckhout Y, Goffinet AM. 1999. Reelin, the extracellular matrix protein deficient in reeler mutant mice, is processed by a metalloproteinase. Exp Neurol. 156:214-217.

LeDoux JE. 2000. Emotion circuits in the brain. Annu Rev Neurosci. 23:155–184.

Liu WS, Pesold C, Rodriguez MA, Carboni G, Auta J, Lacor P, Larson J, Condie BG, Guidotti A, Costa E. 2001. Downregulation of dendritic spine and glutamic acid decarboxylase 67 expression in the reelin haploinsufficient heterozygous reeler mouse. Proc Nat Acad Sci USA. 98:3477-3482.

Luo Y, Ferreira-Cornwell M, Baldwin H, Kostetskii I, Lenox J, Lieberman M, Radice G. 2001. Rescuing the N-cadherin knockout by cardiac-specific expression of N- or Ecadherin. Development. 128:459-469.

Luo J, Treubert-Zimmermann U, Redies C. 2004. Cadherins guide migrating Purkinje cells to specific parasagittal domains during cerebellar development. Mol Cell Neurosci. 25:138-152.

Lumsden A, Krumlauf R. 1996. Patterning the vertebrate neuraxis. Science. 274:1109-1115.

Luskin, MB, Price JL. 1983. The topographic organization of associational fibres of the olfactory system in the rat, including centrifugal fibers to the olfactory bulb. J Comp Neurol. 216:264–291.

Magdaleno S, Keshvara L, Curran T. 2002. Rescue of ataxia and preplate splitting by ectopic expression of reelin in reeler mice. Neuron. 33:573-586.

Manabe T, Togashi H, Uchida N, Suzuki SC, Hayakawa Y, Yamamoto M, Yoda H, Miyakawa T, Takeichi M, Chisaka O. 2000. Loss of cadherin-11 adhesion receptor enhances plastic changes in hippocampal synapses and modifies behavioral responses. Mol Cell Neurosci. 15:534–546.

Marin O, Yaron A, Bagri A, Tessier-Lavigne M, Rubenstein JL. 2001. Sorting of striatal and cortical interneurons regulated by semaphoring-neuropilin interactions. Science. 293:872-875.

Marin O, Rubenstein JL. 2003. Cell migration in the forebrain. Annu Rev Neurosci. 26:441-483.

Marin-Padilla M. 1998. Cajal-Retzius cells and the development of the neocortex. Trends Neurosci. 21:64-71.

Martinez-Marcos A. 2009. On the organization of olfactory and vomeronasal cortices. Prog Neurobiol. 87:21-30.

Matsunami H, Miyatani S, Inoue T, Copeland NG, Gilbert DJ, Jenkins NA, Takeichi M. 1993. Cell binding specificity of mouse R-cadherin and chromosomal mapping of the gene. J Cell Sci. 106:401-409.

McDonald AJ.1998. Cortical pathways to the mammalian amygdala. Prog Neurobiol. 55:257-332.

Medina L, Legaz I, Gonzalez G, de Castro F, Rubenstein JLR, Puelles L. 2004. Expression of Dbx1, Neurogenin 2, Semaphorin 5A, Cadherin 8, and Emx1 distinguish ventral and lateral pallial histogenetic divisions in the developing claustroamygdaloid complex. J Comp Neurol. 474:504–523.

Miyashita-Lin EM, Hevner R, Wassarman KM, Martinez S, Rubenstein JL. 1999. Early neocortical regionalization in the absence of thalamic innervation. Science. 285:906-909.

Molnár Z, Adams R, Goffinet AM, Blakemore C. 1998. The role of the first postmitotic cortical cells in the development of thalamocortical innervation in the reeler mouse. J Neurosci. 18:5746-5765.

Nadarajah B, Brunstrom JE, Grutzendler J, Wong RO, Pearlman AL. 2001. Two modes of radial migration in early development of the cerebral cortex. Nat Neurosci. 4:143-150.

Nakagawa S, Takeichi M. 1998. Neural crest emigration from the neural tube depends on regulated cadherin expression. Development. 125:2963-2971.

Nakagawa Y, Johnson JE, O'Leary DD. 1999. Graded and areal expression patterns of regulatory genes and cadherins in embryonic neocortex independent of thalamocortical input. J Neurosci. 19:10877-10885.

Nern A, Zhu Y, Zipursky SL. 2008. Local N-cadherin interactions mediate distinct steps in the targeting of lamina neurons. Neuron. 58:34-41.

Nery S, Fishell G, Corbin JG. 2002. The caudal ganglionic eminence is a source of distinct cortical and subcortical cell populations. Nat Neurosci. 5:1279–1277.

Neudert F, Nuernberger KK, Redies C. 2008. Comparative analysis of cadherin expression and connectivity patterns in the cerebellar system of ferret and mouse. J Comp Neurol. 511:736-752.

Neudert F, Redies C. 2008. Neural circuits revealed by axon tracing and mapping cadherin expression in the embryonic chicken cerebellum. J Comp Neurol. 509:283-301.

Nollet F, Kools P, van Roy F. 2000. Phylogenetic analysis of the cadherin superfamily allows identification of six major subfamilies besides several solitary members. J Mol Biol. 299:551-572.

Nose A, Nagafuchi A, Takeichi M. 1988. Expressed recombinant cadherins mediate cell sorting in model systems. Cell. 54:993-1001.

Obst-Pernberg K, Medina L, Redies C. 2001. Expression of R-cadherin and N-cadherin by cell groups and fiber tracts in the developing mouse forebrain: relation to the formation of functional circuits. Neuroscience. 106:505-533.

Ogawa M, Miyata T, Nakajima K, Yagyu K, Seike M, Ikenaka K, Yamamoto H, Mikoshiba K. 1995. The Reeler gene-associated antigen on Cajal-Retzius neurons is a crucial molecule for laminar organization of cortical neurons. Neuron. 14:899-912.

Ohkubo N, Vitek MP, Morishima A, Suzuki Y, Miki T, Maeda N, Mitsuda N. 2007. Reelin signals survival through Src-family kinases that inactivate BAD activity. J Neurochem. 103: 820-830.

Ohshima T, Ward JM, Huh CG, Longenecker G, Veeranna, Pant HC, Brady RO, Martin LJ, Kulkarni AB. 1996. Targeted disruption of the cyclin-dependent kinase 5 gene result in abnormal corticogenesis, neuronal pathology and perinatal death. Proc Natl Acad Sci USA. 93:11173-11178.

O´Leary DD, Wilkinson DG. 1999. Eph receptors and ephrins in neural development. Curr Opin Neurobiol. 9:65-73.

Overduin M, Harvey TS, Bagby S, Tong KI, Yau P, Takeichi M, Ikura M. 1995. Solution structure of the epithelial cadherin domain responsible for selective cell adhesion. Science. 267:386-389.

Paxinos G, Franklin KBJ. 2001. The mouse brain in stereotaxic coordinates, 2nd edition. San Diego, CA: Academic Press.

Paxinos G, Watson C. 1998. The rat brain in stereotaxic coordinates, 4th edition. San Diego, CA: Academic Press.

Peinado H, Portillo F, Cano A. 2004. Transcriptional regulation of cadherins during development and carcinogenesis. Int J Dev Biol. 48:365-375.

Persico AM, D´Agruma L, Maiorano N, Totaro A, Militerni R, Bravaccio C, Wassink TH, Schneider C, Melmed R, Trillo S, Montecchi F, Palermo M, Pascucci T, Puglisi-Allegra S, Reichelt KL, Conciatori M, Marino R, Quattrocchi CC, Baldi A, Zelante L, Gasparini P, Keller F; Collaborative Linkage Study of Autism. 2001. Reelin gene alleles and haplotypes as a factor predisposing to autistic disorder. Mol Psychiatry. 6:150-159.

Petrovich GD, Canteras NS, Swanson LW. 2001. Combinatorial amygdalar inputs to hippocampal domains and hypothalamic behavior systems. Brain Res Brain Res Rev. 38:247–289.

Petruzelli L, Takami M, Humes HD. 1999. Structure and function of cell adhesion molecules. Am J Med. 106:467-476.

Pikkarainen M, Rönkkö S, Savander V, Insausti R, Pitkänen A. 1999. Projections from the lateral, basal and accessory basal nuclei of the amygdala to the hippocampal formation in rat. J Comp Neurol. 403:229-260.

Pinto Lord MC, Caviness VS. 1979. Determinants of cell shape and orientation: a comparative Golgi analysis of cell-axon interrelationships in the developing neocortex of normal and reeler mice. J Comp Neurol. 187:49-69.

Pitkänen A. 2001. Connectivity of the rat amygdaloid complex. In: Aggleton JP editor. The amygdala. A functional analysis. 2nd edition. Oxford: Oxford University Press, 31-115.

Pitkänen A, Tuunanen J, Kalviainen R, Partanen K, Salmenpera T. 1998. Amygdala damage in experimental and human temporal lobe epilepsy. Epilepsy Res. 32:233–253.

Polleux F, Dehay C, Kennedy H. 1998. Neurogenesis and commitment of corticospinal neurons in Reeler. J Neurosci. 18:9910-9923.

Polleux F, Dehay C, Goffinet A, Kennedy H. 2001. Pre- and post-mitotic events contribute to the progressive acquisition of area-specific connectional fate in the neocortex. Cereb Cortex. 11:1027-1039.

Puelles L, Kuwana E, Puelles E, Bulfone A, Shimamura K, Keleher J, Smiga S,Rubenstein JLR. 2000. Pallial and subpallial derivatives in the embryonic chick and mouse telencephalon, traced by the expression of the genes Dlx-2, Emx-1, Nkx-2.1, Pax-6, and Tbr-1. J Comp Neurol. 424:409–438.

Puelles L, Rubenstein JLR. 1993. Expression patterns of homeobox and other putative regulatory genes in the embryonic mouse forebrain suggest a neuromeric organization. Trends Neurosci.16:472-479.

Quaggin SE, Heuvel GB, Golden K, Bodmer R, Igarashi P. 1996. Primary structure, neural-specific expression, and chromosomal localization of Cux-2, a second murine homeobox gene related to Drosophila cut. J Biol Chem. 271:22624-22634.

Rakic P. 1972. Mode of cell migration to the superficial layers of fetal monkey neocortex. J Comp Neurol. 145:61-84.

Rakic P. 1974. Neurons in rhesus monkey visual cortex: systematic relation between time of origin and eventual disposition. Science. 183:425-7.

Rakic P, Caviness VS. 1995. Cortical development: view from neurological mutants two decades later. Neuron. 14:1101-1104.

Rakic S, Davis C, Molnar Z, Nikolic M, Parnavelas JG. 2006. Role of p35/Cdk5 in preplate splitting in the developing cerebral cortex. Cereb Cortex. 16:i35-45.

Redies C. 2000. Cadherins in the central nervous system. Prog Neurobiol. 61:611-648.

Redies C, Takeichi M. 1993. Expression of N-cadherin mRNA during development of the mouse brain. Dev Dyn. 197:26-39.

Redies C, Takeichi M. 1996. Cadherins in the developnig central nervous system: an adhesive code for segmental and functional subdivisions. Dev Biol. 180:413-423.

Redies C, Engelhart K, Takeichi M. 1993. Differential expression of N- and R-cadherin in functional neuronal systems and other structures of the developing chicken brain. J Comp Neurol. 333:398-416.

Redies C, Puelles L. 2001. Modularity in vertebrate brain development and evolution. Bioessays. 23:1100-11.

Redies C, Kovjanic D, Heyers D, Medina L, Hirano S, Suzuki ST, Puelles L. 2002. Patch/matrix patterns of gray matter differentiation in the telencephalon of chicken and mouse. Brain Res Bull. 57:489-493.

Redies C, Vanhalst K, Roy F. 2005. Delta-protocadherins: unique structures and functions. Cell Mol Life Sci. 62:2840-2852.

Redies C, Neudert F, Lin J. 2010. Cadherins in cerebellar development: Translation of embryonic patterning into mature functional compartmentalization. Cerebellum. DOI: 10.1007/s12311-010-0207-4 (epub ahead of print).

Remedios R, Huilgol D, Saha B, Hari P, Bhatnagar L, Kowalczyk T, Hevner RF, SudaY, Aizawa S, Ohshima T, Stoykova A, Tole S. 2007. A stream of cells migrating from the caudal telencephalon reveals a link between the amygdala and neocortex. Nat Neurosci. 10:1141-50.

Rice DS, Curran T. 2001. Role of the Reelin signalling pathway in central nervous system development. Annu Rev Neurosci. 24:1005-1039.

Rice DS, Sheldon M, D'Arcangelo G, Nakajima K, Goldowitz D, Curran T. 1998. Disabled-1 acts downstream of Reelin in a signaling pathway that controls laminar organization in the mammalian brain. Development. 125:3719-3729.

Rodriguez MA, Pesold C, Liu WS, Kriho V, Guidotti A, Pappas GD, Costa E. 2000. Colocalization of integrin receptors and reelin in dendritic spine post-synaptic densities of adult non-human primate cortex. Proc Natl Acad Sci USA. 97:3550-3555.

Rubenstein JLR, Shimamura K, MartoAnez S, Puelles L. 1998. Regionalization of the prosencephalic neural plate. Annu Rev Neurosci. 21:445-477.

Rubenstein JL, Anderson S, Shi L, Miyashita-Lin E, Bulfone A, Hevner R. 1999. Genetic control of cortical regionalization and connectivity. Cereb Cortex. 9:524-532.

Sanada K, Gupta A, Tsai LH. 2004. Disabled-1 regulated adhesion of migrating neurons to radial glial fiber contributes to neuronal positioning during early corticogenesis. Neuron. 42:197-211.

Sanes, Reh, Harris. 2006. Development of the nervous system. 2nd edition. Burlington, San Diego, London: Elsevier Academic Press

Santiago AC, Shammah-Lagnado SJ. 2004. Efferent connections of the nucleus of the lateral olfactory tract in the rat. J Comp Neurol. 471:314–332.

Sano K, Tanihara H, Heimark RL, Obata S, Davidson M, St. John T, Taketani S, Suzuki S. 1993. Protocadherins: a large family of cadherin-related molecules in central nervous system. EMBO J. 12:2249-2256.

Schaefer A, Poluch S, Juliano S. 2008. Reelin is essential for neuronal migration but not for radial glia elongation in neonatal ferret cortex. Dev Neurobiol. 68:590-604.

Selemon LD, Goldman-Rakic PS. 1999. The reduced neuropil hypothesis: a circuit board model of schizophrenia. Biol Psychiatry 45:17-25.

Senzaki K, Ogawa M, Yagi T. 1999. Proteins of the CNR family are multiple receptors for Reelin. Cell. 99:635-647.

Shapiro L, Fannon AM, Kwong PD, Thompson A, Lehmann MS, Grubel G, Legrand JF, Als-Nielsen J, Colman DR, Hendrickson WA. 1995. Structural basis of cell-cell adhesion by cadherins. Nature. 374:327-337.

Sheldon M, Rice DS, D'Arcangelo G, Yoneshima H, Nakajima K, Mikoshiba K, Howell BW, Cooper JA, Goldowitz D, Curran T. 1997. Scrambler and yotari

disrupt the disabled gene and produce a Reeler-like phenotype in mice. Nature. 389:730-733.

Shi CJ, Cassell MD. 1999. Perirhinal cortex projections to the amygdaloid complex and hippocampal formation in the rat. J Comp Neurol. 406:229-328.

Shimamura K, Hartigan DJ, MartoAnez S, Puelles L, Rubenstein JLR. 1995. Longitudinal organization of the anterior neural plate and neural tube. Development. 121:3923-3933.

Sklar P, Smoller JW, Fan J, Ferreira MA, Perlis RH, Chambert K, Nimgaonkar VL, McQueen MB, Faraone SV, Kirby A, de Bakker PI, Ogdie MN, Thase ME, Sachs GS, Todd-Brown K, Gabriel SB, Sougnez C, Gates C, Blumenstiel B, Defelice M, Ardlie KG, Franklin J, Muir WJ, McGhee KA, MacIntyre DJ, McLean A, VanBeck M, McQuillin A, Bass NJ, Robinson M, Lawrence J, Anjorin A, Curtis D, Scolnick EM, Daly MJ, Blackwood DH, Gurling HM, Purcell SM. 2008. Whole-genome association study of bipolar disorder. Mol Psychiatry. 13:558-569.

Soronen P, Ollila HM, Antila M, Silander K, Palo OM, Kieseppä T, Lönnqvist J, Peltonen L, Tuulio-Henriksson A, Partonen T, Paunio T. 2010. Replication of GWAS of bipolar disorder: association of SNPs near CDH7 with bipolar disorder and visual processing. Mol Psychiatry.15:4-6.

Stoeckli ET, Landmesser LT. 1998. Axon guidance at choice points. Curr Opin Neurobiol. 8:73-79.

Strasser V, Fasching D, Hauser C, Mayer H, Bock HH, Hiesberger T, Herz J, Weeber EJ, Sweatt JD, Pramatarova A, Howell B, Schneider WJ, Nimpf J. 2004. Receptor clustering is involved in reelin signalling. Mol Cell Biol. 24:1378-1386.

Suetsugu S, Tezuka T, Morimura T, Hattori M, Mikoshiba K, Yamamoto T, Takenawa T. 2004. Regulation of actin cytoskeleton by mDab1 through N-WASP and ubiquitination of mDab1. Biochem J. 384:1-8.

Suzuki SC, Sano K, Tanihara H. 1991. Diversity of the cadherin family: evidence for eight new cadherins in nervous tissue. Cell Regulation. 2:261-270.

Suzuki SC, Inoue T, Kimura Y, Tanaka T, Takeichi M. 1997. Neuronal circuits are subdivided by differential expression of type-II classic cadherins in postnatal mouse brains. Mol Cell Neurosci. 9:433-447.

Suzuki SC, Furue H, Koga K, Jiang N, Nohmi M, Shimazaki Y, Katoh-Fukui Y, Yokoyama M, Yoshimura M, Takeichi M. 2007. Cadherin-8 is required for the first relay synapses to receive functional inputs from primary sensory afferents for cold sensation. J Neurosci. 27:3466-3476.

Swanson LW. 2000. Cerebral hemisphere regulation of motivated behavior. Brain Res. 886:113–164.

Swanson LW, Petrovich GD. 1998. What is the amygdala? Trends Neurosci. 21:323-331.

Sweet HO, Bronson RT, Johnson KR, Cook SA, Davisson MT. 1996. Scrambler, a new neurological mutation of the mouse with abnormalities of neuronal migration. Mamm Genome. 7:798-802.

Takahashi T, Goto T, Miyama S, Nowakowski RS, Caviness VS. 1999. Sequence of neuron origin and neocortical laminar fate: relation to cell cycle of origin in the developing murine cerebral wall. J Neurosci. 19:10357-10371.

Takeichi M. 1977. Functional correlation between cell adhesive properties and some cell surface proteins. J Cell Biol. 75:464-474.

Takeichi M. 1988. The cadherins: cell-cell adhesion molecules controlling animal morphogenesis. Development. 102:639-655.

Takeichi M. 1995. Morphogenetic roles of classic cadherins. Cur Opin Cell Biol. 7:619-627.

Takeichi M. 2007. The cadherin superfamily in neuronal connections and interactions. Nat Rev Neurosci. 8:11-20.

Tanaka H, Shan W, Phillips GR, Arndt K, Bozdagi O, Shapiro L, Huntley GW, Benson DL, Colman DR. 2000. Molecular modification of N-cadherin in response to synaptic activity. Neuron. 25:93-107.

Tang L, Hung CP, Schuman EM. 1998. A role for the cadherin family of cell adhesion molecules in hippocampal long-term potentiation. Neuron. 20:1165–1175.

Taniguchi H, Kawauchi D, Nishida K, Murakami F. 2006. Classic cadherins regulate tangential migration of precerebellar neurons in the caudal hindbrain. Development. 133:1923-1931.

Terry-Lorenzo RT, Carmody LC, Voltz JW, Connor JH, Li S, Smith FD, Milgram SL, Colbran RJ, Shenolikar S. 2002. The neuronal actinbinding proteins, neurabin I and neurabin II, recruit specific isoforms of protein phosphatase-1 catalytic subunits. J Biol Chem. 277:27716-27724.

Tissir F, Goffinet AM. 2003. Reelin and brain development. Nat Rev Neurosci. 4:496-505.

Tole S, Remedios R, Saha B, Stoykova A. 2005. Selective requirement of Pax6, but not Emx2, in the specification and development of several nuclei of the amygdaloid complex. J Neurosci. 25:2753–2760.

Treubert-Zimmermann U, Heyers D, Redies C. 2002. Targeting axons to specific fiber tracts in vivo by altering cadherin expression. J Neurosci. 22:7617-7626.

Tueting P, Costa E, Dwivedi Y, Guidotti A, Impagnatiello F, Manev R, Pesold C. 1999. The phenotypic characteristics of heterozygous reeler mouse. Neuroreport. 10:1329-1334.

Utsunomiya-Tate N, Kubo KI, Tate SC, Kainosho M, Katayama E, Nakajima K, Mikoshiba K. 2000. Reelin molecules assemble together to form a large protein complex, which is inhibited by the function-blocking CR-50 antibody. Proc Natl Acad Sci USA. 97:9729-9734.

Vanhalst K, Kools P, Staes K, van Roy F, Redies C. 2005. Delta-protocadherins: a gene family expressed differentially in the mouse brain. Cell Mol Life Sci. 62:1247-1259.

Visel A, Carson J, Oldekamp J, Warnecke M, Jakubcakova V, Zhou X, Shaw CA, Alvarez-Bolado G, Eichele G. 2007. Regulatory pathway analysis by high-throughput in situ hybridization. PLoS Genet. 3:1867-1883.

Vogt C, Vogt O. 1919. Allgemeine Ergebnisse unserer Hirnforschung. J Psychol Neurol. 25:279-462.

Wang X, Weiner JA, Levi S, Craig AM, Bradley A, Sanes JR. 2002. Gamma protocadherins are required for survival of spinal interneurons. Neuron. 36:843–854.

Ware ML, Fox JW, Gonzalez JL, Davis NM, Lambert de Rouvroit C, Russo CJ, Chua SC, Goffinet AM, Walsh CA. 1997. Aberrant splicing of a mouse disabled homolog, mdab1, in the scrambler mouse. Neuron. 19:239-249.

Winklbauer R, Selchow A, Nagel M, Angres B. 1992. Cell interaction and its role in mesoderm cell migration during Xenopus gastrulation. Dev Dyn. 195:290-302.

Wöhrn JC, Nakagawa S, Ast M, Takeichi M, Redies C. 1999. Combinatorial expression of cadherins in the tectum and the sorting of neurites in the tectofugal pathways of the chicken embryo. Neuroscience. 90:985-1000.

Wöhrn JC, Puelles L, Nakagawa S, Takeichi M, Redies C. 1998. Cadherin expression in the retina and retinofugal pathways of the chicken embryo. J Comp Neurol. 396:20-38.

Wolverton T, Lalande M. 2001. Identification and characterization of three members of a novel subclass of protocadherins. Genomics. 76:66-72.

Wright CI, Beijer AVJ, Groenewegen HJ. 1996. Basal amygdaloid complex afferents to the rat nucleus accumbens are compartmentally organized. J Neurosci. 16:1877-1893.

Yamagata K, Andreasson KI, Sugiura H, Maru E, Dominique M, Irie Y, Miki N, Hayashi Y, Yoshioka M, Kaneko K, Kato H, Worley PF. 1999. Arcadlin is a neural activity-regulated cadherin involved in long term potentiation. J Biol Chem. 274:19473–11979.

Yoshida K, Watanabe M, Kato H, Dutta A, Sugano S. 1999. BHprotocadherin-c, a member of the cadherin superfamily, interacts with protein phosphatase 1 alpha through its intracellular domain. FEBS Lett. 460:93–98.

Yoneshima H, Nagata E, Matsumoto M, Yamada M, Nakajima K, Miyata T, Ogawa M, Mikoshiba K. 1997. A novel neurological mutant mouse, yotari, which exhibits Reeler-like phenotype but expresses CR-50 antigen/reelin. Neurosci Res. 29:217-223.

Zimmer C, Tiveron MC, Bodmer R, Cremer H. 2004. Dynamics of Cux2 expression suggests that an early pool of SVZ precursors is fated to become upper cortical layer neurons. Cereb Cortex. 14:1408-20.

APPENDIX: MATERIALS

Chemicals

All chemicals were ordered from the Sigma-Aldrich, Merck or Roth companies, except when noted otherwise. They were of analytical purity.

Agarose (electrophoresis grade ultra pure)	Invitrogen GmbH, Darmstadt
5-bromo-4-chloro-3-indolyl phosphate, p-toluidine salt (BCIP)	Fermentas GmbH, St. Leon-Rot
Blocking Reagent	Roche Diagnostics GmbH, Mannheim
Chloroform	Sigma-Aldrich GmbH, Steinheim
Denhardt´s solution	Sigma-Aldrich GmbH, Steinheim
Dextran sulfate sodium salt (50x)	Sigma-Aldrich GmbH, Steinheim
3,3-Diaminobenzidine tetrahydrochloride (DAB)	Sigma-Aldrich GmbH, Steinheim
1,4-Diazabicyclo[2.2.2]octan (DABCO)	Sigma-Aldrich GmbH, Steinheim
Diethylpyrocarbonate (DEPC)	Sigma-Aldrich GmbH, Steinheim
Dimethylformamide (DMF)	Merck KGaA, Darmstadt
Entellan®	Merck KGaA, Darmstadt
Fast Red Tablets	Roche Diagnostics GmbH, Mannheim
4-(2-hydroxyethyl)-1-piperazine-ethanesulfonic acid (HEPES)	Roth GmbH, Karlsruhe
Hoechst 34580	Molecular Probes, Inc., Eugene, USA
LB Agar	Invitrogen GmbH, Darmstadt
Mowiol 4-88	Calbiochem-Novabiochem Corporation, La Jolla, USA
Nitroblue tetrazolium salt (NBT)	Fermentas GmbH, St. Leon-Rot
Paraformaldehyde (PFA)	Merck KGaA, Darmstadt
Phenol red	Sigma-Aldrich GmbH, Steinheim
Silicon solution	SERVA GmbH, Heidelberg
Skim milk powder	Merck KGaA, Darmstadt
Sucrose	Sigma-Aldrich GmbH, Steinheim
Thionin	Merck KGaA, Darmstadt
Tissue Tek® O.C.T.	Science Services, München

TritonX-100	Sigma-Aldrich GmbH, Steinheim
Tween-20	Roth GmbH, Karlsruhe

Antibodies

primary

Sheep anti-digoxigenin-AP, Fab fragments, polyclonal, (catalog no. 11093274910)	Roche Diagnostics GmbH, Mannheim
Sheep anti-fluorescein-AP, Fab fragments, polyclonal, (catalog no.11426338910)	Roche Diagnostics GmbH, Mannheim
Rat anti-neural cell adhesion molecule L1, clone 324 (MAB5275)	Millipore, Temecula, CA, USA

secondary

Biotinylated goat anti rat IgG (H+L), (catalog no. 112-065-167)	Jackson ImmunoResearch, Cambridgeshire, UK

Kits

DNeasy® Blood & Tissue Kit	Qiagen GmbH, Hilden
QIAprep® Spin Miniprep Kit	Qiagen GmbH, Hilden
REDTaq® ReadyMix™ PCR Reaction Mix	Sigma-Aldrich GmbH, Steinheim
Vectastain Elite ABC Kit Standard	Vector Laboratories Inc., Burlingame, USA

Enzymes, antibiotics and other proteins

Ampicillin	Invitrogen GmbH, Darmstadt
BSA (bovine serum albumin)	New England Biolabs GmbH, Frankfurt/M.
DNase A	Promega, Madison, WI USA
Horse serum, normal	Vector Laboratories, Inc., Burlingame, USA
Proteinase K (for genotyping)	Qiagen GmbH, Hilden
Proteinase K (for in situ hybridization)	Sigma-Aldrich GmbH, Steinheim

Restriction endonucleases		
ApaI	50,000 unit/ml	New England Biolabs GmbH, Frankfurt/M.
HindIII	100,000 unit/ml	New England Biolabs GmbH, Frankfurt/M.
KpnI	10,000 unit/ml	Fermentas GmbH, St. Leon-Rot
NcoI	10,000 unit/ml	New England Biolabs GmbH, Frankfurt/M.
NotI	10,000 unit/ml	New England Biolabs GmbH, Frankfurt/M.
SmaI	10,000 unit/ml	Fermentas GmbH, St. Leon-Rot
SpeI	10,000 unit/ml	New England Biolabs GmbH, Frankfurt/M.
XhoI	20,000 unit/ml	New England Biolabs GmbH, Frankfurt/M.
Ribonuclease A		Sigma-Aldrich GmbH, Steinheim
RNA inhibitor RiboLock™		Fermentas GmbH, St.Leon-Rot
RNA polymerases		
Sp6		Fermentas GmbH, St. Leon-Rot
T3		Roche Diagnostics GmbH, Mannheim
T7		Fermentas GmbH, St. Leon-Rot
Sheep serum, normal		Merck KGaA, Darmstadt
Taq DNA polymerase		Sigma-Aldrich GmbH, Steinheim

Nucleic acids and nucleotides

DIG-RNA labeling mix (10x)	Roche Diagnostics GmbH, Mannheim
DNA ladder, MassRuler™	Fermentas GmbH, St. Leon-Rot
DNA ladder, Mid Range	Jena Bioscience GmbH, Jena
Fluo-RNA labeling mix (10x)	Roche Diagnostics GmbH, Mannheim
Oligonucleotides (Primer)	Eurofins MWG Operon, Ebersberg
RNA ladder, High Range	Fermentas GmbH, St. Leon-Rot
RNA, transfer, from baker´s yeast	Sigma-Aldrich GmbH, Steinheim
Salmon testes DNA	Sigma-Aldrich GmbH, Steinheim

Solutions and Buffers

All solutions and buffers were prepared, except as noted otherwise, with deionized water (H_2O) from an ultrapure water purification system (ELGA LabWater, Celle) and stored at room temperature. RNase-free solutions were prepared with DEPC-treated water under RNase-free conditions.

ABC-Reagent	Avidin DH	2% v/v
	Reagent B	2% v/v
	NaCl	150mM
	Trizma base	50mM
	$CaCl_2$	1M
	$MgCl_2$	1M
	Skim milk powder	5% w/v
Acetic anhydride solution (ISH)	DEPC-treated water	150ml
	Triethanolamine	2.26ml
	37% HCl	380µl
	Acetic anhydride	380µl
Acetic anhydride solution (D-ISH)	Triethanolamine	0.1M
	Acetic anhydride	375µl
Antibody solution (ISH + D-ISH)	NaCl	0.13M
	Na_2HPO_4 x $2H_2O$	7mM
	NaH_2PO_4 x H_2O	3mM
	Sheep serum, normal	1% v/v
	10% sodium azide	0.2% v/v
	Sheep anti-DIG-AP antibody	1:2000
	Sheep anti-Fluo-AP antibody	1:2000
Antibody solution (primary; IHC)	NaCl	150mM
	Trizma base	50mM
	$CaCl_2$	1M
	$MgCl_2$	1M
	Skim milk powder	5% w/v
	Rat anti-L1 antibody	1:1000
Antibody solution (secondary; IHC)	NaCl	150mM
	Trizma base	50mM

	$CaCl_2$	1M
	$MgCl_2$	1M
	Skim milk powder	5% w/v
	Biotinylated goat anti-rat antibody	1:300
Antibody solution (Northern Blot)	Maleic acid	10mM
	NaCl	15mM
	Blocking reagent	1% w/v
	Maleic acid	100mM
	Sheep-anti-DIG-AP antibody	1:5000
	Sheep-anti-Fluo-AP antibody	1:5000
Blocking buffer (Northern Blot)	Maleic acid	10mM
	NaCl	15mM
	Blocking reagent	1% w/v
	Maleic acid	100mM
	pH 7.5	
Blocking solution (ISH)	NaCl	130mM
	Na_2HPO_4 x $2H_2O$	7mM
	NaH_2PO_4 x H_2O	3mM
	Sheep serum, normal	2% v/v
	pH 7.4	
Blocking solution (D-ISH)	NaCl	130mM
	Na_2HPO_4 x $2H_2O$	7mM
	NaH_2PO_4 x H_2O	3mM
	Sheep serum, heat inactivated	2% v/v
	Blocking reagent	2% w/v
	pH 7.4	
Blocking solution (IHC)	NaCl	150mM
	Trizma base	50mM

	$CaCl_2$	1M
	$MgCl_2$	1M
	Skim milk powder	5% w/v
Buffer 3	Trizma base	100mM
	NaCl	100mM
	$MgCl_2$	50mM
	pH 9.5	
Buffer 4	Trizma base	10mM
	EDTA	1mM
	pH 8.0	
DAB solution	NaCl	150mM
	Trizma base	50mM
	$CaCl_2$	1M
	MgCl	1M
	Skim milk powder	5% w/v
	DAB	0.03% w/v
	$NiCl_2$	0.04% w/v
	30% H_2O_2	0.01% v/v
DEPC-treated water	DEPC	1%
	autoclaved	
Detection buffer (Northern blot)	Trizma base	100mM
	NaCl	100mM
	$MgCl_2$	50mM
	NBT	0.03% w/v
	BCIP	0.02% w/v
HBS stock solution (10x)	NaCl	1.4M
	KCl	50mM

	Glucose	50mM
	Na_2HPO_4 x $2H_2O$	4mM
	Phenol red	0.4mM
	HEPES	0.1M
	pH 7.4	
	stored at 4°C	
Humid chamber solution (for hybridization)	Formamide	50% v/v
	SSC	1x v/v
Hybridization solution A (ISH)	Formamide	50% v/v
	EDTA	10mM
	SSC solution	3x v/v
	Denhardt´s solution	1x v/v
	Dextran sulfate	10% w/v
	stored at -20°C	
Hybridization solution A (D-ISH)	Tris pH 7.5	10mM
	NaCl	600mM
	EDTA	1mM
	SDS	0.25% w/v
	Dextran sulfate	10% w/v
	Denhardt's solution	1x v/v
	Formamide	50% v/v
	stored at -20°C	
Hybridization solution B (ISH)	Baker´s yeast t-RNA	42µg/ml
	Salmon testis DNA	42µg/ml
	probe	1µg/ml
Hybridization solution B (D-ISH)	Baker´s yeast t-RNA	200µg/ml
	Salmon testis DNA	42µg/ml
	probe	1µg/ml

Fast Red substrate solution	Napthol substrate	0.5mg
	Fast Red chromogen	2mg
	Levamisole	0.4mg
	Tris-HCl, pH 8.2	2ml
Formaldehyde in HBS	Paraformaldehyde	4% w/v
	NaCl	140mM
	KCl	5mM
	Glucose	5mM
	Na_2HPO_4 x $2H_2O$	0.4mM
	Phenol red	0.04mM
	HEPES	10mM
	$MgCl_2$	0.1M
	$CaCl_2$	0.1M
	pH 7.4	
Formaldehyde in PBS	Paraformaldehyde	4% w/v
	NaCl	130mM
	Na_2HPO_4 x $2H_2O$	7mM
	NaH_2PO_4 x H_2O	3mM
	pH 7.4	
LB agar	Agar in LB medium	15g/l
	autoclaved, stored at 4°C	
LB medium	Tryptone/peptone	10g/l
	Yeast extract	5g/l
	NaCl	5g/l
	1M NaOH	1ml/l
	autoclaved, stored at 4°C	
LB^{Amp} medium	Ampicillin in LB medium	50µg/ml

MAB stock solution (10x)	Maleic acid	1M
	NaCl	2.5M
	pH 7.5, stored at 4°C	
MABT solution buffer	Maleic acid	0.1M
	NaCl	0.25M
	Tween-20	0.1% w/v
MOPS running buffer	MOPS (4-morpholino-propanesulfonic acid)	20mM
	Sodium acetate	5mM
	EDTA	1mM
	37% Formaldehyde	2% v/v
Mowiol mounting medium	Mowiol 4-88	13.3% w/v
	Glycerin	30% w/v
	Tris-HCl	0.1M
	DABCO	25mg/ml
	pH 8.5	
NBT/BCIP substrate solution	Trizma base	100mM
	NaCl	100mM
	$MgCl_2$	50mM
	BCIP	0.02% w/v
	NBT	0.03% w/v
NTE stock solution (5x)	Trizma base	50mM
	EDTA	5mM
	NaCl	2.5M
	pH 8.0	
NTM buffer	NaCl	100mM

	Tris pH8	100mM
	$MgCl_2$	50mM
	pH 8.0	
PBS stock solution (Phosphate-buffered saline; 10x)	NaCl	1.3M
	Na_2HPO_4 x $2H_2O$	70mM
	NaH_2PO_4 x H_2O	30mM
	pH 7.4	
PBT buffer	NaCl	0.13M
	Na_2HPO_4 x $2H_2O$	7mM
	NaH_2PO_4 x H_2O	3mM
	Tween-20	0.1% w/v
	pH 7.4	
Peroxidase blocking solution	Methanol	100% v/v
	H_2O_2	0.3% v/v
Proteinase K buffer	Trizma base	100mM
	EDTA	50mM
	pH 8.0	
SOC medium	Peptone	20g/l
	Yeast extract	5g/l
	NaCl	0.5g/l
	KCl	2.5mM
	$MgCl_2$	10mM
	1M NaOH	1ml/l
	after autoclaving, add Glucose	
	stored at -20°C	3.6g/l
SSC stock solution (saline sodium citrate; 20x)	NaCl	3M
	Sodium citrate	0.3M
	pH 7.0	

Sucrose solutions	Sucrose	12% w/v; 15% w/v; 18% w/v
	NaCl	140mM
	KCl	5mM
	Glucose	5mM
	Na_2HPO_4 x $2H_2O$	0.4mM
	Phenol red	0.04mM
	HEPES	10mM
	$MgCl_2$	0.1M
	$CaCl_2$	0.1M
	sterile filtered, stored at 4°C	
TAE stock solution (Tris-acetate-EDTA; 50x)	Trizma base	2M
	EDTA, pH 8.0	50mM
	Glacial acetic acid	5.71% v/v
TBS stock solution (Tris-buffered saline; 10x)	NaCl	1.5M
	Trizma base	0.5M
	pH 7.4	
TE buffer	Trizma base	100mM
	EDTA	1mM
	pH 8.0	
Thionin solution	Thionin	0.1% w/v
	Ethanol, absolute	10% v/v
	Sodium acetate	33mM
	Acetic acid	0.48% v/v
Washing buffer	Maleic acid	100mM
	NaCl	150mM
	pH 7.5	

Equipment

Analytical balance CP 2202S	Sartorius AG, Göttingen
Camera, digital, Olympus DP70	Olympus GmbH, Hamburg
Centrifuge (MiniSpin®)	Eppendorf, Wesseling-Berzdorf
Cryostat HM560 Cryo-Star	Microm GmbH, Walldorf
Electrophoresis chamber B1A	Owl Separation Systems, Portsmouth, USA
Electrophoresis chamber B2	Owl Separation Systems, Portsmouth, USA
Gel documentation system BioDocAnalyze	Biometra GmbH, Göttingen
Microscope, confocal laser scanning, SP5	Leica Microsystems, Wetzlar
Microscope, light transmission, BX40	Olympus, Hamburg
Microscope, stereo, SV11	Carl Zeiss AG, Jena
Microscope, stereo, Stemi 2000	Carl Zeiss AG, Jena
Microscope, stereo, MZ FLIII	Leica Microsystems, Wetzlar
Spectrophotometer WPA Biowave	Biometra, Göttingen
Thermocycler T3	Biometra, Göttingen
Ultrapure water purification system PURELAB Maxima	ELGA LabWater, Celle

Consumption items

Coverslips 24x60mm (Size 1)	Menzel GmbH, Braunschweig
Coverslips 24x50mm (Size 1.5)	Menzel GmbH, Braunschweig
Cuvettes (UV)	Brand GmbH, Wertheim
Nylon membrane Hybond™-N	GE Healthcare Europe GmbH, München
Parafilm “M” laboratory film	Pechiney Plastic Packaging, Chicago, USA
Presicion surgical instruments	Fine Science Tools GmbH, Heidelberg
RNase AWAY	Molecular Bio-Products, Bradford, UK
Slices Super Frost® Plus	Menzel GmbH, Braunschweig

Software

Adobe Photoshop CS	Adobe Systems GmbH, München
Microsoft Excel 2003	Microsoft GmbH, Unterschleißheim
Microsoft Word 2002	Microsoft GmbH, Unterschleißheim
Olympus DP Soft	Olympus GmbH, Hamburg

ACKNOWLEDGEMENTS

I wish to express my sincere gratitude to Prof. Dr. Dr. Christoph Redies. He gave me the opportunity to carry out this work in his group. His excellent supervision and the extensive discussions with him enriched this thesis. My work greatly profited from his tireless support and his expertise in the scientific presentation of the results in publications and posters. He also helped me to improve my language skills from simple "school English" to well-versed scientific English.

My warm and sincere thanks to Prof. Dr. Loreta Medina, University of Lleida, Spain, who introduced me to the amygdala, its highly complex structure and complicated development. The intense discussions with her during her visits in Germany and during my stay in Spain have contributed much to the completion of this part of the work. Additionally, I am grateful for her help in selecting the results of the amygdala part of my thesis.

I would like to thank my present and former colleagues of the "Molecular Neuroembryology" group – Juntang Lin, Krishna, Franziska Neudert and Monique Nürnberger – for sharing time with me in the laboratory and for being open to all my questions. Travelling to conferences together with them was always very stimulating and a lot of fun. Particularly, Krishna and my office mate Juntang facilitated my every-day practice of English. Juntang was a great help with the initial problems of the PCR technique. Thank you for everything.

I am particularly grateful to our technical assistants Ms. Carolin Große, Dr. Manuela Schwalbe, Ms. Sylvia Hänßgen and Ms. Silke Schreiber for their support and their expert assistance in laboratory procedures. I always looked forward to our common tea/coffee break in the afternoon. Carolin – I extend my special thanks to you. The friendly and uncomplicated atmosphere in our cooperation in the laboratory and your "willingness to suffer" contributed to the progress of this thesis project.

I thank my colleagues at the Institutes of Anatomy I and II. It has been always a pleasure to work in the institute. Special thanks to Dr. Gudrun Stoya for her help in the hippocampus part of this study and for proof reading, and Dr. Uta Biedermann who was

a great support in the preparation of the brain course. Dr. Cornelius Lemke and Dr. Annett Eitner taught me the secrets of the laser-scanning microscope. Many thanks to all of you.

I am grateful to the staff of the animal care facilities of the University Hospital Jena – Mrs. Zapfe, Mrs. Bierbrauer, Mrs. Dolke, Mr. Dix, Mrs. Tolksdorf and Dr. van der Wall – for the care of the mice and the uncomplicated, friendly cooperation.

I wish to extend my thanks to my friends – Nicky, Matthias, Katja, Martin, Annett, Esther, Axel, Willy and Franzi – for their moral support and for proof reading. Thanks for your understanding that I had so little time for you, especially in recent times.

Hans – you are my bridge over troubled water and I am proud to have you by my side. You have always supported me and encouraged me to achieve my goals. I thank you with all my heart.

Mom, Dad, Grandma Sigrid, and René – you always believed in me and encouraged my work. With your support - often financial - have you secured the success of this work.

DANKSAGUNG

In ganz besonderem Maße möchte ich mich bei Prof. Dr. Dr. Christoph Redies bedanken. Er gab mir die Möglichkeit, die vorliegende Arbeit in seiner Arbeitsgruppe anzufertigen. Seine hervorragende Betreuung und seine große Diskussionsbereitschaft bereicherten diese Dissertation. Seine unermüdliche Hilfe und sein „Know-how" bei der wissenschaftlichen Präsentation der Ergebnisse in Publikationen und Postern prägten meine Arbeit. Die Entwicklung meiner Sprachkenntnisse von „einfachem Schulenglisch" zu wissenschaftlich-versiertem Englisch habe ich ihm zu verdanken.

Ein großes Dankeschön gilt Prof. Dr. Loreta Medina. Sie hat mir den hochkomplexen Aufbau und die komplizierte Entwicklung der Amygdala näher gebracht. Ihre Diskussionsbereitschaft bei ihren Aufenthalten in Deutschland bzw. meinem Aufenthalt in Spanien hat sehr zur Fertigstellung dieses Teils der Arbeit beigetragen. Für die Hilfe bei der Auswahl der Ergebnisse im Amygdala-Teil möchte ich mich zusätzlich bedanken.

Bei meinen, zum Teil ehemaligen, Kollegen der Arbeitsgruppe „Molekulare Neuroembryologie" – Juntang Lin, Krishna, Franziska Neudert und Monique Nürnberger – möchte ich mich für die gemeinsame Zeit im Labor und die „offenen Ohren" bei allen meinen Fragen bedanken. Die gemeinsamen Kongressreisen waren immer sehr abwechslungsreich und haben großen Spaß gemacht. Besonders durch Krishna und meinem „Büronachbarn" Juntang konnte ich täglich das „Englisch-Sprechen" üben. Juntang war mir eine große Hilfe bei den Anfangsschwierigkeiten der PCR. Vielen Dank für Alles.

Bei unseren technischen Assistentinnen Carolin Große, Manuela Schwalbe, Sylvia Hänßgen und Silke Schreiber möchte ich mich herzlich für die Unterstützung und die kompetente Hilfe bei labortechnischen Problemen bedanken. Auf die gemeinsame Tee/Kaffee-Nachmittagsrunde habe ich mich immer sehr gefreut. Carolin – an dieser Stelle möchte ich Dir ein extra Dankeschön aussprechen. Die freundschaftliche und unkomplizierte Atmosphäre bei unserer Zusammenarbeit im Labor und Deine „Leidensbereitschaft" haben einen großen Anteil an dieser Arbeit.

Ich möchte meinen Kollegen und Kolleginnen der Institute für Anatomie I und II meinen Dank aussprechen. Die Arbeit im Institut hat mir stets viel Freude bereitet. Namentlich möchte ich hier besonders Frau Dr. Stoya für ihre Hilfe beim Hippocampus-Teil der vorliegenden Arbeit und beim Korrekturlesen nennen, sowie Frau Dr. Biedermann, die mir bei der Vorbereitung des Hirnkurses eine große Unterstützung war. Herr Dr. Lemke und Frau Dr. Eitner brachten mir die Geheimnisse des Laser-Scanning-Mikroskops näher. Vielen Dank dafür.

Bei den Mitarbeitern der „Service-Einheit Kleinnager“ – Frau Zapfe, Frau Bierbrauer, Frau Dolke, Herr Dix, Frau Tolksdorf und Herr Dr. van der Wall – möchte ich mich für die Betreuung der Mäuse und die unkomplizierte, freundliche Zusammenarbeit sehr herzlich bedanken.

Meinen Freunden – Nicky, Matthias, Katja, Martin, Annett, Esther, Axel, Willy und Franzi – möchte ich für die moralische Unterstützung und das Korrekturlesen danken. Danke, dass Ihr immer Verständnis hattet und akzeptiertet, dass ich vor allem in der letzten Phase so wenig Zeit für Euch hatte.

Hans – Du bist die Stütze in meinem Leben und ich bin stolz, Dich an meiner Seite zu haben. Du hast mich immer aufgefangen und mich bestärkt, an der Verwirklichung meiner Ziele weiter zu arbeiten. Dafür danke ich Dir von ganzem Herzen.

Mama, Papa, Oma Sigrid, René – ich Danke Euch von ganzem Herzen, dass Ihr immer an mich geglaubt und mich in meiner Arbeit bestärkt habt. Durch Eure, oft auch finanzielle, Unterstützung habt Ihr den Erfolg dieser Arbeit mitgetragen.

EHRENWÖRTLICHE ERKLÄRUNG

Hiermit erkläre ich, dass ich die vorliegende Arbeit selbständig und ohne unzulässige Hilfe Dritter angefertigt habe. Es wurden keine anderen als die angegebenen Quellen und Hilfsmittel verwendet. Jegliche aus anderen Quellen sinngemäß oder wörtlich übernommenen Daten und Konzepte sind unter Angabe der Quelle gekennzeichnet. Bei der Auswahl des Materials für die vorliegende Dissertationsschrift, speziell bei der Zusammenstellung der Ergebnisse für die Amygdala, wurde ich von Prof. Dr. Loreta Medina unterstützt. Es wurde von mir weder entgeltliche Hilfe von Promotionsberatern oder anderen Personen in Anspruch genommen, noch haben Dritte von mir unmittelbar oder mittelbar geldwerte Leistungen für Arbeiten erhalten, die im Zusammenhang mit dem Inhalt der vorgelegten Dissertation stehen.

Ich versichere, dass die vorliegende Dissertationsschrift bisher weder im In- noch im Ausland in gleicher oder in wesentlichen Teilen ähnlicher Form als Prüfungsarbeit für eine staatliche oder andere wissenschaftliche Prüfung eingereicht oder einer anderen Hochschule zur Eröffnung eines Verfahrens zum Erwerb eines akademischen Grades vorgelegt wurde. Die geltende Promotionsordnung der Medizinischen Fakultät der Friedrich-Schiller-Universität ist mir bekannt.

Jena, den 28. April 2011 Nicole Hertel

CURRICULUM VITAE

Personal data

Name:	Nicole Hertel
Date of birth:	27/09/1982
Place of birth:	Borna, Saxony, Germany
Nationality:	German

Research experience

06/2007 – present	PhD student Institute of Anatomy I, Friedrich Schiller University Jena School of Medicine, Germany

Education

10/2001 – 05/2007	Friedrich Schiller University Jena, Germany Subject: Biology Degree: Diploma
09/1993 – 07/2001	Gymnasium (Lerchenberggymnasium Altenburg) Degree: Allgemeine Hochschulreife (Abitur)
09/1989 – 07/1993	Primary school (Staatliche Grundschule Treben)

Grant

2009	DAAD, travel grant as part of the DAAD program "Acciones Integradas Hispano-Alemanas" to visit the laboratory of Prof. Dr. Loreta Medina, Lleida, Spain.

Nicole Hertel

PUBLICATIONS AND POSTER PRESENTATIONS

Publications

Hertel N, Krishna-K, Nuernberger M, Redies C. 2008. A cadherin-based code for the divisions of the mouse basal ganglia. *Journal of Comparative Neurology*, 508:511-528.

This dissertation contains material from the following publications:

Hertel N, Redies C. 2011. Absence of layer-specific cadherin expression profiles in the neocortex of the Reeler mutant mouse. *Cerebral Cortex*, 21:1105-1117.

Krishna-K, **Hertel N**, Redies C. 2011. Cadherin expression in the somatosensory cortex: evidence for a combinatorial molecular code at the single-cell level. *Neuroscience*, 175:37-48.

Material from this dissertation will be used in the following publications:

Hertel N, Redies C, Medina L. Cadherin-based code in the postnatal and adult amygdala of mouse. Manuscript in preparation.

Hertel N, Medina L, Redies C. Altered morphogenesis in the amygdala of the Reeler mouse. Manuscript in preparation.

Poster presentations

Hertel N, Krishna-K, Nuernberger M, Redies C. A cadherin-based code for the divisions of the mouse striatum. 24. Arbeitstagung der Anatomischen Gesellschaft, Poster No. 80, 26/09-28/09/2007, Würzburg, Germany.

Hertel N, Redies C. Comparison of the cadherin expression in the cerebral cortex of wild type and Reeler mice. In: Proceedings of the 8th Göttingen Meeting of the German Neuroscience Society/ 32nd Göttingen Neurobiology Conference, Poster No. T10-4B, 25/03-29/03/2009, Göttingen, Germany.

Hertel N, Redies C. Cadherins in the neocortex of the Reeler mutant mouse: change of layer-specific expression profiles. Symposium of the Network of European

Neuroscience Institutes (ENINET) "Cortical Development and Evolution", 11/04-14/04/2010, Alicante, Spain.

Hertel N, Redies C, Medina L. A cadherin-based code for multiple molecular subdivisions within the amygdaloid complex of wild-type and Reeler mutant mouse. In: 7th FENS Forum of European Neuroscience, Volume 5, Poster No. 101.16, 03/07-07/07/2010, Amsterdam, The Netherlands.

Stoya G, **Hertel N**, Redies C. Cadherin expression profiles in the allocortex/periallocortex of wild-type and Reeler mutant mice. 9th Göttingen Meeting of the German Neuroscience Society/ 33rd Göttingen Neurobiology Conference, Poster No. T10-1A, 23/03-27/03/2011, Göttingen, Germany.